

Virtual Compton Scattering off the nucleon

P.A.M. Guichon and M. Vanderhaeghen

CEA-Saclay, DAPNIA/SPhN, F-91191 Gif-sur-Yvette, France

Abstract

We review the recent developments of virtual Compton scattering. We focus on the kinematical regimes which look the most promising. The threshold regime gives access to the generalized polarizabilities of the proton. The hard scattering regime allows tests of perturbative QCD predictions and of the valence quark wave function. The Bjorken regime is closely related to deep inelastic scattering. It gives access to the off-forward parton distributions which generalize the ordinary parton distributions and may shed a new light on the spin problem. For each regime we discuss the experimental perspectives and the role of the Bethe-Heitler background.

to appear in Prog.Part.Nucl.Phys., Vol.41 (1998)

Contents

1	INTRODUCTION	3
2	PRELIMINARIES	6
2.1	Units and constants	6
2.2	Kinematics	6
2.3	BH and FVCS amplitudes	7
2.4	The VCS amplitude	9
2.5	Tensor expansion of the VCS amplitude	10
2.6	The $(e, e' \gamma)$ cross sections	10
2.7	Virtual photon cross sections	12
3	THE THRESHOLD REGIME AND THE POLARIZABILITIES	14
3.1	Introduction	14
3.2	Electron scattering in an external field	15
3.3	The low energy theorem	18
3.4	Multipole expansion of H_{NB}	19
3.5	Low energy behaviour and generalized polarizabilities	20
3.6	Generalized polarizabilities in models	22
3.7	Low energy expansion of the scattering coefficients	23
3.8	Observables	24
3.9	Results for $(e, e' \gamma)$ observables in the threshold regime	27
4	THE HARD SCATTERING REGIME	31
4.1	Introduction	31
4.2	Incoherence between the short and long-distance physics	31
4.3	The diquark model	34
4.4	Compton scattering in PQCD	38
5	DEEPLY VIRTUAL COMPTON SCATTERING	43
5.1	Introduction	43
5.2	Light cone dominance of the amplitude in the Bjorken limit and definition of off-forward parton distributions	44
5.3	Sum rules for off-forward parton distributions	47
5.4	DVCS amplitude	48
5.5	Hard meson electroproduction amplitudes	49
5.6	Models for the off-forward parton distributions	50
5.7	Results for DVCS and hard meson leptonproduction observables	52
6	OUTLOOK AND PERSPECTIVES	59
A	Polarization vectors and spinors	62
B	Vector basis	63

1 INTRODUCTION

Virtual Compton Scattering generally refers to any process where two photons are involved and where at least one of them is virtual. In the following we shall use Virtual Compton Scattering (VCS) in a more restricted sense, that is the reaction where a *space-like* virtual photon is absorbed by a hadronic target which returns to its initial state by emitting one real photon. The reaction can be accessed through electroproduction of photons, $(e, e'\gamma)$. In practice the target will be the proton but one could extend our considerations to other targets provided the experiments, which are very difficult, become feasible. The experimental difficulty has two origins. Firstly, the cross section is suppressed by a factor $\alpha \sim 1/137$ with respect to the purely elastic case. Secondly, the emission of a neutral pion which decays into two photons creates a physical background which may prevent the extraction of the VCS signal. When the target is a proton one can use kinematical conditions where its recoil momentum is large enough to be measured in a high resolution spectrometer, thus allowing to separate the VCS events from the π^0 events. Even in this favourable case the experiments are still delicate and have become possible only due to the advent of the new generation of electron accelerators. This is why, even though VCS has been put forward many times by theorists, the experiments are just beginning.

VCS was first proposed as a possible test of Quantum Electrodynamics (QED) at small distance [Bjo58] but it is amusing to note that the first calculation [Ber58] of the VCS cross section was motivated by the experimental program of the Mark-III accelerator in Stanford, where the electroproduction of photons was considered as an embarrassing background of the electroproduction of pions, the physically interesting reaction. Later the VCS process was recognized as interesting by itself and was studied by the same authors [Ber61] in the framework of dispersion relations. The interest for this reaction then disappeared for a while due to the lack of experimental data. Actually VCS is a small background!

After the discovery of approximate scaling in deep inelastic scattering, VCS was proposed [Geo71] to get further insight in the light cone singularity of current commutators and later the process was analysed using the operator product expansion [Wat82], providing tests of Quantum Chromodynamics (QCD) and of the models of hadrons. In the framework of the hard scattering picture [Bro80], the first, and till now unique, calculation [Far90a] of the VCS amplitudes in the framework of Perturbative QCD (PQCD) was stimulated by physicists who were planning the first experiment of VCS [vBi89] using the high luminosity apparatus of the (abandoned) PEGASYS project.

The VCS program came to live thanks to the advent of the CEBAF accelerator. The high luminosity and high resolution of the latter allowed to propose a convincing program of VCS [Ber93]. Due to the relatively low energy, the best physics case here turned out to be the threshold region where the so called generalized polarizabilities [Gui95] of the proton could be measured. It was then soon realised that a part of this threshold physics was in fact immediately feasible [d'Ho95] at the MAMI accelerator. The data taking took place in 1996 and at the time of writing are still under analysis. In the meanwhile the first few events of VCS were observed [vdB95].

The last important development is the recent proposal [Ji97a][Rad96a] that VCS in the Bjorken regime could be used to extract new structure functions which reduce to the ordinary parton distributions in the forward limit. The first moments of these functions are related to the hadronic form factors and the second moment gives access to the total spin carried by the quarks in the nucleon. This is an unexpected development which illustrates

the interplay between the existence of a performant accelerator and the apparitions of new and promising ideas.

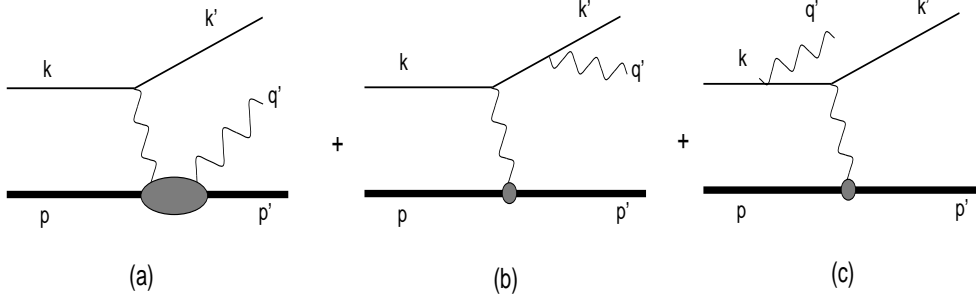


Figure 1: (a) FVCS amplitude, (b,c) BH amplitude.

In the $(e, e'\gamma)$ reaction on the proton

$$e + p \rightarrow e' + p' + \gamma ,$$

the final photon can be emitted either by the proton, giving access to the VCS process, or by the electrons, which is referred to as the Bethe-Heitler (BH) process. If we call $T^{ee'\gamma}$ the amplitude of the $(e, e'\gamma)$ reaction, we have

$$T^{ee'\gamma} = T^{FVCS} + T^{BH} ,$$

where T^{FVCS} and T^{BH} corresponds respectively to graphs (a) and (b,c) of Fig.(1). The meaning of the superscript FVCS is that the corresponding amplitude contains the leptonic current while VCS refers only to the subprocess

$$p + \gamma^* \rightarrow p' + \gamma .$$

The BH amplitude can be calculated exactly in QED, if one knows the elastic form factors of the proton. Therefore it contains no new information on the structure. Unfortunately light particles such as electrons radiate much more than the heavy proton. So the BH process generally dominates or interferes strongly with the VCS process, and this may jeopardize the interpretation of the $(e, e'\gamma)$ reaction, independently of the experimental difficulty. The only way out of this problem is either to find kinematical regions where the BH process is suppressed or to have a very good theoretical control over the interference between the BH and the FVCS amplitudes.

Assuming that this problem is fixed, another difficulty of the theoretical analysis is the complexity of the VCS amplitude itself. For a spin S target, the number of possible helicity states is $2 \times (2S + 1) \times 3 \times 2$ since the virtual and real photons have respectively 3 and 2 degrees of freedom. Parity invariance reduces this number by a factor 1/2 so that for the proton one needs 12 complex functions to specify completely the VCS amplitude. These functions depend, for instance, on the virtuality of the initial photon (Q^2), the scattering angle ($\theta_{\gamma^*\gamma}$) and the energy in the proton-photon center of mass (\sqrt{s}). Extracting the whole set of functions would involve such a huge amount of very difficult experiments that it looks definitely out of reach.

In view of the two difficult points discussed above, the safe attitude has been to restrict the use of the $(e, e'\gamma)$ reaction to cases where the situation is simple enough to allow a fruitful interpretation. Until now 3 cases have been identified:

- The low energy region, below the pion production threshold, where the VCS amplitudes can be parametrised by 6 generalized polarizabilities which are real functions of Q^2 .
- The hard scattering region, where \sqrt{s} is large with respect to the typical hadronic scale, and $\theta_{\gamma^*\gamma}$ is close to 90° . The virtuality needs not to be large. There one can test the prediction of PQCD in the framework of the Hard Scattering Picture (HSP) [Bro80]. In particular the phase of the amplitude which is predicted to be large [Far90a],[Kro91] can be accessed through the interference between the BH and the VCS processes.
- The Bjorken region, where s and Q^2 are large, Q^2/s finite and $\theta_{\gamma^*\gamma}$ close to zero. This is often referred to as Deeply Virtual Compton Scattering (DVCS). In this limit the amplitude depends only on 4 parton distributions (called Off Forward Parton Distributions, OFPD's).

In Section 2 we give our notations and conventions. We present the theoretical framework and collect the formulae that are used in the rest of the paper. Section 3 presents the threshold regime. We have tried to propose a qualitative introduction to the physics of polarizabilities by considering the real photon as an applied external field. The low energy parametrization of the amplitude in terms of six generalized polarizabilities is then discussed in details and we propose an experimental program to determine them. In Section 4 we explain the interest of the hard scattering regime and we use the diquark model to delineate the experimental possibilities. We also discuss real Compton scattering because the experimental prospects are better in this case. Section 5 deals with the Bjorken regime. The DVCS amplitude is computed in the handbag approximation for which the non perturbative input are the OFPD's. We use the same OFPD's to compute the meson production amplitude. Using a simple ansatz for the OFPD's we present some estimates of cross sections in kinematics corresponding to existing and future facilities. We conclude in Section 6 with a discussion of the open problems and perspectives.

	Heaviside-Lorentz	Gauss
Electron mass	$m_e \sim 0$	$m_e \sim 0$
Proton mass	$m = .938\text{GeV}$	$m = .938\text{GeV}$
Planck constant	$\hbar=1$	$\hbar=1$
Light velocity	$c = 1$	$c = 1$
Proton charge	e	e_G
QED fine structure constant	$\alpha_{QED} = e^2/4\pi = 1/137$	$\alpha_{QED} = e_G^2 = 1/137$

Table 1: Constants used in the paper.

	4-momentum	Helicity	Spin projection
Incident electron	k	h	
Scattered electron	k'	$h' = h$	
Target proton	p	h_N	σ
Recoil proton	p'	h'_N	σ'
Final photon	q'	λ'	

Table 2: Notation for the 4-momenta and polarizations.

2 PRELIMINARIES

2.1 Units and constants

The system of units used in this paper is the (natural) Heaviside-Lorentz one [Jac75], but occasionally we shall also write some formulae in the Gauss system so as to fix some misunderstandings. Table (1) summarises our notations or values for the various constants of this paper.

2.2 Kinematics

Greek letters are used to note Lorentz indices. For the space components we use latin letters. Summation over repeated indices is implicit and the metric is $g_{00} = 1$, $g_{ii} = -1$. We have collected in Table (2) our notations for the 4-momenta and helicities or spin projections. We often neglect the mass of the electron with respect to its energy, which is permitted except when the angle between the electrons or between one electron and the final photon is exactly zero. These situations are irrelevant experimentally, so the approximation is safe. As a consequence of this approximation, the electron helicity is conserved, which simplifies a lot the formalism. For the proton the same would happen in the hard scattering regime at very large values of s , but in the threshold region the use of the helicity quantum number is not so compelling. In this case we shall use the (rest frame) spin projection because it leads to a simpler angular analysis.

The virtual photon exchanged in the VCS process has 4-momentum $q = k - k'$, while it is $q - q'$ in the BH process. In the following we shall note with a Roman letter the modulus of a 3-vector, e.g. $q = |\vec{q}|$. A hat on a 3-vector will denote the direction of this vector.

We shall often work in the C.M. frame defined by $\vec{p} + \vec{q} = 0$, and *by default every non*

Lorentz covariant quantity will refer to this particular frame. The unit vectors of this frame are noted $[\vec{e}(1), \vec{e}(2), \vec{e}(3)]$ and are such that the components of the 3-momenta are

$$\begin{aligned}\vec{q} &= q(0, 0, 1) , \\ \vec{q}' &= q'(\sin \theta, 0, \cos \theta) , \\ \vec{k} &= k(\sin \alpha \cos \phi, \sin \alpha \sin \phi, \cos \alpha) , \\ \vec{k}' &= k'(\sin \alpha' \cos \phi, \sin \alpha' \sin \phi, \cos \alpha') ,\end{aligned}\tag{1}$$

and the scattering angle of the electron is $\theta_e = \alpha' - \alpha$. The invariant quantities which appear frequently in the following are:

$$Q^2 = -q^2, t = (q - q')^2, s = (p + q)^2 ,\tag{2}$$

and we have the relations :

$$q' = \frac{s - m^2}{2\sqrt{s}}, q_0 = \frac{s - m^2 - Q^2}{2\sqrt{s}}, p_0 = \frac{s + m^2 + Q^2}{2\sqrt{s}}, p'_0 = \frac{s + m^2}{2\sqrt{s}}.\tag{3}$$

2.3 BH and FVCS amplitudes

For definiteness we consider the case of an electron beam. For a positron beam one must change the relative sign of the BH and FVCS amplitudes. In the one photon exchange approximation and in Lorentz gauge, the BH amplitude is

$$T^{BH} = \frac{-e^3}{t} \varepsilon'^*_{\mu} L^{\mu\nu} \bar{u}(p') \Gamma_{\nu}(p', p) u(p) ,\tag{4}$$

where the spinors are defined in App. A. The polarization of the final photon is $\varepsilon'(q', \lambda')$ and the vertex Γ is defined as

$$\begin{aligned}\Gamma^{\nu}(K', K) &= F_1(X) \gamma^{\nu} + i F_2(X) \sigma^{\nu\rho} (K' - K)_{\rho} / 2m , \\ X &= (K' - K)^2, F_1(0) = 1, F_2(0) = 1.79 .\end{aligned}\tag{5}$$

From QED one has the expression of the non symmetric lepton tensor

$$L^{\mu\nu} = \bar{u}(k') \left(\gamma^{\mu} \frac{1}{\gamma \cdot (k' + q') - m_e + i\epsilon} \gamma^{\nu} + \gamma^{\nu} \frac{1}{\gamma \cdot (k - q') - m_e + i\epsilon} \gamma^{\mu} \right) u(k) ,\tag{6}$$

which explicitly satisfies the gauge invariance conditions

$$q'_{\mu} L^{\mu\nu} = L^{\mu\nu} (q_{\nu} - q'_{\nu}) = 0.\tag{7}$$

The FVCS amplitude has a similar expression

$$T^{FVCS} = \frac{e^3}{q^2} \varepsilon'^*_{\mu} H^{\mu\nu} \bar{u}(k') \gamma_{\nu} u(k).\tag{8}$$

Note that in Eqs.(4, 8) we have extracted a factor e^3 for convenience. The hadronic tensor $H^{\mu\nu}$ depends on the proton structure. At this point we do not want to make hypothesis which are specific of a model. We only assume that it is described by a strong interaction

Hamiltonian H_S which depends on some generic charged field and its momentum (ψ, π) . Under a gauge transformation they transform as

$$\psi \rightarrow \exp(-ie\alpha(x))\psi, \quad \pi \rightarrow \exp(ie\alpha(x))\pi, \quad (9)$$

with analogous transformation for (ψ^*, π^*) . The distinction between Fermi and Bose fields is irrelevant here. For definiteness we assume canonical commutation rules

$$[\pi(\vec{x}, t), \psi(\vec{x}', t)] = -i\delta(\vec{x} - \vec{x}'). \quad (10)$$

The explicit form of H_S is not necessary for the moment. We simply assume the following form

$$H_S = \int d\vec{x} \mathcal{H}_S(\pi, \psi, \partial_i \psi, \pi^*, \psi^*, \partial_i \psi^*), \quad (11)$$

and that H_S is invariant under the transformations (9) when α is constant. In general \mathcal{H}_S does not depend on the gradient of the momenta but including such a dependence would not lead to any difficulty, apart the fact that the formulae would be longer. Also one could include non localities in \mathcal{H}_S which are stronger than the first derivative.

To introduce the coupling to the electromagnetic field one imposes that the Hamiltonian equations of motion

$$\begin{aligned} \frac{\partial \psi}{\partial t} &= i[H_S, \psi], \\ \frac{\partial \pi}{\partial t} &= i[H_S, \pi], \end{aligned} \quad (12)$$

be invariant under the gauge transformations (9). This is achieved by the minimal substitution

$$\begin{aligned} \partial_i \psi &\rightarrow \partial_i \psi + ie A_i \psi, \\ \partial_i \psi^* &\rightarrow \partial_i \psi^* - ie A_i \psi^*, \\ \mathcal{H}_S &\rightarrow \mathcal{H}_S + ie(\psi^* \pi^* - \psi \pi) A_0, \end{aligned} \quad (13)$$

where the gauge transformation for the electromagnetic field A_μ is

$$A_\mu \rightarrow A_\mu + \partial_\mu \alpha. \quad (14)$$

We need to compute T^{FVCS} only to lowest significant order in e . Therefore when we perform the substitution (13) in Eq.(11) we only need to expand the Hamiltonian to order e^2 . This leads to the effective Hamiltonian

$$H_{eff} = H_S + V, \quad \text{with : } V = \int d\vec{x} e j_\mu A^\mu + \frac{e^2}{2} S_{\mu\nu} A^\mu A^\nu, \quad (15)$$

where we have defined

$$\begin{aligned} j^0 &= i\psi^* \pi^* + \text{h.c.}, \quad j^i = -i\psi^* \frac{\partial \mathcal{H}_S}{\partial \partial_i \psi^*} + \text{h.c.}, \\ S^{ij} &= \psi \psi^* \frac{\partial^2 \mathcal{H}_S}{\partial \partial_i \psi \partial \partial_j \psi^*} - \psi^2 \frac{\partial^2 \mathcal{H}_S}{\partial \partial_i \psi \partial \partial_j \psi} + \text{h.c.}, \\ S^{\mu 0} &= S^{0\mu} = 0, \end{aligned} \quad (16)$$

and h.c. denotes the hermitian conjugate. If we note the field strength $F^{\mu\nu} = \partial^\mu A^\nu - \partial^\nu A^\mu$, Eq.(15) implies the field equations

$$\partial_\mu F^{\mu\nu} = ej^\nu + e^2 S^{\nu\mu} A_\mu . \quad (17)$$

Note that the contact (or seagull) term $S^{\mu\nu}$ has only space components. This is characteristic of the Hamiltonian formulation where the variables are the fields and their momenta. In the Lagrangian formalism the time components $S^{0\mu}$, $S^{\mu 0}$ of the contact term are not zero but they disappear when one builds the Hamiltonian. Here the use of the Hamiltonian formalism is compulsory because we must use perturbation theory without too specific hypotheses about the structure. So even if we had started from the Lagrangian we would have been forced to go to the Hamiltonian at some point.

By computing the effect of V in Eq.(15) in perturbation theory to lowest significant order in e one gets the following expression for $H^{\mu\nu}$

$$\begin{aligned} H^{\mu\nu} &= \int d\vec{x} e^{-i\vec{q}' \cdot \vec{x}} \langle \vec{p}' | j^\mu(\vec{x}, 0) \frac{1}{p'_0 + q' - H_S + i\epsilon} j^\nu(0) \\ &\quad + j^\nu(0) \frac{1}{p_0 - q' - H_S + i\epsilon} j^\mu(\vec{x}, 0) | \vec{p} \rangle + H_{seagull}^{\mu\nu}, \\ H_{seagull}^{\mu\nu} &= \langle \vec{p}' | S^{\mu\nu}(0) | \vec{p} \rangle . \end{aligned} \quad (18)$$

This can also be written

$$H^{\mu\nu} = -i \int d^4x e^{-iq \cdot x} \langle p' | T [j^\nu(x), j^\mu(0)] | p \rangle + H_{seagull}^{\mu\nu} , \quad (19)$$

with T the time ordering symbol, and since the equations of motion are by construction gauge invariant, $H^{\mu\nu}$ satisfies the gauge invariance conditions

$$q'_\mu H^{\mu\nu} = H^{\mu\nu} q_\nu = 0.$$

In the C.M. frame one has $\vec{p} = -\vec{q}$ and $\vec{p}' = -\vec{q}'$. The hadronic tensor, which depends on (\vec{p}, \vec{p}') and the spin labels (σ, σ') or helicity labels (h, h') will be noted $H^{\mu\nu}(\vec{q}', \sigma', \vec{q}, \sigma)$ or $H^{\mu\nu}(\vec{q}', h', \vec{q}, h)$ when necessary .

2.4 The VCS amplitude

It is convenient to expand the lepton current which appears in Eq.(8) on the basis of the polarization vector of the virtual photon which are defined in App. A. Using the expressions for the helicity spinors (App. A) one gets

$$\begin{aligned} \bar{u}(k', h) \gamma^\nu u(k, h) &= \sum_{\lambda=0, \pm 1} \Omega(h, \lambda) \varepsilon^\nu(q, \lambda), \\ \Omega(h, \lambda) &= \left(-\lambda e^{-i\lambda\phi} \alpha(\lambda h) + \delta(\lambda, 0) \frac{q_0}{Q} \sqrt{2\varepsilon} \right) \frac{Q}{\sqrt{1-\varepsilon}}, \\ \alpha(z) &= \frac{\sqrt{1+\varepsilon} + 2z\sqrt{1-\varepsilon}}{\sqrt{2}}, \\ \varepsilon &= \frac{(k+k')^2 - q^2}{(k+k')^2 + q^2} = \left[1 + 2 \frac{q^2}{Q^2} \tan^2 \theta_e / 2 \right]^{-1}, \end{aligned} \quad (20)$$

where ε is the usual linear polarization parameter. It is equal to 1 when the virtual photon is linearly polarized in the lepton scattering plane. We *define* the VCS amplitude by

$$T^{VCS}(\lambda', \lambda) = \varepsilon_{\mu}^{\prime*}(\lambda') H^{\mu\nu} \varepsilon_{\nu}(\lambda), \quad (21)$$

which allows us to write

$$T^{FVCS}(\lambda') = \frac{e^3}{-Q^2} \sum_{\lambda} \Omega(h, \lambda) T^{VCS}(\lambda', \lambda). \quad (22)$$

Thanks to the decoupling of the lepton current in Eq.(22) one can take the limit $Q^2 \rightarrow 0$ in T^{VCS} . In this limit the transverse part $T^{VCS}(\lambda = \pm 1)$ coincides (up to a factor e^2) with the amplitude for real Compton scattering.

2.5 Tensor expansion of the VCS amplitude

It is often useful to have a general expansion of the VCS amplitude defined by Eq.(22). A convenient, though not unique, tensor expansion in the C.M. frame and in Lorentz gauge has been proposed in [Gui95]. For the longitudinal part ($\lambda = 0$) it has the form

$$\begin{aligned} \mathcal{N}^{-1} T^{VCS} &= a^l \vec{\varepsilon}^{\prime*} \cdot \hat{q} \\ &+ i[b_1^l \vec{\varepsilon}^{\prime*} \cdot (\hat{q} \times \hat{q}') \vec{\sigma} \cdot \vec{e}(1) + b_2^l \vec{\varepsilon}^{\prime*} \cdot \hat{q} \vec{\sigma} \cdot \vec{e}(2) + b_3^l \vec{\varepsilon}^{\prime*} \cdot (\hat{q} \times \hat{q}') \vec{\sigma} \cdot \vec{e}(3)] , \end{aligned} \quad (23)$$

and for the transverse one ($\lambda = \pm 1$)

$$\begin{aligned} \mathcal{N}^{-1} T^{VCS} &= a^t \vec{\varepsilon}^{\prime*} \cdot \vec{\varepsilon} + a^{tt} \vec{\varepsilon}^{\prime*} \cdot \hat{q} \vec{\varepsilon} \cdot \hat{q}' \\ &+ i[b_1^t \vec{\varepsilon}^{\prime*} \cdot \hat{q} \vec{\varepsilon} \cdot (\hat{q} \times \hat{q}') + b_1^{tt} \vec{\varepsilon}^{\prime*} \cdot (\hat{q} \times \hat{q}') \vec{\varepsilon} \cdot \hat{q}] \vec{\sigma} \cdot \vec{e}(1) \\ &+ i[b_2^t \vec{\varepsilon}^{\prime*} \cdot \vec{\varepsilon} + b_2^{tt} \vec{\varepsilon}^{\prime*} \cdot \hat{q} \vec{\varepsilon} \cdot \hat{q}'] \vec{\sigma} \cdot \vec{e}(2) \\ &+ i[b_3^t \vec{\varepsilon}^{\prime*} \cdot \hat{q} \vec{\varepsilon} \cdot (\hat{q} \times \hat{q}') + b_3^{tt} \vec{\varepsilon}^{\prime*} \cdot (\hat{q} \times \hat{q}') \vec{\varepsilon} \cdot \hat{q}] \vec{\sigma} \cdot \vec{e}(3) , \end{aligned} \quad (24)$$

where the normalisation factor $\mathcal{N} = 2\sqrt{p_0 p'_0}$ is for future convenience and $\vec{\sigma}$ are the Pauli matrices acting on the nucleon spin. The helicity labels λ, λ' have been omitted to simplify the equations.

The 12 scattering coefficients (a^l, b_1^l, \dots) are complex functions of ($q, q', \cos \theta$) which become real below the pion threshold due to time reversal invariance [Gui95].

2.6 The ($e, e' \gamma$) cross sections

In this section, we are giving the observables of the ($e, e' \gamma$) reaction. Due to the small cross sections the experiments will require such high luminosities that the use of polarized hydrogen targets seems excluded. Moreover detecting the polarization of the outgoing electron or photon looks impossible as this can be done only through another electromagnetic process, thereby decreasing by a factor $\sim 1/137$ the already small counting rates. Therefore it looks reasonable to restrict our considerations to the case of a polarized beam and to the detection of the recoil proton polarization.

Let (ξ_e^μ, ξ_p^μ) the 4-vectors which describe the polarization state of the initial electron and final proton. By definition ξ^μ is orthogonal to the particle momentum (that is $\xi_e \cdot k =$

$\xi_p \cdot p' = 0$), and, *in the particle rest frame*, $\vec{\xi}$ is twice the expectation value of the particle spin. We define the following density matrices

$$\begin{aligned}\rho_{h\bar{h}}^e(\xi^e) &= \frac{1}{2m_e} \bar{u}(k, h) \frac{(1 + \gamma^5 \gamma \cdot \xi^e)}{2} u(k, \bar{h}), \\ \rho_{\sigma'\bar{\sigma}'}^p(\xi^p) &= \frac{1}{2m} \bar{u}(p', \sigma') \frac{(1 + \gamma^5 \gamma \cdot \xi^p)}{2} u(p', \bar{\sigma}').\end{aligned}\quad (25)$$

and the Lorentz invariant quantity

$$\mathcal{M}(\xi^e, \xi^p) = \frac{1}{2} \sum_{\sigma\sigma'\lambda'h'h'} T^{ee'\gamma}(\lambda'\sigma'h', \sigma h) \rho_{h\bar{h}}^e(\xi^e) T^{ee'\gamma\dagger}(\lambda'\bar{\sigma}'h', \sigma\bar{h}) \rho_{\sigma'\bar{\sigma}'}^p(\xi^p), \quad (26)$$

in terms of which the invariant cross section is

$$d\sigma(\xi^e, \xi^p) = \frac{(2\pi)^{-5}}{32\sqrt{(p \cdot k)^2 - m^2 m_e^2}} \frac{d\vec{k}' d\vec{p}' d\vec{q}'}{k'_0 p'_0 q'_0} \delta^4(p + k - p' - k' - q') \mathcal{M}(\xi^e, \xi^p). \quad (27)$$

Note that in the above expression, the states are supposed to be normalized as

$$\langle \vec{p} | \vec{p}' \rangle = (2\pi)^3 2p_0 \delta(\vec{p} - \vec{p}'). \quad (28)$$

After integration over the energy of the final photon and defining

$$\mathcal{M} = \mathcal{M}(0, \xi^p) + \mathcal{M}(0, -\xi^p) = 2\mathcal{M}(0, 0), \quad (29)$$

one gets for the unpolarized cross section

$$\frac{d\sigma}{dQ^2 ds dt d\phi d\phi_e} = \frac{(2\pi)^{-5}}{128 m^2 k_{0,lab}^2 \Lambda(s, -Q^2, m^2)} \mathcal{M}, \quad (30)$$

where the azimuthal angle of the electron ϕ_e is arbitrary and

$$\Lambda(x, y, z) = \sqrt{x^2 + y^2 + z^2 - 2xy - 2xz - 2yz}. \quad (31)$$

The experiment is often performed by detecting the electron in coincidence with the proton and the $(e, e' \gamma)$ event is tagged by a zero missing mass, $(k + p - k' - p')^2 = 0$. The corresponding laboratory cross section is then

$$\frac{d\sigma}{dk'_{lab} d\hat{k}'_{lab} d\hat{p}'_{cm}} = \frac{(2\pi)^{-5}}{64m} \frac{k'_{lab}}{k_{lab}} \frac{s - m^2}{s} \mathcal{M}. \quad (32)$$

The next interesting observable is the single (electron) spin asymmetry (SSA) because it should be measurable with the existing highly polarized beams. We define it as

$$\mathcal{A} = \frac{\mathcal{M}(\xi^e, 0) - \mathcal{M}(-\xi^e, 0)}{\mathcal{M}(\xi^e, 0) + \mathcal{M}(-\xi^e, 0)}. \quad (33)$$

In practice ξ^e is proportional to k which corresponds to a longitudinal polarization of the electron. Then, because of time reversal invariance and up to corrections of order α_{QED} ,

one has $\mathcal{A} = 0$ below the pion production threshold (see discussion of Section 4). Also \mathcal{A} vanishes by reflection symmetry if the electron and hadron planes coincide.

Finally for a fixed electron polarisation ξ^e one can try to measure the average polarization \mathcal{P} of the recoiling proton. The components along ξ^p of this double polarization observable are

$$-\mathcal{P}.\xi^p = \frac{\mathcal{M}(\xi^e, \xi^p) - \mathcal{M}(\xi^e, -\xi^p)}{\mathcal{M}(\xi^e, \xi^p) + \mathcal{M}(\xi^e, -\xi^p)}. \quad (34)$$

2.7 Virtual photon cross sections

The $(e, e'\gamma)$ reaction is somewhat unique among the electroproduction reactions due to the presence of the BH process. However, there may be situations where this process can be neglected in which case it is interesting to present the cross sections in the usual manner that is in terms of virtual photon cross sections. To this aim we define the following helicity amplitudes [Kro96]

$$\begin{aligned} \Phi_1 &= e^2 T^{VCS}(\lambda=1, h_N=1/2, \lambda'=1, h'_N=1/2), \\ \Phi_2 &= e^2 T^{VCS}(\lambda=1, h_N=1/2, \lambda'=1, h'_N=-1/2), \\ \Phi_3 &= e^2 T^{VCS}(\lambda=1, h_N=1/2, \lambda'=1, h'_N=1/2), \\ \Phi_4 &= e^2 T^{VCS}(\lambda=1, h_N=1/2, \lambda'=1, h'_N=-1/2), \\ \Phi_5 &= e^2 T^{VCS}(\lambda=1, h_N=1/2, \lambda'=1, h'_N=1/2), \\ \Phi_6 &= e^2 T^{VCS}(\lambda=1, h_N=1/2, \lambda'=1, h'_N=-1/2), \\ \Phi_7 &= e^2 T^{VCS}(\lambda=1, h_N=1/2, \lambda'=1, h'_N=1/2), \\ \Phi_8 &= e^2 T^{VCS}(\lambda=1, h_N=1/2, \lambda'=1, h'_N=-1/2), \\ \Phi_9 &= e^2 T^{VCS}(\lambda=1, h_N=1/2, \lambda'=0, h'_N=1/2) q_0/Q, \\ \Phi_{10} &= e^2 T^{VCS}(\lambda=1, h_N=1/2, \lambda'=0, h'_N=1/2) q_0/Q, \\ \Phi_{11} &= e^2 T^{VCS}(\lambda=1, h_N=1/2, \lambda'=0, h'_N=1/2) q_0/Q, \\ \Phi_{12} &= e^2 T^{VCS}(\lambda=1, h_N=1/2, \lambda'=0, h'_N=1/2) q_0/Q, \end{aligned} \quad (35)$$

where $T^{VCS}(\lambda', h'_N, \lambda, h_N)$ is the amplitude defined in Eq.(21). The factor q_0/Q which multiplies the longitudinal amplitudes (Φ_9 to Φ_{12}) is a matter of convention and is consistent with the polarization vector of App.A.

The unpolarized ($e, e'\gamma$) cross section where one retains only the VCS contribution reads then

$$\frac{d\sigma}{dk'_{lab} d\hat{k}'_{lab} d\phi dt} = \frac{1}{2\pi} \Gamma_v \left(\frac{d\sigma_T}{dt} + \varepsilon \frac{d\sigma_L}{dt} + \varepsilon \cos 2\phi \frac{d\sigma_{TT}}{dt} + \sqrt{2\varepsilon(1+\varepsilon)} \cos \phi \frac{d\sigma_{LT}}{dt} \right), \quad (36)$$

where the virtual photon flux is

$$\Gamma_v = \frac{\alpha_{QED}}{2\pi^2} \frac{k'_{0,lab}}{k_{0,lab}} \frac{s - m^2}{2m Q^2(1 - \varepsilon)}, \quad (37)$$

and the various virtual photon cross sections ¹ are defined as

¹Note that only σ_T and σ_L can be considered as cross sections. The other ones may be negative.
i) The cross-section for transverse photons (which, at $Q^2 = 0$, reduces to the unpolarized cross section $d\sigma/dt$ for real Compton scattering)

$$\frac{d\sigma_T}{dt} = \frac{c}{2} \sum_{i=1}^8 |\Phi_i|^2. \quad (38)$$

ii) The cross-section for longitudinal photons

$$\frac{d\sigma_L}{dt} = c \sum_{i=9}^{12} |\Phi_i|^2. \quad (39)$$

iii) The transverse-transverse interference term

$$\frac{d\sigma_{TT}}{dt} = -\frac{c}{2} \Re e [\Phi_1^* \Phi_7 - \Phi_2^* \Phi_8 + \Phi_3^* \Phi_5 - \Phi_4^* \Phi_6]. \quad (40)$$

iv) The longitudinal-transverse interference term

$$\frac{d\sigma_{LT}}{dt} = -\frac{c}{\sqrt{2}} \Re e [\Phi_9^* (\Phi_1 - \Phi_7) + \Phi_{10}^* (\Phi_2 + \Phi_8) + \Phi_{11}^* (\Phi_3 - \Phi_5) + \Phi_{12}^* (\Phi_4 + \Phi_6)]. \quad (41)$$

The two-body phase space factor c is given by

$$c = \frac{1}{16\pi(s - m^2)^2}. \quad (42)$$

3 THE THRESHOLD REGIME AND THE POLARIZABILITIES

3.1 Introduction

The best way to understand the physics case of the VCS at threshold is to imagine that the final photon plays the role of an external applied field A^{ext} . This may look strange but is possible provided the applied field has the adequate asymptotic conditions. Near the threshold, the energy of the final photon of VCS is small. So the applied field and its electric and magnetic fields are almost constant in time and space. So *VCS at threshold can be interpreted as electron scattering by a target which is in constant electric and magnetic fields*. The physics is exactly the same as if one were performing an *elastic* electron scattering experiment on a target placed between the plates of a capacitor or between the poles of a magnet.

From elementary physics we all know what happens: under the influence of the applied field, the charge J^0 and the current density \vec{J} inside the target get modified. For a weak field this modification is linear in the field and the coefficients of proportionality are the so called polarizabilities. For a uniform isotropic medium only two are necessary: the electric and magnetic ones. In the general case one needs a tensor which moreover depends on the space point. If we note $\delta J^\mu(x)$ the modification of the current density we have, in the linear response approximation

$$\delta J^\mu(x) = \int d^4y P^{\mu\nu}(x, y) A_\nu^{ext}(y). \quad (43)$$

The polarizability tensor $P^{\mu\nu}$ actually quantifies how the system adjusts its internal structure to the applied field. The way to measure it is obviously to measure $\delta J^\mu(x)$ and we do this by electron scattering, exactly in the same way as we measure the *equilibrium* current $J^\mu(x)$ of a free target. In the latter case we know that the experiment can be interpreted in term of the Fourier transform of $J^\mu(x)$, given by

$$J^\mu(q) = \int d^4x e^{iq \cdot x} J^\mu(x). \quad (44)$$

Similarly a VCS experiment measures the Fourier transform of $\delta J^\mu(x)$, the current induced by the applied field.

At this point we can see how the VCS generalizes the real Compton scattering. Though we always think of the zero energy limit, in practice this energy is of course never exactly zero. The corresponding non zero frequency of A^{ext} induces a non uniform time dependence in $\delta J^\mu(x)$ which then radiates an electromagnetic field. The latter, having a non uniform time dependence, decreases only as $1/r$. So it can be detected at large distance. This is the final real photon of the Compton scattering. What we get is again the Fourier transform of $\delta J^\mu(x)$ but now computed along the real photon line, that is for $q^0 = |\vec{q}| \simeq 0$ by energy conservation. This is to be contrasted with the case of VCS for which q^0 and \vec{q} are independent. Moreover since the photon is transverse in the real Compton scattering, only the transverse component of $\delta J^\mu(x)$ come into play.

Now we come to the difficult point of the problem, at least for the experimentalists. In the above reasoning we have tacitely assumed that $\delta J^\mu(x)$ contains only the response of the internal degrees of freedom of the target. The reason is that it is the interesting part. However if the target has a global charge and/or a global magnetic moment, $\delta J^\mu(x)$ also

contains a trivial part due to the global motion under the influence of the applied field. If we put a proton in an electric field the first effect that we observe is that it moves as a whole. Similarly the magnetic field produces a precession of the magnetic moment. Since in a weak field the acceleration is not large, if we scatter an electron on this object we will learn no more than what we learn with a *fixed* target! This problem is absent when one studies the polarizability of a macroscopic sample because it can be fixed in space by appropriate means, which is not possible for the proton. This absence of restoring force explains why the trivial response due to the motion as a whole of the position and magnetic moment dominates over the response of the internal degrees of freedom. This is the physical origin of the low energy theorem [Low58] for VCS.

According to the above development, it is clear that to extract a physically interesting information from a VCS experiment one will have to subtract the trivial part which is due to the global motion. This part must be defined carefully and this will be done in a precise way through the low energy theorem. As stated above, this theorem originates from the fact that at low energy the response is dominated by the global motion of the proton in the external field. So one can ignore the internal structure to calculate this part of the response. All what we need are the parameters which control the motion, that is the mass, the charge, and the magnetic moment. Once the motion is known, we have to compute the amplitude for scattering an electron on this moving proton. For this we only need the elastic form factors and they are known. The calculation in this way is rather involved, mainly due to relativistic effects. This has been done only in the case of real Compton scattering [Gel54]. In the VCS case, one prefers to go directly to the quantum derivation where the use of gauge invariance and perturbation theory greatly simplifies the work. Nevertheless we think it is useful to keep in mind that the LET has a well identified classical origin.

3.2 Electron scattering in an external field

Let us put the above considerations on a more quantitative level. In the presence of the external field the total ² current is, from Eq.(17)

$$J^\mu = ej^\mu + e^2 S^{\mu\nu} A_\nu^{ext}. \quad (45)$$

Note that we have set $A = A^{ext}$ in the seagull term as the other part of the field would only give a contribution of order e^3 or more.

To get the full current we need to evaluate the effect of A^{ext} on the motion. In quantum mechanics this amounts to compute the modification of the nucleon state by A^{ext} . The perturbation is given by Eq.(15) but clearly the seagull term would again produce an effect of order e^3 . So we can write the relevant Schroedinger equation in the form

$$i\frac{\partial}{\partial t}|t\rangle = (H_S + V)|t\rangle, \quad (46)$$

with

$$V = e \int d\vec{x} j^\mu A_\mu^{ext} = e\hat{V}. \quad (47)$$

Note that we work in Schroedinger representation so that j^μ does not depend on time.

²that is the one that scatters the electron

To specify the boundary conditions we assume that the electron scattering happens at time t . The scattering takes place on a hadronic state $|t, in\rangle$ whose time evolution under the perturbation due to A^{ext} is such that

$$|t, in\rangle \rightarrow |N_i\rangle \text{ when } t \rightarrow -\infty. \quad (48)$$

Similarly the scattering leads to a state $|t, out\rangle$ such that

$$|t, out\rangle \rightarrow |N_f\rangle \text{ when } t \rightarrow +\infty. \quad (49)$$

To make the boundary conditions consistent with the dynamics, we assume an adiabatic switching of the interaction by multiplying V by $e^{\epsilon t}$ when computing $|t, in\rangle$ and by $e^{-\epsilon t}$ when computing $|t, out\rangle$.

Using standard time dependent perturbation theory we get to lowest order

$$\begin{aligned} |t, in\rangle &= e^{-iH_S t} \left(1 - i \int_{-\infty}^t dt' e^{iH_S t'} V e^{\epsilon t'} e^{-iH_S t'} \right) |N_i\rangle \\ |t, out\rangle &= e^{-iH_S t} \left(1 - i \int_t^{\infty} dt' e^{iH_S t'} V e^{\epsilon t'} e^{-iH_S t'} \right) |N_f\rangle. \end{aligned} \quad (50)$$

At low energy we know that the target feels essentially a constant electric and magnetic fields (\vec{E}, \vec{B}). In this limiting situation the perturbation is time independent and, combining Eqs.(45, 50) we get

$$\begin{aligned} \langle t, out | J^\mu(\vec{r}) | t, in \rangle &= e^{i(E_f - E_i)t} \left\{ \langle N_f | e j^\mu(\vec{r}) + e^2 S^{\mu\nu}(\vec{r}) A_\nu^{ext}(\vec{r}) \right. \\ &\quad \left. + e^2 (\hat{V} \frac{1}{E_f - H_S + i\epsilon} j^\mu(\vec{r}) + j^\mu(\vec{r}) \frac{1}{E_i - H_S + i\epsilon} \hat{V}) | N_i \rangle \right\} \end{aligned} \quad (51)$$

and we can identify the induced current as the part which goes like e^2 .

In Eq.(51) we see that if we insert a complete set of intermediate states between V and j^μ the state corresponding to the nucleon itself is singular. This pathology is due to the fact that we have taken the strict limit of a constant field and is the quantum manifestation of the global motion discussed previously. Since this part contains no new information, we define the intrinsic induced current by excluding the nucleon from the intermediate states. Since the next possible state is a nucleon and a pion, the energy difference is then finite and we can set $\epsilon = 0$. Thus we get (at $t = 0$)

$$\begin{aligned} \delta J_{int.}^\mu(\vec{r}) &= e^2 \left\{ \langle N_f | S^{\mu\nu}(\vec{r}) A_\nu^{ext}(\vec{r}) | N_f \rangle \right. \\ &\quad \left. + \sum_{n \neq N} \frac{\langle N_f | \hat{V} | n \rangle \langle n | j^\mu(\vec{r}) | N_i \rangle}{E_f - E_n} + \frac{\langle N_f | j^\mu(\vec{r}) | n \rangle \langle n | \hat{V} | N_i \rangle}{E_i - E_n} \right\}. \end{aligned} \quad (52)$$

To simplify a little we set $E_i = E_f = m$ which amounts to neglect the recoil energy of the proton in the electron scattering event. This is only justified at small Q^2 so in the full treatment later we shall not make this approximation.

We now consider separately the effect of a constant electric or magnetic field. The gauge potential corresponding to a constant electric field is

$$A_{ext}^0 = -\vec{r} \cdot \vec{E}, \quad \vec{A}_{ext} = 0. \quad (53)$$

Using Eq.(47) and remembering that the seagull has no time component we get

$$\delta J_{int.,E}^\mu(\vec{r}) = e^2 \sum_{n \neq N} \frac{\langle N_f | \vec{d} \cdot \vec{E} | n \rangle \langle n | j^\mu(\vec{r}) | N_i \rangle}{E_n - m} + \text{c.c.}, \quad (54)$$

where we have defined the dipole moment operator

$$\vec{d} = \int d\vec{r} \vec{r} j^0(\vec{r}). \quad (55)$$

For a constant magnetic field the gauge field is

$$A_{ext}^0 = 0, \quad \vec{A}_{ext} = -\frac{1}{2} \vec{r} \times \vec{B}. \quad (56)$$

So we get

$$\begin{aligned} \delta J_{int.,B}^\mu(\vec{r}) &= \frac{e^2}{2} \langle N_f | S^{\mu i}(\vec{r}) \varepsilon_{ijk} r^j | N_i \rangle B^k \\ &+ e^2 \sum_{n \neq N} \frac{\langle N_f | \vec{\mu} \cdot \vec{B} | n \rangle \langle n | j^\mu(\vec{r}) | N_i \rangle}{E_n - m} + \text{c.c.}, \end{aligned} \quad (57)$$

where the magnetic dipole operator is

$$\vec{\mu} = \frac{1}{2} \int d\vec{r} \vec{r} \times \vec{j}(\vec{r}). \quad (58)$$

If we succeed in eliminating the trivial part of the response, then a low energy VCS experiment will allow to measure the Fourier transform of the induced currents of Eqs.(54, 57).

We can compute from Eqs.(54, 57) the induced dipole moments. After averaging over the nucleon spin projection σ we get

$$\begin{aligned} \delta \vec{d} &= \int d\vec{r} \vec{r} \delta J_{int.,E}^0 = \alpha \vec{E}, \\ \alpha &= \frac{e^2}{3} \sum_{n \neq N, \sigma, \sigma'} \frac{|\langle N, \sigma | \vec{d} | n, \sigma' \rangle|^2}{E_n - m} > 0. \end{aligned} \quad (59)$$

For the magnetic dipole we assume that the seagull term is as in a scalar field theory, that is $S^{ij}(\vec{r}) = -2\delta(i, j)j^0(\vec{r})$, and we get

$$\begin{aligned} \delta \vec{\mu} &= \frac{1}{2} \int d\vec{r} \vec{r} \times \vec{J} = (\beta_{para} + \beta_{dia}) \vec{B}, \\ \beta_{para} &= \frac{e^2}{3} \sum_{n \neq N, \sigma, \sigma'} \frac{|\langle N, \sigma | \vec{\mu} | n, \sigma' \rangle|^2}{E_n - m} > 0, \\ \beta_{dia} &= -\frac{e^2}{6} \sum_{\sigma} \langle N, \sigma | \int d\vec{r} r^2 j^0(\vec{r}) | N, \sigma \rangle < 0. \end{aligned} \quad (60)$$

Note that in the above formulae the polarizabilities α and β are in Heaviside-Lorentz units. To get them in Gauss units, one must replace e by e_G .

3.3 The low energy theorem

Here we abandon the semi-quantitative picture and go back to the true reaction. As explained above we need to separate the trivial part due to the global motion of the proton. However it is easy to see that this separation is not gauge invariant. By itself this is not a problem since only the full amplitude must be gauge invariant, but it is much more comfortable from the theoretical point of view to deal with two parts which are independently gauge invariant.

To this aim we start from the expression of the full VCS amplitude, Eq.(18), and instead of separating the on mass-shell nucleon contribution we write

$$H = H_B + H_{NB}, \quad (61)$$

with H_B , the so called Born term, *defined* by

$$\begin{aligned} H_B^{\mu\nu} &= \bar{u}(p')\Gamma^\mu(p', p' + q') \frac{\gamma \cdot (p' + q') + m}{(p' + q')^2 - m^2} \Gamma^\nu(p' + q', p) u(p) \\ &+ \bar{u}(p')\Gamma^\nu(p', p - q') \frac{\gamma \cdot (p - q') + m}{(p - q')^2 - m^2} \Gamma^\mu(p - q', p) u(p). \end{aligned} \quad (62)$$

Clearly H_B contains not only the nucleon contribution but also the pair excitation term. Moreover the vertex Γ is now evaluated for off mass shell values of one of its arguments because neither $(p' + q')^2$ nor $(p - q')^2$ are equal to m^2 . The advantage is that, if one uses the vertex decomposition of Eq.(62), it is a simple exercise to show that

$$q'_\mu H_B^{\mu\nu} = H_B^{\mu\nu} q_\nu = 0, \quad (63)$$

which in turn implies the gauge invariance of the non Born term H_{NB} .

It has been shown in ref.[Gui95] that H_{NB} is a regular function of the 4-vector q'^μ , which amounts to say that H_{NB} has a polynomial expansion of the form (this also holds for q^μ but we do not need it for the moment)

$$H_{NB}^{\mu\nu} = a^{\mu\nu}(q) + b_\alpha^{\mu\nu}(q)q'^\alpha + c_{\alpha\beta}^{\mu\nu}(q)q'^\alpha q'^\beta + \dots \quad (64)$$

Since the final photon is real we have $q'^0 = q'$ and therefore we can write

$$H_{NB}^{\mu\nu} = a^{\mu\nu} + b_\alpha^{\mu\nu} q'^\alpha + O(q'^2). \quad (65)$$

The gauge invariance of H_{NB} implies

$$0 = q'_\mu a^{\mu\nu} + O(q'^2) = q'a^{0\nu} + q'_i a^{i\nu} + O(q'^2). \quad (66)$$

The coefficients $a^{\mu\nu}$ are constant with respect to \vec{q}' . So averaging Eq.(66) over the direction \vec{q}' on the one hand or multiplying Eq.(66) by \vec{q}' and averaging again on the other hand, we get

$$0 = q'a^{0\nu} = q'_i a^{i\nu}, \quad (67)$$

which implies that $a^{\mu\nu} = 0$. This low energy theorem (LET), which was first shown in ref.[Low58], tells us that the expansion of H_{NB} , the unknown part of the VCS amplitude, starts at order q' . Since, for finite Q^2 the Born part starts at order $1/q'$ we conclude that the first two terms of the VCS amplitude are known as soon as the form factors which define the vertex Γ are known.

3.4 Multipole expansion of H_{NB}

The LET defines in a precise way the separation between the trivial and non trivial part of the VCS amplitude. The non trivial part begins at order q' and is contained in H_{NB} . There is of course a contribution of order q' in H_B but it is exactly known and therefore can be subtracted, at least in principle. So what we need now is an adequate parametrisation of H_{NB} . For this we use the multipole expansion so as to take advantage of angular momentum and parity conservation. Such an expansion implies the choice of a frame and the natural one is the C.M. frame.

Because H_{NB} is a regular function of q and q' , we know from elementary analysis that

$$\int d\hat{q}' H_{NB}^{\mu\nu}(\vec{q}', \vec{q}) Y_{m'}^{l'}(\hat{q}') \sim (q')^{l'}, \quad (68)$$

where \sim means “at least of order”. A similar property holds for an average over \hat{q} . Here $Y_{m'}^{l'}$ stands for the spherical harmonic of rank (l', m') . Since we are interested only in the first power of q' , we can restrict our considerations to the multipoles of rank $l' = 1$, which amounts to say that we are keeping only the *dipole* contribution of the outgoing photon.

To factorize the angular and spin dependence of $H^{\mu\nu}(\vec{q}'\sigma', \vec{q}\sigma)$ we introduce the reduced multipoles

$$\begin{aligned} & 4\pi \mathcal{N} H_{NB}^{(\rho' L', \rho L)S}(q', q) \\ &= \frac{1}{2S+1} \sum_{\sigma\sigma' M' M} (-)^{1/2+\sigma'+L+M} < \frac{1}{2} - \sigma', \frac{1}{2}\sigma | Ss > < L' M', L - M | Ss > \\ & \int d\hat{q}' d\hat{q} V_{\mu}^*(\rho' L' M', \hat{q}') H_{NB}^{\mu\nu}(\vec{q}'\sigma', \vec{q}\sigma) V_{\nu}(\rho L M, \hat{q}), \end{aligned} \quad (69)$$

where the basis vectors $V^{\mu}(\rho L M, \hat{q})$ are defined in Appendix B. The Clebsch-Gordan coefficients are the same as in Ref.[Edm57]. In Eq.(69), L (L') represents the angular momentum of the initial (final) electromagnetic transition whereas S differentiates between the spin-flip ($S = 1$) or non spin-flip ($S = 0$) transition at the nucleon side.

The index ρ can take a priori 4 values: $\rho = 0$ (charge), $\rho = 1$ (magnetic), $\rho = 2$ (electric), $\rho = 3$ (longitudinal), but gauge invariance relates the charge and longitudinal multipoles according to

$$\begin{aligned} q' H_{NB}^{(3L', \rho L)S} + q_0 H_{NB}^{(0L', \rho L)S} &= 0, \\ q H_{NB}^{(\rho' L', 3L)S} + q_0 H_{NB}^{(\rho' L', 0L)S} &= 0. \end{aligned} \quad (70)$$

So if we define the new basis

$$\begin{aligned} W^{\mu}(\rho L M, \hat{q}) &= V^{\mu}(\rho L M, \hat{q}), \quad \rho = 1, 2, \\ W^{\mu}(0, L M, \hat{q}) &= V^{\mu}(0 L M, \hat{q}) + \frac{q_0}{q} V^{\mu}(3 L M, \hat{q}), \end{aligned} \quad (71)$$

which satisfy $q_{\mu} W^{\mu}(\rho L M) = 0$, $\rho = 0, 1, 2$, we have the following manifestly gauge invariant expansion of $H_{NB}^{\mu\nu}$

$$H_{NB}^{\mu\nu}(\vec{q}'\sigma', \vec{q}\sigma) = 4\pi \mathcal{N} \sum_{\rho' L' M' \rho L M} g_{\rho' \rho'} W^{\mu}(\rho' L' M', \hat{q}') g_{\rho \rho} W^{\nu*}(\rho L M, \hat{q})$$

$$\sum_{Ss} (-)^{1/2+\sigma'+L+M} < \frac{1}{2} - \sigma', \frac{1}{2} \sigma | Ss > < L' M', L - M | Ss > H_{NB}^{(\rho' L', \rho L)S}(q', q), \quad (72)$$

where the sum over (ρ', ρ) is now restricted to $(0,1,2)$. The expansion (72) is valid even if the two photons are virtual but for the real final photon only the multipole $\rho' = 1, 2$ can appear. This of course does not mean that the charge multipole does not exist: it is the contraction of the basis vector W with the transverse polarization vector of the photon ε' which vanishes.

The selections rules due to parity and angular momentum conservation are

$$S = 0, 1, \quad |L' - S| \leq L \leq L' + S, \quad (-)^{\rho'+L'} = (-)^{\rho+L}, \quad (73)$$

and in addition one knows that the electric and magnetic multipoles are zero for $L = L' = 0$.

3.5 Low energy behaviour and generalized polarizabilities

Using Eq.(68) and the definition of the basis vectors V^μ it is clear that for small values of q' the multipoles behave as

$$H_{NB}^{(\rho' L', \rho L)S}(q', q) \sim q'^{L'} \quad \text{for } \rho' = 0, 1, \quad (74)$$

A similar relation holds for small values of q . This follows from the fact that in the charge and magnetic vectors the spherical harmonic has rank $l = L$. For the electric multipoles one has the same behaviour, but this does not follow from such a simple argument because in this case the spherical harmonic has rank $l = L \pm 1$. One has to use the Siegert relation [Sie37] (see also Ref.[Gui95]) which is a consequence of gauge invariance and which states that

$$H_{NB}^{(2L', \rho L)S}(q', q) = -\sqrt{\frac{L'+1}{L'}} \frac{q'^0}{q'} H_{NB}^{(0L', \rho L)S}(q', q) + O(q'^{L'+1}), \quad (75)$$

with an analogous relation for the virtual photon. Since $q'^0 = q'$ for the real photon, and $q'^0 < q$ for the (space-like) virtual photon, we see that at small (q', q) all the multipoles behave at least as $q'^{L'} q^L$. As we are looking for the part of H_{NB} which goes like q' and using the selections rules we find that, *a priori*, this involves the following multipoles

$$\begin{aligned} & H_{NB}^{(11,00)1}, H_{NB}^{(11,02)1}, H_{NB}^{(11,22)1}, H_{NB}^{(11,11)0}, H_{NB}^{(11,11)1}, \\ & H_{NB}^{(21,01)0}, H_{NB}^{(21,01)1}, H_{NB}^{(21,21)0}, H_{NB}^{(21,21)1}, H_{NB}^{(21,12)1}. \end{aligned} \quad (76)$$

So the low energy (but arbitrary q) behaviour of the non Born VCS amplitude could be parametrized by 10 functions of q defined by

$$\text{Limit of } \frac{1}{q'} \frac{1}{q^L} H_{NB}^{(\rho' L', \rho L)S}(q', q) \text{ when } q' \rightarrow 0. \quad (77)$$

with $(\rho' L', \rho L)S$ as in Eq.(76).

However this parametrization is not adequate. The first reason is that the $(\rho' = 2, L' = 1)$ multipoles actually behave as q' because of gauge invariance. It often happens that in model calculations gauge invariance is violated by some approximation which otherwise

would be innocuous. In this case the definition (77) may lead to a divergence. The second reason is more serious. In a VCS experiment the functions defined in Eq.(77) are measured by taking the limit $q' \rightarrow 0$ at fixed q . When one lets $q \rightarrow 0$ one would like to recover the polarizabilities measured in real Compton scattering, but in the latter case the experiment realizes the limit ($q' = q \rightarrow 0$) and there is no guarantee that the two limits are the same. It is not difficult to show [Gui95] that for the charge and magnetic multipoles the two limits are actually the same. This is again due to the fact that in those multipoles the rank of the spherical harmonic is $l = L$ or $l' = L'$. By contrast, from Eq.(75) one can understand that it will not be the case for the electric multipoles due to the factor q^0/q which goes to 1 in the Compton case while it obviously goes to 0 in the VCS case. This problem was overcome in Ref.[Gui95] by the introduction of mixed multipoles which were neither electric nor longitudinal. However the findings of a recent work [Dre98] allow for a much more elegant solution.

First one introduces the generalized polarizabilities (GP's) for the multipoles which are not problematic, that is

$$\begin{aligned} P^{(11,00)1}(q) &= \left[\frac{1}{q'} H_{NB}^{(11,00)1}(q', q) \right]_{q'=0}, \quad P^{(11,02)1}(q) = \left[\frac{1}{q' q^2} H_{NB}^{(11,02)1}(q', q) \right]_{q'=0}, \\ P^{(11,11)S}(q) &= \left[\frac{1}{q' q} H_{NB}^{(11,11)S}(q', q) \right]_{q'=0}. \end{aligned} \quad (78)$$

Next one considers the multipoles where only the real photon is electric. In this case one can use Siegert relation to relate them to the corresponding charge multipoles which again are safe. So one defines

$$P^{(01,01)S}(q) = \left[\frac{1}{q' q} H_{NB}^{(01,01)S}(q', q) \right]_{q'=0}, \quad P^{(01,12)1}(q) = \left[\frac{1}{q' q^2} H_{NB}^{(01,12)1}(q', q) \right]_{q'=0}, \quad (79)$$

which, using Eq.(75), specifies the low energy behaviour of $H_{NB}^{(21,01)S}$ and $H_{NB}^{(21,12)1}$. In Ref.[Dre98] it has been shown that $P^{(11,00)1}$ is not independent and can be eliminated according to

$$P^{(11,00)1}(q) = \sqrt{3} \frac{q^2}{\tilde{q}_0} P^{(01,01)1} - \frac{1}{\sqrt{2}} q^2 P^{(11,02)1}, \quad (80)$$

with \tilde{q}_0 the limit of q_0 when $q' \rightarrow 0$, that is $\tilde{q}_0 = m - \sqrt{m^2 + q^2}$.

The remaining problematic multipoles are $H_{NB}^{(11,22)1}$, $H^{(21,21)0}$, $H^{(21,21)1}$. The great value of the work of Refs.[Dre97][Dre98] is that their authors have been able to express the low energy limit of these multipoles in term of the generalized polarizabilities already defined by Eqs.(78, 79). Using their results, the definitions (78,79) and the relations (75,80) one gets the following low energy parametrization of all the needed multipoles

$$\begin{aligned} H_{NB}^{(11,00)1}(q', q) &= q' \left(\sqrt{3} \frac{q^2}{\tilde{q}_0} P^{(01,01)1}(q) - \frac{1}{\sqrt{2}} q^2 P^{(11,02)1}(q) \right) + O(q'^2), \\ H_{NB}^{(11,02)1}(q', q) &= q' q^2 P^{(11,02)1}(q) + O(q'^2), \\ H_{NB}^{(11,11)S}(q', q) &= q' q P^{(11,11)S}(q) + O(q'^2), \\ H_{NB}^{(21,01)S}(q', q) &= -q' q \sqrt{2} P^{(01,01)S}(q) + O(q'^2), \end{aligned}$$

$$\begin{aligned}
H_{NB}^{(21,12)1}(q', q) &= -q'q^2\sqrt{2}P^{(01,12)1}(q) + O(q'^2), \\
H_{NB}^{(11,22)1}(q', q) &= q'qP^{(11,11)1}(q) + O(q'^2), \\
H_{NB}^{(21,21)0}(q', q) &= -q'\tilde{q}_0P^{(11,11)0}(q) + O(q'^2), \\
H_{NB}^{(21,21)1}(q', q) &= -q'\left(2\frac{q^2}{\tilde{q}_0}P^{(11,11)1}(q) - \sqrt{2}q^2P^{(01,12)1}(q)\right) + O(q'^2), \quad (81)
\end{aligned}$$

Thus only 6 GP's, that is

$$P^{(01,01)S}(q), P^{(11,11)S}(q), P^{(11,02)1}(q), P^{(01,12)1}(q), \quad (82)$$

are necessary to give the low energy behaviour of H_{NB} . Moreover it was shown in Ref.[Dre98] that one has the relations

$$P^{(01,01)1}(0) = P^{(11,11)1}(0) = 0. \quad (83)$$

The relations of Ref.[Dre98] which allow to eliminate 4 of the GP's introduced in Ref.[Gui95] can be proved by combining the nucleon crossing symmetry with the charge conjugation invariance. These symmetries hold in any relativistic theory but to exploit them one needs a covariant parametrization of the amplitude. The reason is that nucleon crossing relates the reaction

$$\gamma^* + N(p) \rightarrow \gamma + N(p'), \quad (84)$$

to the reaction

$$\gamma^* + \overline{N}(-p') \rightarrow \gamma + \overline{N}(-p). \quad (85)$$

So to implement the symmetry one needs an expression where the 4-momentum formally appears while in the partial wave expansion only the 3 momentum appears. Though the correctness of the relations makes no doubt, their physical origin is not yet clear. In particular one sees on Eqs.(81) that a purely magnetic GP parametrizes a purely electric multipole. Since Lorentz transformations mix the electric and magnetic field, one may suspect that the origin of the relation is relativistic but a physical interpretation is still lacking.

3.6 Generalized polarizabilities in models

In a static model one neglects all the effects which go like the velocity of the initial or final nucleon. This allows to derive simple expressions for the GP's. Here we recall the expressions derived in Ref.[Gui95] for the most important ones

$$P^{(01,01)0}(q) = \sqrt{\frac{2}{3}} \sum_{n \neq N} \frac{1}{m - E_n} \quad (86)$$

$$\begin{aligned}
P^{(11,11)0}(q) &= \frac{4}{\sqrt{6}} \sum_{n \neq N} \frac{1}{m - E_n} \\
&\quad [< N | d_z(0) | X > < X | d_z(q) | N > + < N | d_z(q) | X > < X | d_z(0) | N >], \\
&\quad [< N | \mu_z(0) | X > < X | \mu_z(q) | N > + < N | \mu_z(q) | X > < X | \mu_z(0) | N >], \quad (87)
\end{aligned}$$

where the generalized dipole moments are defined as

$$\begin{aligned}\vec{d}(\mathbf{q}) &= \int d\vec{r} \frac{3j_1(qr)}{qr} j^0(\vec{r}) \vec{r}, \\ \vec{\mu}(\mathbf{q}) &= \frac{1}{2} \int d\vec{r} \frac{3j_1(qr)}{qr} \vec{r} \times \vec{j}(\vec{r}),\end{aligned}\tag{88}$$

where j_1 is the spherical Bessel function and we have omitted a possible seagull term to simplify.

In the limit $q \rightarrow 0$, if we compare with Eqs.(59, 60) we find the relations with the usual polarizabilities

$$\begin{aligned}P^{(01,01)0}(0) &= -\sqrt{\frac{2}{3}} \frac{\alpha}{e^2} = -\sqrt{\frac{2}{3}} \frac{\alpha_G}{e_G^2}, \\ P^{(11,11)0}(0) &= -\sqrt{\frac{8}{3}} \frac{\beta}{e^2} = -\sqrt{\frac{8}{3}} \frac{\beta_G}{e_G^2}.\end{aligned}\tag{89}$$

The generalized polarizabilities have been calculated in various more or less realistic nucleon structure models. A first estimate was proposed using the constituent quark model [Gui95]. In Refs.[Met97a][Met97b], calculations have been given in the linear sigma model. Calculations and a discussion of the polarizabilities in Chiral Perturbation Theory were given in Refs.[Hem97a] [Hem97b].

3.7 Low energy expansion of the scattering coefficients

The calculation of the observables is easier and more transparent in terms of the tensor expansion defined in Eqs.(23, 24). The relation between the scattering coefficients (a^l, b^l, \dots) and the multipoles has been derived [Gui95] using a generalization of the method used in pion electroproduction [Ber67]. Combining the results of Ref.[Gui95] and the relations of Ref.[Dre98] one gets

$$\begin{aligned}a_{NB}^l &= -\sqrt{\frac{3}{2}} \varepsilon_s P^{(01,01)0}(q) qq' + O(q'^2), \\ b_{NB,1}^l = \frac{q \cos \theta - \tilde{q}_0}{q - \tilde{q}_0 \cos \theta} b_{NB,2}^l &= \frac{3\varepsilon_s}{2 \sin \theta} \left(\frac{q}{\tilde{q}_0} \cos \theta - 1 \right) P^{(01,01)1}(q) qq' + O(q'^2), \\ b_{NB,3}^l &= -\frac{3\varepsilon_s}{2} \left(\frac{q}{\tilde{q}_0} P^{(01,01)1}(q) - q \sqrt{\frac{3}{2}} P^{(11,02)1}(q) \right) qq' + O(q'^2), \\ a_{NB}^t = -\left(\cos \theta - \frac{\tilde{q}_0}{q} \right) a_{NB}^t &= \sqrt{\frac{3}{8}} \left(\cos \theta - \frac{\tilde{q}_0}{q} \right) P^{(11,11)0}(q) qq' + O(q'^2), \\ b_{NB,1}^t = -b_{NB,2}^t &= \frac{3}{2 \sin \theta} \left(\frac{q^2}{\tilde{q}_0} P^{(11,11)1}(q) - \sqrt{2} q^2 P^{(01,12)1}(q) \right) q' + O(q'^2), \\ b_{NB,1}^t \sim b_{NB,2}^t &= O(q'^2), \\ b_{NB,3}^t = \frac{q \cos \theta - \tilde{q}_0}{q - \tilde{q}_0 \cos \theta} b_{NB,3}^t &= -\frac{3}{2 \sin^2 \theta} \left(1 - \frac{q}{\tilde{q}_0} \cos \theta \right) P^{(11,11)1}(q) qq' + O(q'^2),\end{aligned}\tag{90}$$

where NB indicates that we consider only the non Born part of the scattering coefficients and where $\varepsilon_s = Q^2/(q_0 q)$.

3.8 Observables

We now investigate how one can analyse the $(e, e' \gamma)$ observables in order to extract the GP's. We recall that the observables can be expressed in term of the Lorentz invariant quantity $\mathcal{M}(\xi_e, \xi_p)$ defined in Section 2. We consider it in the C.M. frame and we choose as independent variables $(q', q, \varepsilon, \theta, \phi)$. The tilde will denote the value of a dependent variable in the limit $q' = 0$.

For the polarization observables we consider an electron beam in a pure helicity state $h = \pm 1/2$, which amounts to take $\xi_e = 2hk/m_e$ up to terms of order m_e that we can neglect. (this yields from Eq.(25) $\rho_{hh}^e(\xi^e) = 1/2m_e \bar{u}(k, h) (1 + \gamma^5 2h)/2 u(k, h)$). Below the pion threshold only the recoil polarization \mathcal{P} , Eq.(34), is interesting. Since $\mathcal{P} \cdot p' = 0$ one only needs the space part of \mathcal{P} and we consider its components along the basis $[\vec{e}(1), \vec{e}(2), \vec{e}(3)]$ defined in Section 2. We shall denote

$$\Delta \mathcal{M}(h, i) = \mathcal{M}[\xi_e = 2hk/m_e, \vec{\xi}_p = \vec{e}(i)] - \mathcal{M}[\xi_e = 2hk/m_e, \vec{\xi}_p = -\vec{e}(i)]. \quad (91)$$

We *assume* that, at fixed $(q, \varepsilon, \theta, \phi)$, the experiment is able to determine \mathcal{M} and $\Delta \mathcal{M}$ in the form

$$\begin{aligned} \mathcal{M}^{\text{exp}} &= \frac{\mathcal{M}_{-2}^{\text{exp}}}{q'^2} + \frac{\mathcal{M}_{-1}^{\text{exp}}}{q'} + \mathcal{M}_0^{\text{exp}} + O(q'), \\ \Delta \mathcal{M}^{\text{exp}} &= \frac{\Delta \mathcal{M}_{-2}^{\text{exp}}}{q'^2} + \frac{\Delta \mathcal{M}_{-1}^{\text{exp}}}{q'} + \Delta \mathcal{M}_0^{\text{exp}} + O(q'). \end{aligned} \quad (92)$$

Due to the low energy theorem, the threshold coefficients \mathcal{M}_{-2} , \mathcal{M}_{-1} , $\Delta \mathcal{M}_{-2}$, $\Delta \mathcal{M}_{-1}$ are known. If we define

$$\begin{aligned} \mathcal{M}^{\text{BH+Born}} &= \frac{\mathcal{M}_{-2}^{\text{BH+Born}}}{q'^2} + \frac{\mathcal{M}_{-1}^{\text{BH+Born}}}{q'} + \mathcal{M}_0^{\text{BH+Born}} + O(q'), \\ \Delta \mathcal{M}^{\text{BH+Born}} &= \frac{\Delta \mathcal{M}_{-2}^{\text{BH+Born}}}{q'^2} + \frac{\Delta \mathcal{M}_{-1}^{\text{BH+Born}}}{q'} + \Delta \mathcal{M}_0^{\text{BH+Born}} + O(q'), \end{aligned} \quad (93)$$

where the index BH+Born means that the quantity is computed by keeping only the BH and Born contributions in the $(e, e' \gamma)$ amplitude, then we have the following constraints due to the LET :

$$\mathcal{M}_{-k}^{\text{exp}} = \mathcal{M}_{-k}^{\text{BH+Born}}, \quad \Delta \mathcal{M}_{-k}^{\text{exp}} = \Delta \mathcal{M}_{-k}^{\text{BH+Born}}, \quad k = 1, 2. \quad (94)$$

The information on the GPs is contained in $\mathcal{M}_0^{\text{exp}}$, and $\Delta \mathcal{M}_0^{\text{exp}}$. These coefficients contain a part which comes from the (BH+Born) part of the amplitude and another one which is a linear combination of the GPs with coefficients determined by the kinematics. After some algebra [Gui95],[Vdh97a] one finds that the observables depend on the 6 following structure functions

$$\begin{aligned}
P_{LL}(q) &= -2\sqrt{6}mG_E P^{(01,01)0}(q) , \\
P_{TT}(q) &= -3G_M \frac{q^2}{\tilde{q}_0} \left(P^{(11,11)1}(q) - \sqrt{2}\tilde{q}_0 P^{(01,12)1}(q) \right) , \\
P_{LT}(q) &= \sqrt{\frac{3}{2}} \frac{mq}{\tilde{Q}} G_E P^{(11,11)0}(q) + \frac{3}{2} \frac{\tilde{Q}q}{\tilde{q}_0} G_M P^{(01,01)1}(q) , \\
P_{LT}^z(q) &= \frac{3\tilde{Q}q}{2\tilde{q}_0} G_M P^{(01,01)1}(q) - \frac{3mq}{\tilde{Q}} G_E P^{(11,11)1}(q) , \\
P_{LT}^{'z}(q) &= -\frac{3}{2} \tilde{Q} G_M P^{(01,01)1}(q) + \frac{3mq^2}{\tilde{Q}\tilde{q}_0} G_E P^{(11,11)1}(q) , \\
P_{LT}^{'\perp}(q) &= \frac{3q\tilde{Q}}{2\tilde{q}_0} G_M \left(P^{(01,01)1}(q) - \sqrt{\frac{3}{2}} \tilde{q}_0 P^{(11,02)1}(q) \right) , \tag{95}
\end{aligned}$$

where G_E and G_M stand for $G_E(\tilde{Q}^2)$ and $G_M(\tilde{Q}^2)$. Clearly measuring the 6 structure functions³ defined in Eq.(95) amounts to measure the 6 independent GP's. For convenience we also introduce the combinations

$$\begin{aligned}
P_{LT}^{\perp} &= \frac{RG_E}{2G_M} P_{TT} - \frac{G_M}{2RG_E} P_{LL} , \\
P_{TT}^{\perp} &= \frac{G_M}{RG_E} (P_{LT}^z - P_{LT}) = -\frac{q}{2} G_M \left(3P^{(11,11)1} + \sqrt{\frac{3}{2}} P^{(11,11)0} \right) , \\
P_{TT}^{'\perp} &= \frac{G_M}{RG_E} \left(P_{LT}^{'z} + \frac{\tilde{q}_0}{q} P_{LT} \right) = \frac{q}{2} G_M \left(3\frac{q}{\tilde{q}_0} P^{(11,11)1} + \sqrt{\frac{3}{2}} \frac{\tilde{q}_0}{q} P^{(11,11)0} \right) , \tag{96}
\end{aligned}$$

where $R = 2m/\tilde{Q}$. The observables⁴ can then be written as (using the notation (x, y, z) for the directions (1,2,3)) [Gui95],[Vdh97a]

$$\begin{aligned}
&\mathcal{M}_0^{\text{exp}} - \mathcal{M}_0^{\text{BH+Born}} \\
&= 2K_2 \left\{ v_1 [\epsilon P_{LL}(q) - P_{TT}(q)] + \left(v_2 - \frac{\tilde{q}_0}{q} v_3 \right) \sqrt{2\varepsilon(1+\varepsilon)} P_{LT}(q) \right\} , \\
&\Delta \mathcal{M}_0^{\text{exp}}(h, z) - \Delta \mathcal{M}_0^{\text{BH+Born}}(h, z) \\
&= 4(2h)K_2 \left\{ -v_1 \sqrt{1-\varepsilon^2} P_{TT}(q) + v_2 \sqrt{2\varepsilon(1-\varepsilon)} P_{LT}^z(q) + v_3 \sqrt{2\varepsilon(1-\varepsilon)} P_{LT}^{'z}(q) \right\} ,
\end{aligned}$$

³The unpolarized cross section and the double polarization observables yield 6 independent structure functions and not 7 as mentionned originally in Ref.[Vdh97a]. Afterwards [Dre98], four relations were found between the polarizabilities which yield then 6 independent observables to determine the 6 independent polarizabilities.

⁴Note the misprint in Eq.(4) of Ref.[Vdh97a]: $h\varepsilon$ should be replaced by ε .

$$\begin{aligned}
& \Delta \mathcal{M}_0^{\text{exp}}(h, x) - \Delta \mathcal{M}_0^{\text{BH+Born}}(h, x) \\
&= 4(2h)K_2 \left\{ v_1^x \sqrt{2\varepsilon(1-\varepsilon)} P_{LT}^\perp(\mathbf{q}) + v_2^x \sqrt{1-\varepsilon^2} P_{TT}^\perp(\mathbf{q}) \right. \\
&\quad \left. + v_3^x \sqrt{1-\varepsilon^2} P_{TT}'^\perp(\mathbf{q}) + v_4^x \sqrt{2\varepsilon(1-\varepsilon)} P_{LT}'^\perp(\mathbf{q}) \right\}, \\
& \Delta \mathcal{M}_0^{\text{exp}}(h, y) - \Delta \mathcal{M}_0^{\text{BH+Born}}(h, y) \\
&= 4(2h)K_2 \left\{ v_1^y \sqrt{2\varepsilon(1-\varepsilon)} P_{LT}^\perp(\mathbf{q}) + v_2^y \sqrt{1-\varepsilon^2} P_{TT}^\perp(\mathbf{q}) \right. \\
&\quad \left. + v_3^y \sqrt{1-\varepsilon^2} P_{TT}'^\perp(\mathbf{q}) + v_4^y \sqrt{2\varepsilon(1-\varepsilon)} P_{LT}'^\perp(\mathbf{q}) \right\}, \tag{97}
\end{aligned}$$

with

$$K_2 = e^6 \frac{\mathbf{q}}{\tilde{Q}^2} \frac{2m}{1-\varepsilon} \sqrt{\frac{2E_q}{E_q+m}}, \quad E_q = \sqrt{m^2 + \mathbf{q}^2}. \tag{98}$$

The angular dependent functions (v_1, v_2, \dots) are given by

$$\begin{aligned}
v_1 &= \sin \theta \left(\omega'' \sin \theta - k_T \omega' \cos \theta \cos \phi \right), \\
v_2 &= - \left(\omega'' \sin \theta \cos \phi - k_T \omega' \cos \theta \right), \\
v_3 &= - \left(\omega'' \sin \theta \cos \theta \cos \phi - k_T \omega' (1 - \sin^2 \theta \cos^2 \phi) \right), \\
v_1^x &= \sin \theta \cos \phi \left(\omega'' \sin \theta - k_T \omega' \cos \theta \cos \phi \right), \\
v_2^x &= -\omega'' \sin \theta + k_T \omega' \cos \theta \cos \phi, \\
v_3^x &= -\cos \theta \left(\omega'' \sin \theta - k_T \omega' \cos \theta \cos \phi \right), \\
v_4^x &= k_T \omega' \sin \theta \sin^2 \phi, \\
v_1^y &= \sin \theta \sin \phi \left(\omega'' \sin \theta - k_T \omega' \cos \theta \cos \phi \right), \\
v_2^y &= k_T \omega' \cos \theta \sin \phi, \\
v_3^y &= k_T \omega' \sin \phi, \\
v_4^y &= -k_T \omega' \sin \theta \sin \phi \cos \phi, \tag{99}
\end{aligned}$$

and finally ⁵

$$\begin{aligned}
\omega &= \left[-\mathbf{q}' \left(\frac{1}{p \cdot \mathbf{q}'} + \frac{1}{k \cdot \mathbf{q}'} \right) \right]_{\mathbf{q}'=0}, \quad \omega' = \left[\mathbf{q}' \left(\frac{1}{k' \cdot \mathbf{q}'} - \frac{1}{k \cdot \mathbf{q}'} \right) \right]_{\mathbf{q}'=0}, \\
\omega'' &= \omega \mathbf{q} - \omega' \sqrt{\tilde{k}'^2 - k_T^2}, \quad k_T = \tilde{Q} \sqrt{\frac{\varepsilon}{2(1-\varepsilon)}}. \tag{100}
\end{aligned}$$

⁵In Ref.[Gui95] there is a misprint in Eq.(119) for ω , which should be corrected by replacing $p' \cdot q'$ by $p \cdot q'$.

3.9 Results for $(e, e'\gamma)$ observables in the threshold regime

In the previous sections, we have outlined the observables of the $p(e, e'\gamma)p$ reaction below threshold and have detailed how the nucleon structure effect can be parametrized in terms of six independent polarizabilities. In this section, results will be shown for the $p(e, e'\gamma)p$ observables in the threshold region in kinematics where the experiments are performed at MAMI [d'Ho95] and at CEBAF [Ber93].

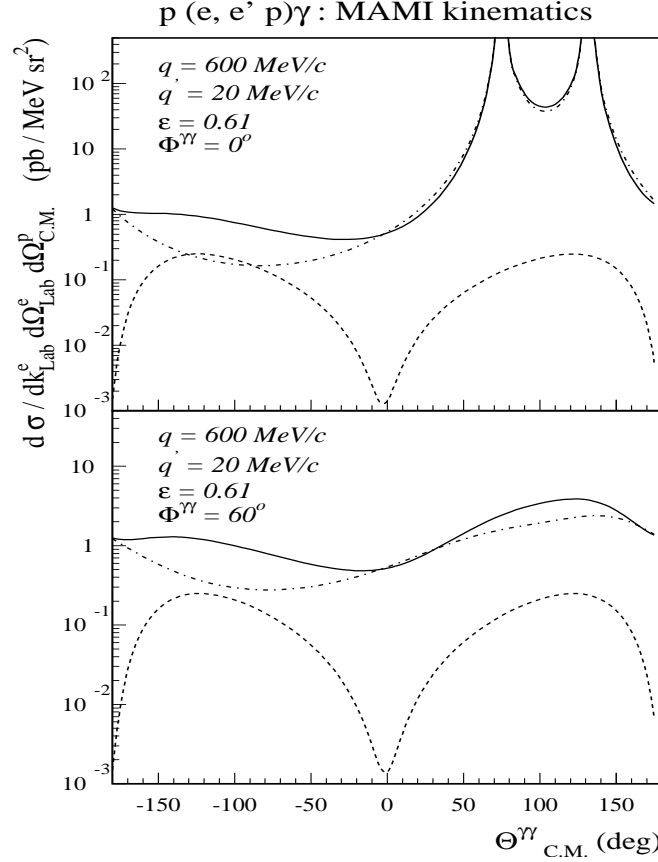


Figure 2: $p(e, e'\gamma)p$ differential cross section in MAMI kinematics : BH (dashed-dotted lines), Born (dashed lines) and BH + Born contributions (full lines) in plane ($\phi = 0^\circ$) and out-of-plane ($\phi = 60^\circ$).

The experimental strategy of VCS in the threshold region consists of two steps. One measures the VCS cross section at several values of the outgoing photon energy. At low outgoing photon energies, the measurement of the VCS observables provides a test of the LET as can be seen from Eqs.(92, 94). Once the LET is verified, the relative effect of the polarizabilities can be extracted using Eq.(97).

The predictions for the Bethe-Heitler (BH) and Born cross sections are shown in Fig.(2) for an outgoing photon of low energy. The BH cross section has a characteristic angular shape and displays two "spikes". These "spikes" occur when the direction of the outgoing photon coincides with either the initial or final electron directions. In these regions, the

cross section is completely dominated by the BH contributions. In order to measure the VCS contribution, one clearly has to detect the photon in the half-plane opposite to the electron directions where the BH contamination is the smallest.

The first absolute measurement of the VCS cross section on the nucleon performed at MAMI [d’Ho95] has shown that radiative corrections provide an important contribution to the $p(e, e'p)\gamma$ reaction. All diagrams that contribute to the cross section to order α_{em}^4 have been calculated in Ref.[Vdh98b]. A preliminary comparison to the MAMI data at low outgoing photon energy shows that the VCS cross section can be understood by the radiatively corrected Bethe-Heitler (BH) + Born processes [d’Ho97] which provides a test of the LET.

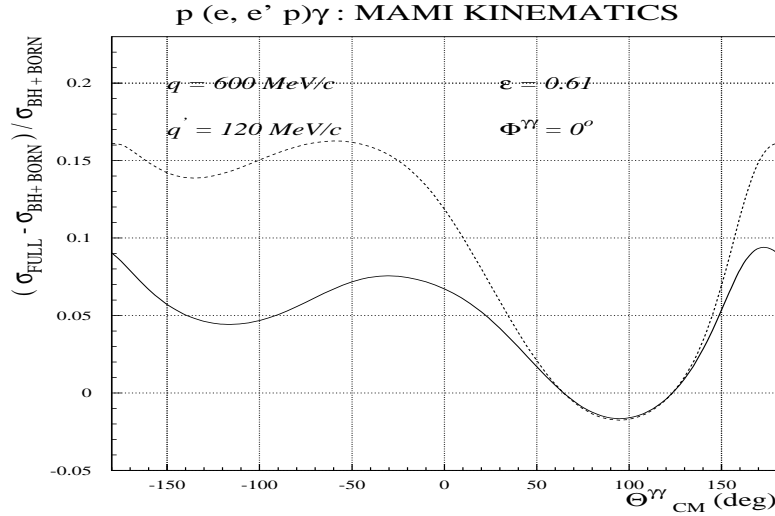


Figure 3: Relative nucleon structure effect in VCS in MAMI kinematics. σ_{FULL} represents the $p(e, e'p)\gamma$ differential cross section in the full model described in the text and $\sigma_{BH+BORN}$ represents the BH + Born contribution. The ratio calculated with all non-Born VCS diagrams is shown by the solid curve, whereas the ratio calculated with only the Δ diagram contribution to the non-Born VCS amplitude is shown by the dashed curve.

For the sake of providing estimates of the nucleon structure effect accessible through VCS, the relativistic effective Lagrangian model of Ref.[Vdh96] is used here as it takes into account the nucleon structure effects to all orders in the outgoing photon energy. In this model, the $p(e, e'p)\gamma$ reaction below pion production threshold is described in terms of BH, Born and non-Born diagrams. For the non-Born diagrams, a tree-level calculation was performed consisting of exchanges of the resonances in the s - and u -channel and the exchanges of the π^0 and σ in the t -channel. For the resonances, the most important contributions come from the $\Delta(1232)$ and $D_{13}(1520)$ for which the radiative couplings were taken from pion photo/electro production [Vdh95]. The model was tested against available data for real Compton scattering below pion threshold and yields for the proton polarizabilities at the photon point : $\alpha_G = 7.29 \cdot 10^{-4} fm^3$ and $\beta_G = 1.56 \cdot 10^{-4} fm^3$, which should be compared to the values extracted from experiment [MGi95] : $\alpha_G^{exp} = 12.1 \pm 0.8 \pm 0.5 \cdot 10^{-4} fm^3$

and $\beta_G^{exp} = 2.1 \pm 0.8 \pm 0.5 \cdot 10^{-4} fm^3$. The underestimation of α_G is probably due to the simplicity of the present tree-level effective Lagrangian model which does not include non-resonant πN intermediate states.

To see the magnitude of the non-Born contributions, we plot in Figs.(3) and (4) the BH+B+NB differential cross section (σ_{FULL}) relative to the BH+B differential cross section (σ_{BH+B}) for MAMI kinematics and for CEBAF kinematics respectively. In Figs.(3, 4), σ stands for the fivefold differential $p(e, e'p)\gamma$ cross section $d\sigma/(d\Omega_e')_{Lab} d|k'|_{Lab} (d\Omega_p')_{CM}$. The in-plane $p(e, e'p)\gamma$ differential cross section ratios are shown for a momentum of the outgoing real photon of $q' = 120$ MeV, which is close to but below the pion threshold. The MAMI experiment [d'Ho95] was performed for a virtual photon momentum $q = 600$ MeV and a value of the virtual photon polarization around $\varepsilon = 0.61$. In the MAMI kinematics, the non-Born contribution is a 10-15 % effect to the $p(e, e'p)\gamma$ reaction at backward angles (where the photon is emitted opposite to the electron directions).

The kinematics of the CEBAF experiment [Ber93], corresponds to a larger value of

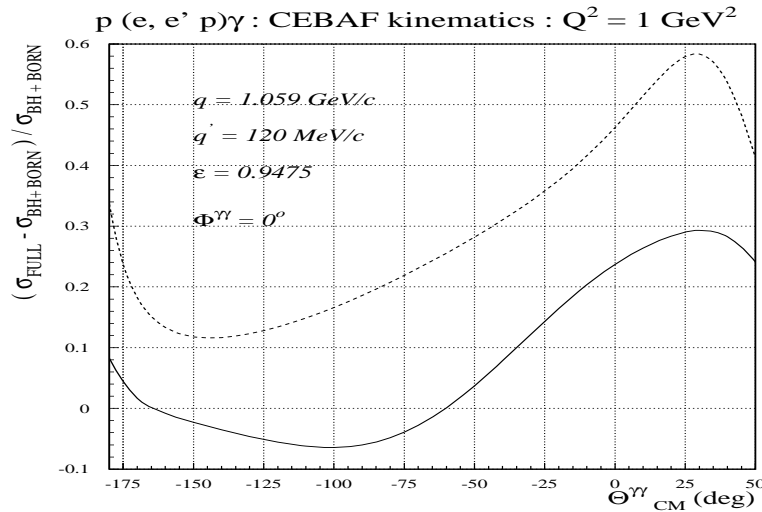


Figure 4: Same ratio and curve conventions as in Fig.(3) but for CEBAF kinematics.

$\epsilon \approx 0.95$ due to the higher beam energy. The correspondingly larger virtual photon flux factor which goes like $1/(1 - \epsilon)$ increases the VCS contribution relative to the BH cross section. Thus one expects a larger effect in CEBAF kinematics as is also seen from the model calculations on Fig.(4) which are performed at $q \approx 1.06$ GeV/c.

If one wants to extract the polarizabilities from experiment, we have seen that an unpolarized experiment is not sufficient as it gives access to only 3 independent response functions. To separate the polarizabilities, one has to resort to double polarization observables. Experimentally, at existing high duty cycle electron facilities with a polarized electron beam such as at MAMI, MIT-Bates and CEBAF, double polarization VCS experiments can be performed by measuring the recoil polarization of the outgoing nucleon with a focal plane polarimeter.

In Fig.(5) the double polarization asymmetry of Eq.(34), where the recoil proton po-

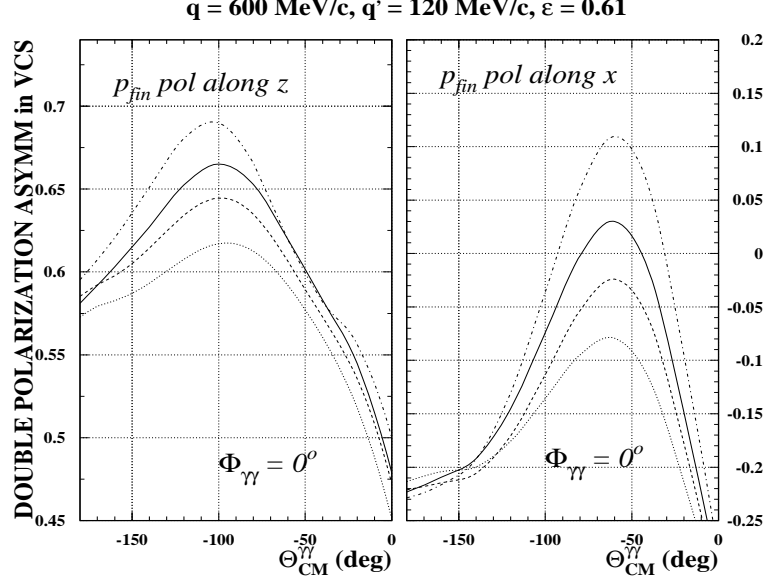


Figure 5: VCS double polarization asymmetry (polarized electron, recoil proton polarization along either the x - or z -directions) in MAMI kinematics ($Q^2 = 0.33 \text{ GeV}^2$) as function of the CM angle between real and virtual photon. The BH + Born contribution is shown by the dashed lines. The result of the BH + Born + Δ contribution is shown by the dotted lines, whereas the BH + Born + $D_{13} + \sigma$ contribution is shown by the dashed-dotted lines. The total effect in the model is shown by the full lines.

larization is measured either along the x - or z - directions, is shown at $q = 600 \text{ MeV}/c$ for in-plane kinematics. It is seen that the asymmetry where the final proton is polarized parallel to the virtual photon yields a large value (between 0.6 and 0.7). Remark that in Fig.(5), the electric and magnetic contributions in the present effective Lagrangian calculation yield large and opposite effects to the asymmetry.

4 THE HARD SCATTERING REGIME

4.1 Introduction

Here we come to the hard part of this review. The threshold regime presented in Section 3 and the deep VCS which is the subject of Section 5 are going well. In both cases the theoretical activity is important and while in the first case the experiments are running, in the second case they are already at the stage of experiment proposals. By an irony of history the threshold regime and the deep VCS should be considered as the wealthy descendants of the VCS in the hard scattering regime, a domain now somewhat sleeping. Though everybody agrees that this is a splendid physics case for VCS, it suffers from a severe drawback, namely the extreme difficulty of the experiments. It was the conclusion of the first feasibility study [Arv93] that no existing accelerator is adequate for such experiments. A new type of electron accelerator with a high energy (> 30 GeV), high duty factor ($\sim 100\%$), very good energy resolution (much better than the pion mass) and high intensity ($> 100\mu\text{A}$) is actually necessary. Unfortunately no decision about the ELFE project [Arv95], which meets with these requirements, is expected in the coming years. The consequence is that, despite its evident interest, the subject is in standby. In particular there is no motivation to develop the very complicated perturbative QCD calculations for this process.

However we want to hope that one day the field will have the opportunity to take off and the role of this review may be to prepare the way. We shall do it by first introducing the physics of the hard scattering regime. Then we shall use the diquark model to get realistic estimates of the cross sections. We shall see that, even though the energy of CEBAF is too low to achieve a fruitful VCS program in the hard scattering regime, some preliminary studies can be performed with the polarized beam. Finally we shall switch to the case of real Compton scattering. The first reason is that the physics, though less rich, is closely related to the VCS because the relevant energy scales are (s, t, u) and not Q^2 , which can be zero. The second reason is that the experimental prospects are better in this case [d'Ho96][D'An97].

4.2 Incoherence between the short and long-distance physics

This regime is defined by requiring that all three variables (s, t, u) be large with respect to a typical hadronic scale, say 1 GeV. In this case there is a prejudice (actually proved in the case of elastic electron scattering [Ste97]) that the amplitude factorizes in a soft non-perturbative part, the distribution amplitude, and a hard scattering kernel which is calculable from perturbative QCD. Because of asymptotic freedom, the perturbative approach must be to some degree relevant to the hard scattering regime. However, since the binding of the quarks and gluons in the hadrons is a long distance, non-perturbative effect, the description of the reaction requires a consistent analysis of both large and small scales. Here we follow the nice argument of Ref.[Ste97]. When the reaction is hard enough the relative velocities of the participating particles are nearly lightlike. Time dilatation increases the lifetime of the quantum configurations which build the hadron. So the partonic content, as seen by the other particles, is frozen. Moreover, due to the apparent contraction of the hadron size, the time during which momentum can be exchanged is decreased. Therefore one expects a lack of coherence between the long-distance confining effects and the short distance reaction. This incoherence between the soft and hard physics is the origin of the factorization which is illustrated on Fig.(6).

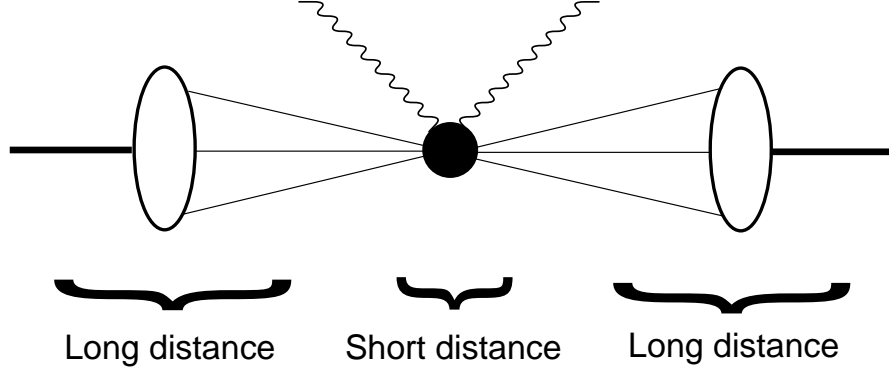


Figure 6: Factorization of the scattering amplitude in the hard scattering regime.

The calculation of the amplitude can be done using the Brodsky-Lepage formalism [Bro80] which leads to the factorized expression

$$T(\lambda', h'_N, \lambda, h_N) = \int dx_i dy_j \phi_N^*(y_j) T_H(\lambda', h'_N, y_j, \lambda, h_N, x_i; s, t) \phi_N(x_i), \quad (101)$$

where (x_i, y_i) are respectively the momentum fractions of the quarks in the initial and final nucleon, T_H is the hard scattering kernel and ϕ_N is the distribution amplitude (D.A.). The evaluation of Eq.(101) requires a four-fold convolution integral since there are two constraint equations ($x_1 + x_2 + x_3 = 1$ and $y_1 + y_2 + y_3 = 1$). In Eq.(101) a sufficiently large momentum transfer is assumed so as to neglect the transverse momentum dependence in the hard scattering amplitude T_H . In this limit, the integration over the transverse momenta $\vec{k}_{\perp i}$ (where $\sum_i \vec{k}_{\perp i} = \mathbf{0}$) acts only on the valence wavefunction

$$\Psi_V(x_1, x_2, x_3; \vec{k}_{\perp 1}, \vec{k}_{\perp 2}, \vec{k}_{\perp 3}), \quad (102)$$

which is the amplitude of the three quark state in the Fock expansion of the proton:

$$|P\rangle = \Psi_V |qqq\rangle + \Psi_{q\bar{q}} |qqq, q\bar{q}\rangle + \Psi_g |qqq, g\rangle + \dots \quad (103)$$

This valence wavefunction Ψ_V integrated up to a scale μ (which separates the soft and hard parts of the wavefunction) defines the D.A. which appears in Eq.(101) :

$$\phi_N(x_i, \mu) = \int^\mu d^2 \vec{k}_{\perp i} \Psi_V(x_i; \vec{k}_{\perp i}). \quad (104)$$

For μ much larger than the average value of the transverse momentum in the proton, this function ϕ_N depends only weakly on μ [Bro80] and this dependence can be neglected.

The interest of the formalism is that the distribution amplitude is universal, that is independent of the particular reaction considered. Several distribution amplitudes have been modeled using QCD sum rules [Che84][Che89][Kin87]. They have a characteristic shape and predict that in a proton, the u -quark with helicity along the proton helicity carries about 2/3 of its longitudinal momentum (see Fig.(7)).

For the computation of the hard scattering amplitude T_H , the leading order PQCD contribution corresponds to the exchange of the minimum number of gluons (in the present case two) between the three quarks as shown on Fig.(8). The number of diagrams grows rapidly with the number of elementary particles involved in the reaction (42 diagrams for the nucleon form factor, 336 diagrams in the case of real or virtual Compton scattering). Despite the large number of diagrams, the calculation of T_H is a parameter free calculation once the scale $\Lambda_{QCD} \approx 200 \text{ MeV}$ in $\alpha_s(Q^2)$ is given. Note that configurations with more than three valence quarks are a priori allowed but since this implies to exchange more hard gluons the corresponding contribution is suppressed by powers of $1/t$.

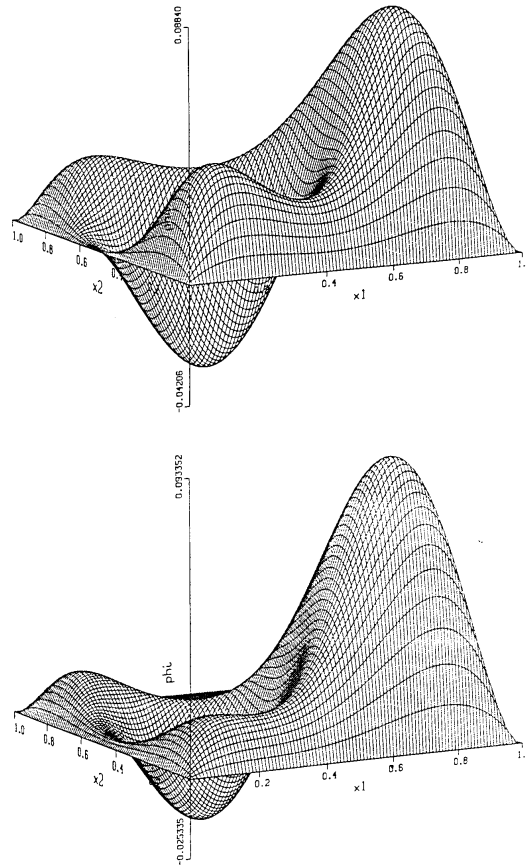


Figure 7: Model distribution amplitudes for the nucleon : KS (upper figure) and COZ (lower figure), as function of the valence quark momentum fractions x_1 and x_2 ($x_1 + x_2 + x_3 = 1$).

There are two characteristic features of the Brodsky-Lepage model which are almost direct consequences of QCD: the dimensional counting rules [Bro73] and the conservation of hadronic helicities [Bro81]. The latter feature implies that any helicity flip amplitude is zero

and, hence, any single spin asymmetry too. The helicity sum rule is a consequence of utilizing the collinear approximation and of dealing with (almost) massless quarks which conserve their helicities when interacting with gluons. Whereas the dimensional counting rules are in reasonable agreement with experiment, the helicity sum rule seems to be violated even at moderately large momentum transfers. The prevailing opinion is that these phenomena cannot be explained in terms of perturbative QCD (see, for example, Ref. [Siv89]), rather they are generated by an interplay of perturbative and non-perturbative physics.

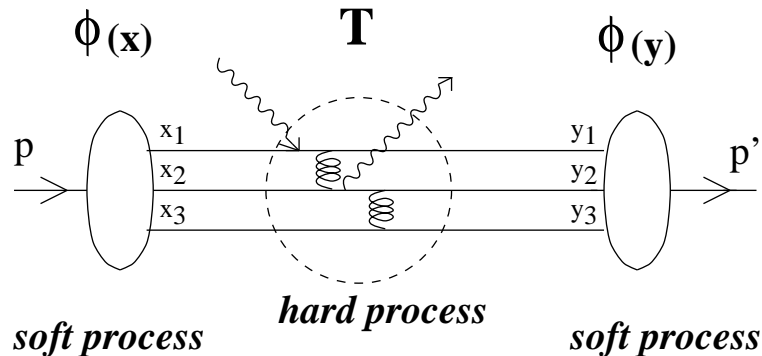


Figure 8: The hard scattering kernel in leading order PQCD.

An interesting aspect of real and virtual Compton scattering is that they are the simplest processes in which the integrals over the longitudinal momentum fractions yield imaginary parts. The reason is that, as in any scattering process, there are kinematical regions where internal quarks and gluons can go on their mass shell. The appearance of imaginary parts to leading order in α_s is a non-trivial prediction of PQCD which should be tested experimentally. As explained below, the $(e, e'\gamma)$ reaction with polarized incoming electrons seems to be a good candidate for this investigation.

4.3 The diquark model

The only calculation [Far90a] of VCS in the Brodsky-Lepage formalism is unfortunately not reliable due to a treatment of the singularities which leads to inaccurate results. This is discussed in details in Section 4.4. To get realistic predictions and to delineate what would be the most interesting VCS experiments we rely on the diquark model calculation of Ref.[Kro96]. Due to the (relative) simplicity of this model it has been possible to analytically integrate the singularities, which eliminates the problems encountered in Ref. [Far90a].

In the diquark model [Ans87] baryons are viewed as made up of quarks and diquarks, the latter being treated as quasi-elementary constituents which partly survive medium hard collisions. The composite nature of the diquarks is taken into account by diquark form factors. Diquarks are an effective description of correlations in the wave functions and constitute a particular model for non-perturbative effects. The diquark model has been applied to a variety of processes and successfully confronted to data. Among these applications is a study of the nucleon's electromagnetic form factors [Jak93]. In fact, predictions are achieved for both the magnetic and the electric form factors. For the latter quantity no result is obtained in the pure quark hard scattering model because it requires helicity flips of the nucleon and,

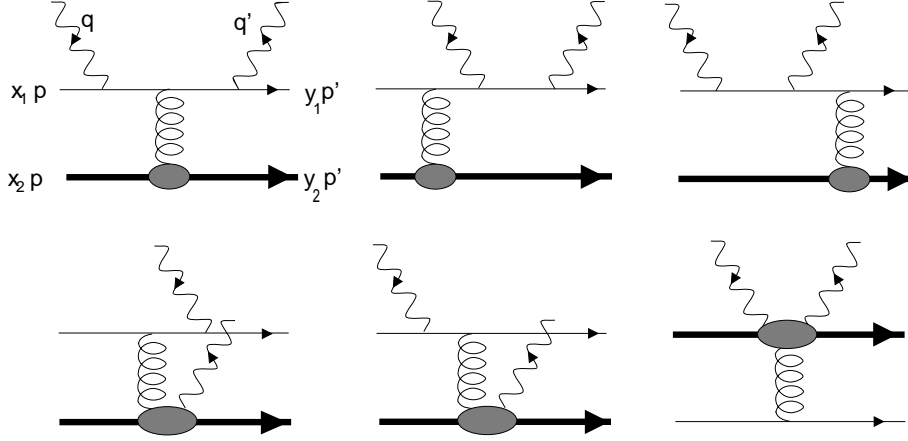


Figure 9: Feynman graphs contributing to the VCS process $\gamma^* p \rightarrow \gamma p$. Graphs with the two photons interchanged are not shown, and the thick line represents a diquark.

in so far, the electric form factor also represents a polarization effect. In the diquark model helicity flips are generated through spin 1 diquarks. The diquark model is designed in such a way that it turns into the theoretically well established pure quark picture asymptotically. So the pure quark picture of Brodsky-Lepage and the diquark model do not oppose each other, they are not alternatives but rather complements.

Representative Feynman graphs contributing to the gauge invariant hard-scattering amplitudes are displayed in Fig.(9). The blobs appearing at the gD , γgD and $\gamma\gamma D$ vertices symbolize three-, four- and five-point functions. These n-point functions are evaluated for point-like diquarks and the results are multiplied with phenomenological vertex form factors which take into account the composite nature of the diquarks. The perturbative part of the model, i.e. the coupling of gluons (and photons) to diquarks follows standard prescriptions. The results for VCS shown below have been obtained with the same diquark parameters taken from previous applications of the diquark model [Kro96].

The first point to consider is the relative strength of the VCS and BH processes. A strong interference between them, though not uninteresting by itself, would obscure the interpretation of the results because it would prevent the familiar analysis in terms of the virtual photon cross sections defined in Eq.(36). For that purpose we plot in Fig.(10) the difference between the full $ep \rightarrow ep\gamma$ cross section and the VCS contribution to it divided by the full cross section. This represents the BH contamination. Clearly the dominance of the VCS contribution requires a high energy and requires to detect the outgoing photon in the half-plane opposite to the electron directions ($\phi = 180^\circ$).

The Q^2 dependence of the cross sections is obviously the new information we can get from VCS by comparison with the real Compton scattering. In Fig.(11) the Q^2 dependence of the VCS cross sections is shown in a hard scattering situation ($s = 10 \text{ GeV}^2$, $\cos\theta = \pm 0.6$). The transition from real Compton scattering to large Q^2 as predicted by the diquark model, is obviously non-trivial. In particular one observes that in the forward direction

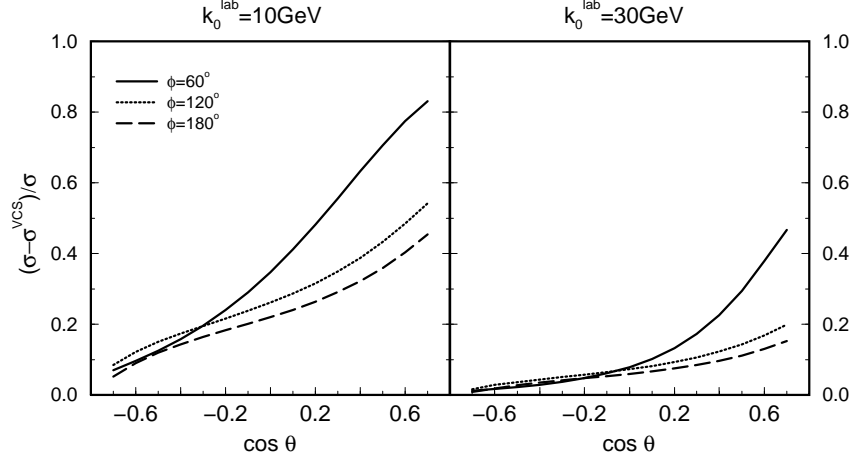


Figure 10: The difference between the full photon electroproduction cross section and the VCS contribution to it over the full cross section vs. $\cos \theta$ for $Q^2 = 1 \text{ GeV}^2$, $s = 10 \text{ GeV}^2$, two values of the beam energy k_{0L} , and for several values of the azimuthal angle ϕ .

($\cos \theta = 0.6$), the variation is smooth, compatible with the diquark form factor. In the backward region ($\cos \theta = -0.6$) there is a rapid variation at small Q^2 and the slope seems to be related to the scale of the diquark mass. So by studying the Q^2 variation as a function of the angle, one can observe the interplay of the two characteristic scales of the model.

The (L , LT , TT) cross sections have relative sizes with respect to the dominant transverse cross section which are not negligible and their Q^2 dependence seems to merit a thorough investigation. However one must keep an eye on the very small value of the cross sections. Without a dedicated accelerator nobody will have the opportunity to contemplate the actual curves. Remark that at the real photon point, the diquark calculations predict a very small (non-zero) value for the photon asymmetry (TT/T) over most of the angular range which should be compared with the PQCD prediction shown in the next section.

By contrast to the above comments where the BH is considered as a nuisance, the regions of strong BH contaminations offer an interesting possibility to measure the phases of the VCS amplitudes. These phases, due to the possible poles of the quarks, diquarks or gluon propagators, induce in the (e , $e'\gamma$) amplitudes non-trivial phases beyond the phases due to the azimuthal angle dependence (see Eq. (20)). In other words, the perturbative phases manifest themselves in the fact that the T matrix is not self-adjoint. For the BH process on the other hand, $T = T^\dagger$ obviously holds. As shown in [Kro96], information on the absorptive part $T - T^\dagger$ can be obtained from the electron single spin asymmetry. Since at CEBAF the electron beam is polarized a measurement of the asymmetry seems feasible. It is important to note that this possibility of measuring the absorptive part of the T matrix by the electron asymmetry follows from parity and time reversal invariance and does not rely on any model hypothesis.

As is well known, a one-particle helicity state transforms under the combined parity and time reversal operation as

$$|\vec{k}, \lambda\rangle \longrightarrow \eta(\lambda)|\vec{k}, -\lambda\rangle, \quad (105)$$

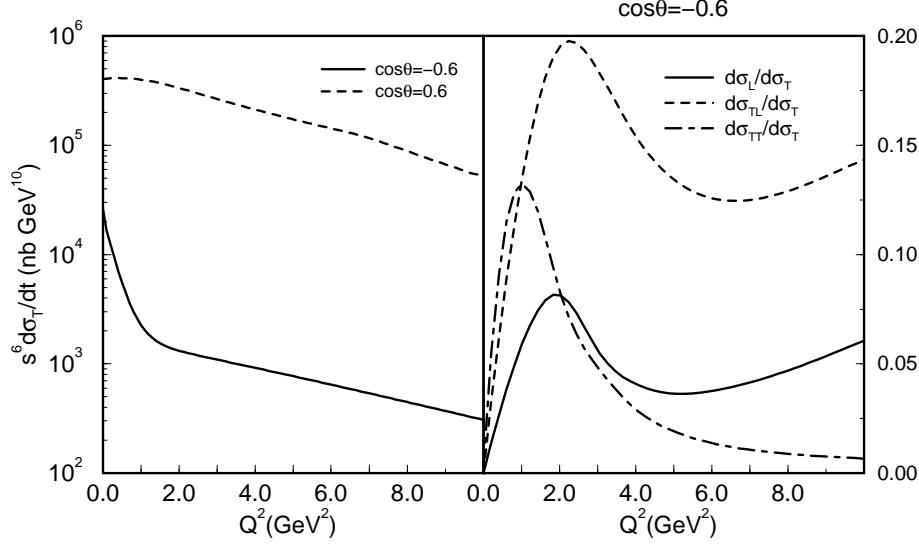


Figure 11: The cross section for virtual Compton scattering vs. Q^2 at $s = 10 \text{ GeV}^2$.

where $\eta(\lambda)$ is ± 1 depending on λ , the spin of the particle and on its internal parity. So the combined parity and time reversal operations transform a given helicity state into a state with the same momentum but with reversed helicity. If the interaction is invariant under the parity and time reversal operations, the T -matrix elements for, say, a $2 \rightarrow 3$ process satisfy the relation

$$\begin{aligned} & \langle \vec{k}'_1, \lambda'_1; \vec{k}'_2, \lambda'_2; \vec{k}'_3, \lambda'_3 | T | \vec{k}_1, \lambda_1; \vec{k}_2, \lambda_2 \rangle \\ &= \left(\prod_i \eta_i \right) \langle \vec{k}'_1, -\lambda'_1; \vec{k}'_2, -\lambda'_2; \vec{k}'_3, -\lambda'_3 | T^\dagger | \vec{k}_1, -\lambda_1; \vec{k}_2, -\lambda_2 \rangle^* . \end{aligned} \quad (106)$$

Let us now assume that particle 1 is a spin 1/2 one, say an electron and note $\sigma(\pm)$ is the differential cross section for photon electroproduction with specified helicity of the incoming electron. Then, ignoring all kinematical variables, the cross section with particle 1 in a definite helicity state is

$$\sigma(\pm) = \sum_{\{\lambda_i, \lambda'_i\}} |T^{e, e' \gamma}(\lambda'_1, \lambda'_2, \lambda'_3; \pm, \lambda_2)|^2. \quad (107)$$

The difference of these cross sections $\Delta\sigma = \sigma(+)-\sigma(-)$ may be written as

$$\begin{aligned} \Delta\sigma = \Re e \sum_{\{\lambda_i, \lambda'_i\}} & [T^{e, e' \gamma}(\lambda'_1, \lambda'_2, \lambda'_3; +, \lambda_2) + \prod_i \eta_i T^{e, e' \gamma}(-\lambda'_1, -\lambda'_2, -\lambda'_3; -, -\lambda_2)^*] \\ & \times [T^{e, e' \gamma}(\lambda'_1, \lambda'_2, \lambda'_3; +, \lambda_2)^* - \prod_i \eta_i T^{e, e' \gamma}(-\lambda'_1, -\lambda'_2, -\lambda'_3; -, -\lambda_2)]. \end{aligned} \quad (108)$$

If there would be no absorptive part of T , i. e., $T = T^\dagger$, then, according to Eq.(106), the difference of the two helicity cross sections and hence the electron asymmetry would be zero.

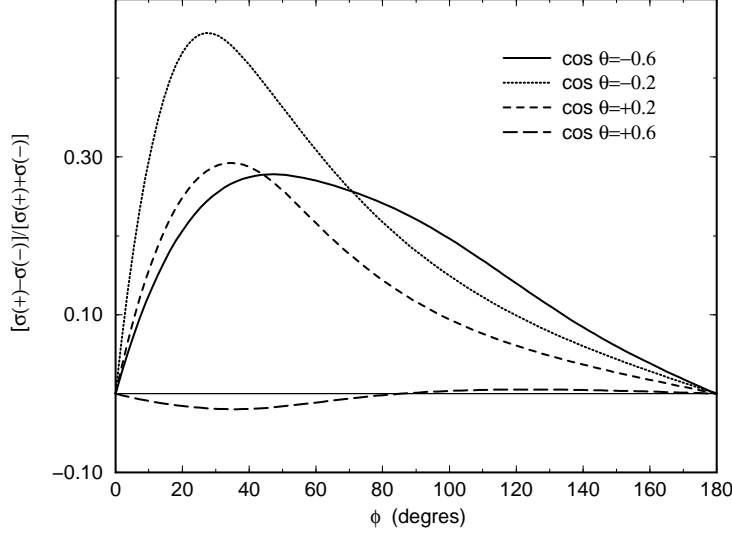


Figure 12: The electron asymmetry at CEBAF (6 GeV) as function of ϕ for several values of $\cos \theta$ for $s = 5 \text{ GeV}^2$ and $Q^2 = 1 \text{ GeV}^2$.

Therefore, the asymmetry measures the non-trivial phase as stated above. If we consider only the VCS contribution, we find (dropping irrelevant kinematical factors)

$$\Delta\sigma \simeq \sin \phi \Im m [\Phi_9^* (\Phi_1 - \Phi_7) + \Phi_{10}^* (\Phi_2 + \Phi_8) + \Phi_{11}^* (\Phi_3 - \Phi_5) + \Phi_{12}^* (\Phi_4 + \Phi_6)] \quad (109)$$

Thus, we see that in this case $\Delta\sigma$ measures the imaginary part of the longitudinal-transverse interference term whereas σ_{LT} measures its real part. In other words, $\Delta\sigma$ measures the relative phase between the longitudinal and transverse VCS helicity amplitudes.

It turns out that the diquark model predicts very small values for $\Delta\sigma$ in the pure VCS case. The ultimate reason is that the longitudinal helicity amplitudes are much smaller than the transverse ones for VCS as illustrated on Fig.(11).

However $\Delta\sigma$ can be strongly enhanced by the interference with the BH process. In the regions of strong BH contaminations it then essentially measures the relative phase between the transverse VCS amplitudes and the BH amplitudes. This enhancement can be seen on Fig.(12) where we show the electron asymmetry for a kinematical situation accessible in the future at CEBAF ($s = 5 \text{ GeV}^2$, $k_{0L} = 6 \text{ GeV}$, $Q^2 = 1 \text{ GeV}^2$). As can be seen from that figure, the asymmetry is large in the diquark model for small values of $|\cos \theta|$ ($\simeq 0.2$) and values of the azimuthal angle around 30° . The magnitude of the effect is of course sensitive to details of the model and, therefore, should not be taken literally. However, this suggests that preliminary tests of the theoretical predictions can be made with the low energy polarized beam of CEBAF even though the cross section is in this case dominated by the BH process.

4.4 Compton scattering in PQCD

The VCS estimates in the diquark model make clear that a measurement of VCS at high energy and large angle will be very difficult and will require a dedicated accelerator even

for moderate values of Q^2 ($\sim 1 \text{ GeV}^2$). At these rather low values of Q^2 , the cross section is dominated by its transverse part. Therefore, it is natural to consider real Compton scattering at high energy and large angle to study the hard scattering. From the experimental point of view, there are much better hopes to realize a real Compton scattering experiment. Firstly, the count rates are much higher than for electroproduction. Also, the required high intensity, high energy ($E_\gamma \sim 10 - 15 \text{ GeV}$) real photon beam might be feasible at the existing HERA ring [d’Ho96][D’An97]. This motivated us [Vdh97b] to perform a leading order PQCD calculation for real Compton scattering.

In a first stage, we simplified the calculations by approximating the x, y dependence in the gluon virtuality Q^2 in $\alpha_s(Q^2)$ by their average values for a given distribution amplitude. In this way we also avoid large contributions in the end-point region ($x_i \approx 0, x_i \approx 1$) where the asymptotic formula for $\alpha_s(Q^2)$ is no longer valid.

Once the hard scattering amplitude T_H is evaluated, the four-fold convolution integral of Eq.(101) has to be performed to obtain the Compton helicity amplitudes. The numerical integration requires some care because the quark and/or gluon propagators can go on-shell which leads to (integrable) singularities. The different numerical implementations of these singularities are probably at the origin of the different results obtained in two previous calculations [Far90a][Kro91]. In Refs.[Far90a][Far90b], the propagator singularities were integrated by taking a finite value for the imaginary part $+i\epsilon$ of the propagator. Then the behaviour of the result was studied by decreasing the value of ϵ . To obtain convergence with a practical number of samples in the Monte Carlo integration performed in Refs.[Far90a][Far90b], the smallest feasible value for ϵ was $\epsilon \approx 0.005$. In Ref.[Kro91] the propagator singularities were integrated by decomposing the propagators into a principal value (off-shell) part and an on-shell part. To compare these methods, we implemented both of them and found for the $+i\epsilon$ method differences of the order of 10% for every diagram as compared with the result of our final method. It is not surprising that, when summing hundreds of diagrams, an error of 10% on every diagram can easily be amplified due to the interference between the diagrams. To have confidence in the evaluation of the convolution of Eq.(101), we compared the principal value integration method with a third independent method. This third method starts from the observation that the diagrams can be classified into four categories depending upon the number of propagators which can develop singularities : in the present case this number is 0, 1, 2 or 3. Besides the trivial case of zero singularities which can be integrated immediately, the diagrams with one or two propagator singularities can be integrated by performing a contour integration in the complex plane for one of the four integrations. For the most difficult case of three propagator singularities, we found it possible to evaluate it by performing two contour integrations in the complex plane. In doing so, one achieves quite a fast convergence because the integrations along the real axis are replaced by integrations along semi-circles in the complex plane which are far from the propagator poles. We checked this method by also implementing the principal value integration method and found the same result up to 0.1% for each type of singularity. The principal value method was found to converge much slower and is more complicated to implement especially for the case with three singularities due to the fact that the three principal value integrals are coupled.

Having exposed the PQCD calculational framework for Compton scattering, we now come to the calculations which are performed with several model distribution amplitudes denoted as CZ [Che84], COZ [Che89] and KS [Kin87].

The highest energy data which exist for real Compton scattering were taken around

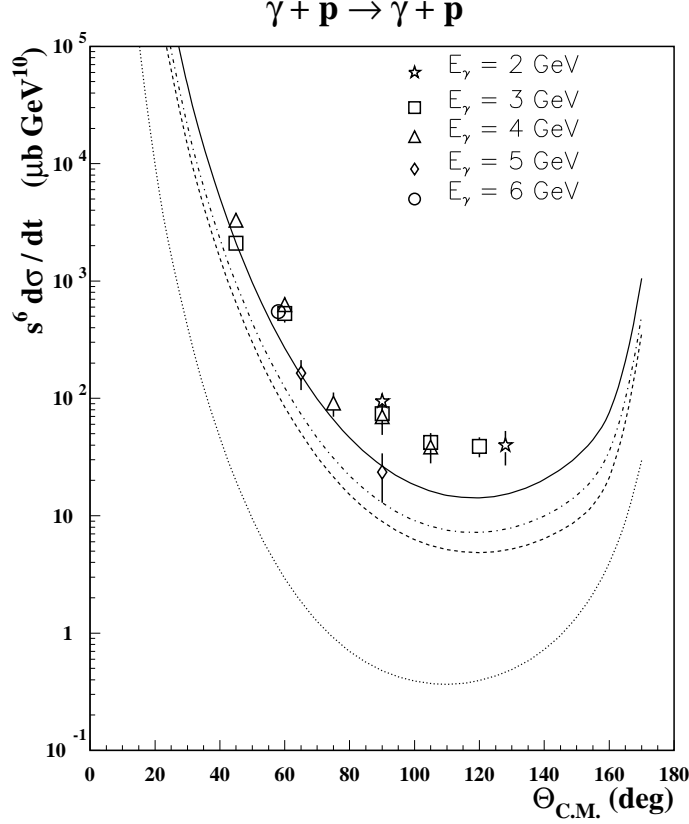


Figure 13: Unpolarized Compton cross section on the proton for different nucleon D.A. : KS (full line), COZ (dashed-dotted line), CZ (dashed line) and asymptotic D.A. (dotted line). Data are from Refs.[Deu73][Dud83][Shu79].

5 GeV and are shown in Fig.(13). Although the energy at which these experiments were performed is probably too low to justify a PQCD calculation, we nevertheless show the comparison with these existing data for illustrative purposes.

Let us first mention that the hard scattering amplitude has the s -dependence ($T \sim s^{-2}$) which leads to the QCD scaling laws [Bro73], that is $\frac{d\sigma}{dt} \sim s^{-6}$ for Compton scattering or VCS.

The unpolarized real Compton differential cross section (multiplied by the scaling factor s^6) is shown as function of the photon C.M. angle. We first remark that the result with the asymptotic D.A. ($\sim 120 x_1 x_2 x_3$) is more than one decade below the results obtained with the QCD sum rules motivated amplitudes KS, COZ, CZ. The results with KS, COZ and CZ show a similar characteristic angular dependence which is asymmetric around 90° . Note that in the forward and backward directions, which are dominated by diffractive mechanisms, a PQCD calculation is not reliable. Comparing the results obtained with KS, COZ and CZ, one notices that although these distribution amplitudes have nearly the same lowest

moments, they lead to differences of a factor of two in the Compton scattering cross section. Consequently, this observable is sensitive enough to distinguish between various distribution amplitudes.

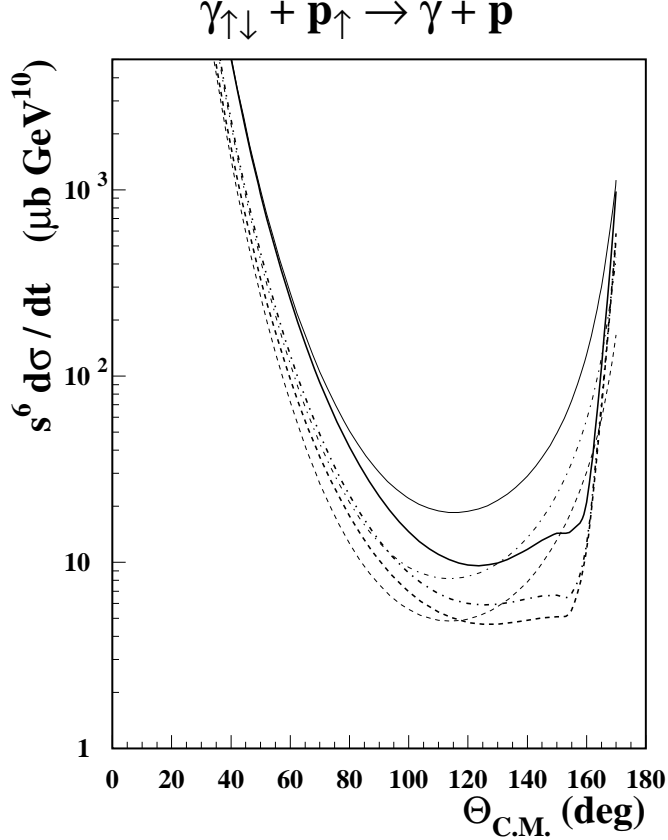


Figure 14: Calculations for the polarized Compton cross section for two helicity states of the photon : $\lambda = +1$ (thick lines), $\lambda' = -1$ (thin lines). Results are shown with KS (full lines), COZ (dashed-dotted lines), CZ (dashed lines).

In Fig.(14), we show the polarized Compton cross sections for the two helicity states of the photon and for a target proton with positive helicity. We remark that for all three D.A. there is a marked difference both in magnitude and angular dependence between the cross sections for the two photon helicities. Consequently, the resulting photon asymmetry Σ defined as

$$\Sigma_{\uparrow} = \frac{\frac{d\sigma}{dt}(\uparrow, \lambda = 1) - \frac{d\sigma}{dt}(\uparrow, \lambda = -1)}{\frac{d\sigma}{dt}(\uparrow, \lambda = 1) + \frac{d\sigma}{dt}(\uparrow, \lambda = -1)}, \quad (110)$$

where λ is the helicity of the incoming photon and where \uparrow means a positive helicity for the hadron, changes sign for different values of θ_{CM} as shown in Fig.(15). This suggests

that the photon asymmetry might be a useful observable to distinguish between nucleon distribution amplitudes.

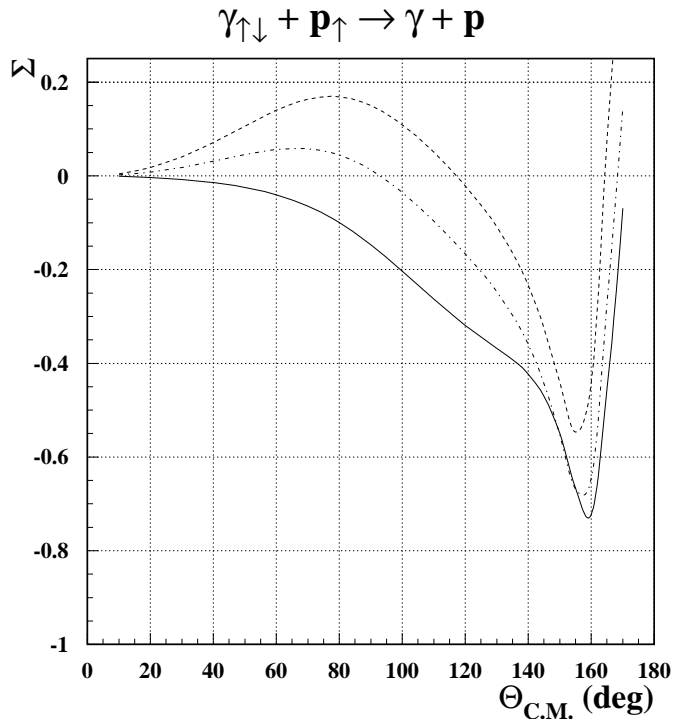


Figure 15: Calculations of the photon asymmetry for Compton scattering. Results are shown with KS (full lines), COZ (dashed-dotted lines) and CZ (dashed lines) D.A.'s.

The predicted sensitivity of the asymmetry to the nucleon D.A. can be used in the extraction of a D.A. from Compton scattering data in the scaling region. In Ref.[Vdh97b] we have outlined a procedure to extract a D.A. from Compton data in a model independent way by expanding the D.A. first in a set of basis functions and then using the angular informations of the cross sections to fit the expansion coefficients. It was seen that the precision on these coefficients is greatly improved when one measures both unpolarized cross sections and photon asymmetries. Such an experiment might be feasible at the HERA ring in the foreseeable future and might open up prospects to study the nucleon valence wave function in a direct way.

5 DEEPLY VIRTUAL COMPTON SCATTERING

5.1 Introduction

Deep-inelastic lepton scattering (DIS) in the Bjorken regime ($Q^2 \rightarrow \infty$ and $x_B = Q^2/2p \cdot q$ finite) is a powerful tool for the study of nucleon structure [Ste95]. In particular, polarized DIS experiments have revealed that only about 23% of the nucleon spin is carried by the quarks [Sti96]. This has stimulated new investigations to understand the nucleon spin. Exclusive virtual Compton scattering in the Bjorken regime (DVCS) has been proposed recently [Ji97a][Ji97b][Rad96a] to access a new type of parton distributions, referred to as *off-forward parton distributions* (OFPD's) which are generalizations of the parton distributions measured in DIS. Their first moments link them to the nucleon elastic form factors and it has been shown [Ji97a] that their second moment gives access to the contribution of the quark spin and quark orbital angular momentum to the nucleon spin.

The off-forward or off-diagonal correlations of quark operators in the proton have a long history (see e.g. [Dit88][Bal88][Jai93] and references therein). They appear in the recent literature also under the name of *nonforward parton distributions* or *double parton distributions* [Rad97]. Despite their different names and definitions, the generalized parton distributions have in common that they include the additional degrees of freedom brought in by their non forward nature.

It has been proposed that these OFPD's can also be accessed through the hard exclusive electroproduction of mesons (π^0, ρ^0, \dots) for which a QCD factorization proof was given recently [Col97]. This factorization is illustrated in Fig.(16b) and is valid for the leading power in Q and all logarithms. Furthermore, it is valid for all x_B and thus generalizes previous results [Rys93][Bro94][Rad96b]. According to Ref.[Col97], the factorization between hard and soft processes applies when the virtual photon is *longitudinally* polarized because in this case the end-point contributions in the meson wavefunction are power suppressed.

In two very recent independent works [Col98][Ji98], it has been shown that factorization also holds for the DVCS amplitude in QCD, up to power suppressed terms, to all orders in perturbation theory. It has furthermore been shown in these works that the factorization remains valid independent of the virtuality of the final photon, so that it also applies to the production of a real photon.

In Ref.[Vdh98a], the leading order of the γ, π^0 and ρ_L^0 ⁶ leptonproduction amplitudes were calculated and first estimates for the cross sections were given using an educated guess for the OFPD's. These three reactions are highly complementary because apart from isospin factors, they depend on the same OFPD's. In the following, we present in more detail the γ, π^0 and ρ_L^0 amplitudes at the leading order in PQCD. We then explore the experimental opportunities which may allow to determine the OFPD's.

⁶the index L means longitudinally polarized ρ^0

5.2 Light cone dominance of the amplitude in the Bjorken limit and definition of off-forward parton distributions

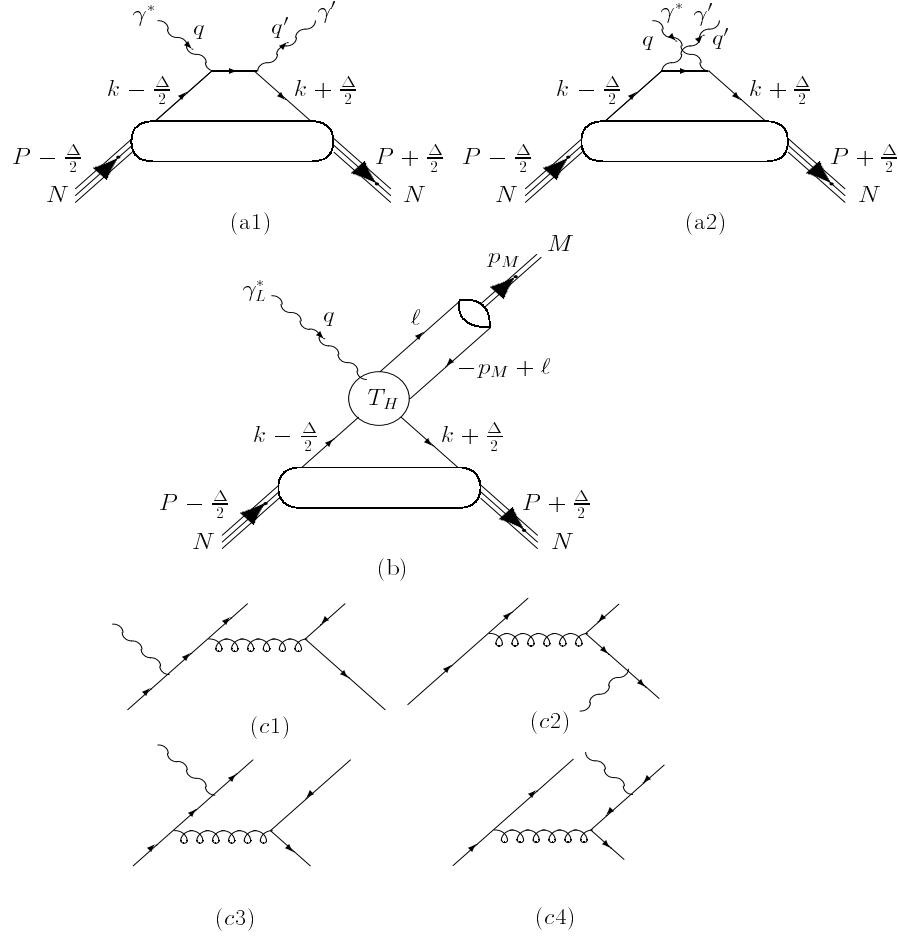


Figure 16: Direct (a1) and crossed (a2) handbag diagrams for DVCS; (b) diagram for the factorized meson electroproduction amplitude; (c) leading order diagrams for the hard scattering part T_H of the meson electroproduction amplitude.

The leading twist contribution to the DVCS amplitude in the forward direction is given [Ji97b] by the handbag diagrams shown in Figs.(16)(a1, a2). To calculate the corresponding amplitudes, it is convenient to use a frame where the virtual photon momentum q^μ and the average nucleon momentum P^μ (see Fig.(16) for the kinematics) are collinear and along the z -axis. Furthermore, in the Bjorken regime it is natural to express the momenta in terms

of the lightlike vectors

$$\tilde{p}^\mu = \frac{P^+}{\sqrt{2}}(1, 0, 0, 1), \quad n^\mu = \frac{1}{P^+\sqrt{2}}(1, 0, 0, -1), \quad (111)$$

where the light-cone components a^\pm are defined by $a^\pm \equiv 1/\sqrt{2}(a^0 \pm a^3)$. The physical momenta have the following decomposition :

$$P^\mu = \tilde{p}^\mu + \frac{\bar{m}^2}{2} n^\mu, \quad q^\mu = -2\xi' \tilde{p}^\mu + \frac{Q^2}{4\xi'} n^\mu, \quad (112)$$

$$\Delta^\mu \equiv p'^\mu - p^\mu = -2\xi \tilde{p}^\mu + \xi \bar{m}^2 n^\mu + \Delta_\perp^\mu, \quad (113)$$

where the variables \bar{m}^2 , ξ' and ξ are given by

$$\begin{aligned} \bar{m}^2 &= m^2 - \frac{\Delta^2}{4}, \\ 2\xi' &= \frac{P \cdot q}{\bar{m}^2} \left[-1 + \sqrt{1 + \frac{Q^2 \bar{m}^2}{(P \cdot q)^2}} \right] \xrightarrow{Bj} \frac{x_B}{1 - \frac{x_B}{2}}, \\ 2\xi &= 2\xi' \frac{Q^2 - \Delta^2}{Q^2 + \bar{m}^2 (2\xi')^2} \xrightarrow{Bj} \frac{x_B}{1 - \frac{x_B}{2}}. \end{aligned} \quad (114)$$

Remark that for a fast moving proton along the positive z-axis (such as e.g. is the case in an infinite momentum frame) the P^+ component will be very large whereas the P^- component will be negligible. For DVCS, the outgoing photon momentum is

$$q'^\mu \equiv q^\mu - \Delta^\mu = -2(\xi' - \xi) \tilde{p}^\mu + \left(\frac{Q^2}{4\xi'} - \xi \bar{m}^2 \right) n^\mu - \Delta_\perp^\mu. \quad (115)$$

In the Bjorken limit, the q^- component of the virtual photon momentum is of order Q^2 whereas the component q^+ is of order 1. Therefore, the operator product in the VCS tensor of Eq.(19) is dominated, as in DIS, by free quark currents separated by a lightlike distance. This is due on the one hand to the dominance of the 4-fold integral in Eq.(19) by the region $y^+ \sim 1/|q^-|$ and on the other hand to causality which forces $y^2 > 0$ [Ell77]. So, in the Bjorken regime Eq.(19) reduces to a one dimensional integral along a lightlike line. DVCS and hard electroproduction of mesons in the Bjorken regime will therefore select the leading twist part of the matrix element of the bilocal quark operator represented by the lower blob in Fig.(16)

$$\begin{aligned} & \frac{P^+}{2\pi} \int dy^- e^{ixP^+y^-} \langle p' | \bar{\psi}_\beta(-\frac{y}{2}) \psi_\alpha(\frac{y}{2}) | p \rangle \Big|_{y^+=\vec{y}_\perp=0} \\ &= \frac{1}{4} \left\{ (\gamma^-)_{\alpha\beta} \left[H^q(x, \xi, t) \bar{u}(p') \gamma^+ u(p) + E^q(x, \xi, t) \bar{u}(p') i\sigma^{+\kappa} \frac{\Delta_\kappa}{2m} u(p) \right] \right. \\ & \quad \left. + (\gamma_5 \gamma^-)_{\alpha\beta} \left[\tilde{H}^q(x, \xi, t) \bar{u}(p') \gamma^+ \gamma_5 u(p) + \tilde{E}^q(x, \xi, t) \bar{u}(p') \gamma_5 \frac{\Delta^+}{2m} u(p) \right] \right\}, \quad (116) \end{aligned}$$

where ψ is the quark field and u the nucleon spinor. In writing down the matrix element Eq.(116) we are implicitly working in the light-cone gauge $n \cdot A = 0$ for the gluon field A . If one works in a covariant gauge, one has to add a gauge link between the quark fields.

The leading twist matrix element of Eq.(116) is parametrized in terms of four OFPD's $H^q, E^q, \tilde{H}^q, \tilde{E}^q$. These OFPD's are defined for each quark flavor ($q = u, d$ and s) and depend upon the variables x, ξ and t . The light-cone momentum fraction x is defined by $k^+ = xP^+$ and $t = \Delta^2$. The support in x of the OFPD's is $[-1, 1]$ and a negative momentum fraction corresponds to the antiquark contribution. Note that in writing down Eq.(116), we have taken $\xi' = \xi$ to simplify the presentation. As shown in Eqs.(114), these two variables have the same value in the Bjorken limit. From Eq.(113) one realizes that ξ is the longitudinal momentum transfer. As the longitudinal momentum fractions of the nucleons cannot be negative, ξ is bounded by

$$0 < \xi < \frac{\sqrt{-\Delta^2}/2}{\bar{m}} < 1. \quad (117)$$

A glance at Figs.(16a, b) shows that the active quark with momentum $k - \Delta/2$ has longitudinal (+ component) momentum fraction $x + \xi$, whereas the one with momentum $k + \Delta/2$ has longitudinal momentum fraction $x - \xi$. As negative momentum fractions correspond to antiquarks, one can identify two regions according to whether $|x| > \xi$ or $|x| < \xi$. When $x > \xi$, both quark propagators represent quarks, whereas for $x < -\xi$ both represent antiquarks. In these regions, the OFPD's are the generalizations of the usual parton distributions from DIS. Actually, in the forward direction, the OFPD's H and \tilde{H} respectively reduce to the quark density distribution $q(x)$ and quark helicity distribution $\Delta q(x)$:

$$H^q(x, \xi = 0, t = 0) = q(x), \quad (118)$$

$$\tilde{H}^q(x, \xi = 0, t = 0) = \Delta q(x), \quad (119)$$

where q and Δq are defined as [Jaf96]

$$q(x) = \frac{p^+}{2\pi} \int dy^- e^{ixp^+y^-} \langle p | \bar{\psi}(0) \gamma \cdot n \psi(y) | p \rangle \Big|_{y^+ = \vec{y}_\perp = 0}, \quad (120)$$

$$\Delta q(x) = \frac{p^+}{2\pi} \int dy^- e^{ixp^+y^-} \langle p S_\parallel | \bar{\psi}(0) \gamma \cdot n \gamma_5 \psi(y) | p S_\parallel \rangle \Big|_{y^+ = \vec{y}_\perp = 0}. \quad (121)$$

In Eqs.(120, 121), p represents the initial nucleon momentum in the DIS process and S_\parallel is the longitudinal nucleon spin projection. From Eqs.(120, 121) the quark distributions for negative momentum fractions are related to the antiquark distributions as $q(-x) = -\bar{q}(x)$ and $\Delta q(-x) = +\Delta \bar{q}(x)$.

In the region $-\xi < x < \xi$, one quark propagator represents a quark and the other one an antiquark. In this region, the OFPD's behave like a meson distribution amplitude.

5.3 Sum rules for off-forward parton distributions

By integrating Eq.(116) over x one gets the following relations between the first moments of the OFPD's and the elastic form factors (for one quark flavor)

$$\int_{-1}^{+1} dx H^q(x, \xi, t) = F_1^q(t), \quad \int_{-1}^{+1} dx E^q(x, \xi, t) = F_2^q(t), \quad (122)$$

$$\int_{-1}^{+1} dx \tilde{H}^q(x, \xi, t) = g_A^q(t), \quad \int_{-1}^{+1} dx \tilde{E}^q(x, \xi, t) = h_A^q(t), \quad (123)$$

where F_1^q , F_2^q are the Dirac and Pauli form factors respectively, g_A^q is the axial form factor and h_A^q is the induced pseudoscalar form factor. Note that in the sum rules of Eqs.(122) and (123), the ξ -dependence drops out.

According to the considered reaction, the proton OFPD's enter in different combinations due to the charges and isospin factors. For the DVCS on the proton, the combination is

$$H_{DVCS}^p(x, \xi, t) = \frac{4}{9}H^{u/p} + \frac{1}{9}H^{d/p} + \frac{1}{9}H^{s/p}, \quad (124)$$

and similarly for \tilde{H} , E and \tilde{E} . For the electroproduction of ρ^0 and π^0 on the proton, the isospin structure yields the combination

$$H_{\rho^0}^p(x, \xi, t) = \frac{1}{\sqrt{2}} \left\{ \frac{2}{3}H^{u/p} + \frac{1}{3}H^{d/p} \right\}, \quad \tilde{H}_{\pi^0}^p(x, \xi, t) = \frac{1}{\sqrt{2}} \left\{ \frac{2}{3}\tilde{H}^{u/p} + \frac{1}{3}\tilde{H}^{d/p} \right\}, \quad (125)$$

and similar for E and \tilde{E} . The elastic form factors for one quark flavor have to be related to the physical ones. Restricting oneself to the u, d and s quark flavors, this yields

$$F_1^{u/p} = 2F_1^p + F_1^n + F_1^s, \quad F_1^{d/p} = 2F_1^n + F_1^p + F_1^s, \quad (126)$$

where F_1^p and F_1^n are the proton and neutron electromagnetic form factors respectively. The strange form factor is given by $F_1^{s/p} \equiv F_1^s$, but since it is small and not so well known we set it to zero in the following. Relations similar to Eq.(126) hold also for the form factor F_2^q . For the axial vector form factors one uses the isospin decomposition :

$$g_A^{u/p} = \frac{1}{2}g_A + \frac{1}{2}g_A^0, \quad g_A^{d/p} = -\frac{1}{2}g_A + \frac{1}{2}g_A^0. \quad (127)$$

The isovector axial form factor g_A is known from experiment ($g_A(0) \approx 1.26$) and for the unknown isoscalar axial form factor g_A^0 we use the quark model relation : $g_A^0(t) = 3/5 g_A(t)$. For h_A^q we have relations similar to Eq.(127).

The second moment of the OFPD's is relevant for the nucleon spin structure. It was shown in Ref.[Ji97a] that there exists a (color) gauge-invariant decomposition of the nucleon spin:

$$\frac{1}{2} = J_q + J_g, \quad (128)$$

where J_q and J_g are respectively the total quark and gluon spin contributions to the nucleon spin. The second moment of the OFPD's gives

$$J_q = \frac{1}{2} \int_{-1}^{+1} dx x [H^q(x, \xi, t=0) + E^q(x, \xi, t=0)], \quad (129)$$

and this relation is independent of ξ . The total quark spin contribution J_q decomposes as

$$J_q = \frac{1}{2}\Delta\Sigma + L_q, \quad (130)$$

where $1/2 \Delta\Sigma$ and L_q are respectively the quark spin and quark orbital contributions to the nucleon spin. We recall that $\Delta\Sigma$ is measured through polarized DIS experiments. So if one can measure the OFPD's through exclusive hard electroproduction reactions, the sum rule of Eq.(129) will determine the quark orbital contribution to the nucleon spin.

5.4 DVCS amplitude

In the following, we assume as in Refs.[Ji97a][Ji97b] that a factorization between hard and soft processes is valid for DVCS. A formal factorization proof has been given very recently [Col98][Ji98]. Using the parametrization of Eq.(116) for the bilocal quark operator, the leading order DVCS tensor $H_{L.O.DVCS}^{\mu\nu}$ (defined by Eq.(19)) follows from the two handbag diagrams of Fig.(16a) as

$$\begin{aligned} & H_{L.O.DVCS}^{\mu\nu} \\ &= \frac{1}{2} \left\{ [\tilde{p}^\mu n^\nu + \tilde{p}^\nu n^\mu - g^{\mu\nu}] \cdot \int_{-1}^{+1} dx \left[\frac{1}{x - \xi + i\epsilon} + \frac{1}{x + \xi - i\epsilon} \right] \right. \\ & \quad \cdot \left[H_{DVCS}^p(x, \xi, t) \bar{u}(p') \gamma \cdot n u(p) + E_{DVCS}^p(x, \xi, t) \bar{u}(p') i\sigma^{\kappa\lambda} \frac{n_\kappa \Delta_\lambda}{2m} N(p) \right] \\ & \quad + [-i\varepsilon^{\mu\nu\kappa\lambda} \tilde{p}_\kappa n_\lambda] \cdot \int_{-1}^{+1} dx \left[\frac{1}{x - \xi + i\epsilon} - \frac{1}{x + \xi - i\epsilon} \right] \\ & \quad \cdot \left[\tilde{H}_{DVCS}^p(x, \xi, t) \bar{N}(p') \gamma \cdot n \gamma_5 N(p) + \tilde{E}_{DVCS}^p(x, \xi, t) \bar{N}(p') \gamma_5 \frac{\Delta \cdot n}{2m} N(p) \right] \left. \right\}, \quad (131) \end{aligned}$$

with $\varepsilon_{0123} = +1$. Tests of the handbag approximation to the DVCS amplitude have been proposed in Ref.[Die97] and experiments are proposed to check the hypothesis [Ber98].

The leading order DVCS amplitude of Eq.(131) as given first in Refs.[Ji97a][Ji97b], is exactly gauge invariant with respect to the virtual photon, i.e. $q_\nu H_{L.O.DVCS}^{\mu\nu} = 0$. However gauge invariance is violated by the real photon except in the forward direction. In fact $q'_\mu H_{L.O.DVCS}^{\mu\nu} \sim \Delta_\perp$. This violation of gauge invariance is a higher twist effect of order $1/Q^2$ compared to the leading order term $H_{L.O.DVCS}^{\mu\nu}$. So in the limit $Q^2 \rightarrow \infty$ it is innocuous but for actual experiments it matters. Actually for any cross section estimate one needs to choose a gauge and this explicit gauge dependence for $\theta \neq 0$ is unpleasant. In the absence of a dynamical gauge invariant higher twist calculation of the DVCS amplitude, we propose to restore gauge invariance in a heuristic way based on physical considerations. We propose to write

$$H_{DVCS}^{\mu\nu} = H_{L.O.DVCS}^{\mu\nu} - \frac{a^\mu}{(a \cdot q')} \left(q'_\lambda H_{L.O.DVCS}^{\lambda\nu} \right), \quad (132)$$

where a^μ is a four-vector specified below. Obviously $H_{DVCS}^{\mu\nu}$ respects gauge invariance for both the virtual and the real photon :

$$q_\nu H_{DVCS}^{\mu\nu} = 0, \quad q'_\mu H_{DVCS}^{\mu\nu} = 0. \quad (133)$$

Furthermore, as

$$q'_\lambda H_{L.O. DVCS}^{\lambda\nu} = -(\Delta_\perp)_\lambda H_{L.O. DVCS}^{\lambda\nu}, \quad (134)$$

the gauge restoring term gives zero in the forward direction ($\Delta_\perp = 0$) which is natural. We choose $a^\mu = \tilde{p}^\mu$ because $\tilde{p} \cdot q'$ is of order Q^2 , which gives automatically a gauge restoring term of order $O(1/Q^2)$. This choice for a^μ is furthermore motivated by the fact that in the derivation of the leading order amplitude of Eq.(131), only the \tilde{p}^μ components at the electromagnetic vertices are retained [Ji97a][Ji97b]. The above arguments lead to the following fully gauge invariant DVCS amplitude:

$$H_{DVCS}^{\mu\nu} = H_{L.O. DVCS}^{\mu\nu} + \frac{\tilde{p}^\mu}{(\tilde{p} \cdot q')} (\Delta_\perp)_\lambda H_{L.O. DVCS}^{\lambda\nu}. \quad (135)$$

We will illustrate the influence of this gauge invariance prescription, by comparing DVCS observables calculated with Eq.(135) and with the leading order formula of Eq.(131).

5.5 Hard meson electroproduction amplitudes

For the electroproduction of π^0 and ρ_L^0 mesons ⁷ at large values of x_B (i.e. in the valence region), the leading order amplitude is given by the diagrams of Fig.(16c). This amplitude was calculated in Ref.[Vdh98a] where the following gauge invariant expressions were found for the current operators

$$\begin{aligned} J_{\rho_L^0}^\mu = & (ie4\pi\alpha_s) \frac{4}{9} \frac{x_B}{Q^2} \left[\int_0^1 dz \frac{\Phi_\rho(z)}{z} \right] \cdot \left\{ \tilde{p}^\mu + \frac{Q^2}{2x_B^2} n^\mu \right\} \\ & \cdot \frac{1}{2} \int_{-1}^{+1} dx \left[\frac{1}{x - \xi + i\epsilon} + \frac{1}{x + \xi - i\epsilon} \right] \\ & \cdot \left\{ H_{\rho_L^0}^p(x, \xi, t) \bar{u}(p') \gamma \cdot n u(p) + E_{\rho_L^0}^p(x, \xi, t) \bar{u}(p') i\sigma^{\kappa\lambda} \frac{n_\kappa \Delta_\lambda}{2m} u(p) \right\}, \quad (136) \end{aligned}$$

$$\begin{aligned} J_{\pi^0}^\mu = & (ie4\pi\alpha_s) \frac{4}{9} \frac{x_B}{Q^2} \left[\int_0^1 dz \frac{\Phi_\pi(z)}{z} \right] \cdot \left\{ \tilde{p}^\mu + \frac{Q^2}{2x_B^2} n^\mu \right\} \\ & \cdot \frac{1}{2} \int_{-1}^{+1} dx \left[\frac{1}{x - \xi + i\epsilon} + \frac{1}{x + \xi - i\epsilon} \right] \\ & \cdot \left\{ \tilde{H}_{\pi^0}^p(x, \xi, t) \bar{u}(p') \gamma \cdot n \gamma_5 u(p) + \tilde{E}_{\pi^0}^p(x, \xi, t) \bar{u}(p') \gamma_5 \frac{\Delta \cdot n}{2m} u(p) \right\}, \quad (137) \end{aligned}$$

where $\Phi_\rho(z)$ and $\Phi_\pi(z)$ are the ρ and π distribution amplitude (DA) respectively. For the pion, recent data [Gro98] for the $\pi^0 \gamma^* \gamma$ transition form factor up to $Q^2 = 9 \text{ GeV}^2$ support the asymptotic form:

$$\Phi_\pi(z) = \sqrt{2} f_\pi 6z(1-z), \quad (138)$$

with $f_\pi = 0.093 \text{ GeV}$ from the pion weak decay. For the rho meson, the DA is not as well known. A recent theoretical analysis [Bal96] updating the QCD sum rule analysis by

⁷Note that although we will only show results for the ρ^0 and π^0 in this work, the formalism also applies for other vector mesons such as the ω and ϕ or other pseudoscalar mesons such as the η .

including $O(\alpha_s)$ radiative corrections, favors a DA that is rather close to its asymptotic form. In the calculations shown below, we use the asymptotic DA for the rho :

$$\Phi_\rho(z) = \sqrt{2}f_\rho 6z(1-z) , \quad (139)$$

with $f_\rho = 0.153$ GeV determined from the electromagnetic decay $\rho^0 \rightarrow e^+e^-$. Note that the CZ DA for the ρ [Che84], which is more concentrated near the end points, would yield an amplitude larger by a factor 5/3.

The $(e, e' M)$ cross section for a meson M is given by the formula of Eq.(36). The T, L, TT, TL cross sections appearing in Eq.(36) are calculated from the helicity amplitudes for meson electroproduction. In the following, we give only predictions for σ_L as, at large Q^2 , only the meson production by a longitudinal virtual photon survives and because the factorization theorem [Col97] only applies for a longitudinal virtual photon. The longitudinal $\gamma^* + p \rightarrow M + p$ two body cross section $d\sigma_L/dt$ of Eq.(36) is

$$\frac{d\sigma_L}{dt} = \frac{1}{16\pi(s-m^2)^2} \frac{1}{2} \sum_{h_N} \sum_{h'_N} \left| \frac{q_0}{Q} \varepsilon_\mu(\lambda=0) \cdot J^\mu(\lambda_M=0, h'_N; h_N) \right|^2 , \quad (140)$$

where $\varepsilon_\mu(\lambda=0)$ is the polarization vector for a longitudinal photon (following the convention of App.A, Eq.(152)). It is expressed in terms of the lightlike vectors \tilde{p}^μ and n^μ as

$$\frac{q_0}{Q} \varepsilon^\mu(\lambda=0) = -\frac{1}{Q} \left\{ x_B \tilde{p}^\mu + \frac{Q^2}{2x_B} n^\mu \right\} . \quad (141)$$

In Eq.(140), J^μ is the current operator for production of a ρ_L^0 or π^0 defined in Eqs(136, 137). One can see from Eqs.(136, 137) that the large Q^2 behaviour of the amplitude for ρ_L^0 and π^0 production is

$$\frac{q_0}{Q} \varepsilon_\mu(\lambda=0) \cdot J^\mu(\lambda_M=0, h'_N; h_N) \sim \frac{q_0}{Q} \varepsilon_\mu(\lambda=0) \cdot \left\{ \tilde{p}^\mu + \frac{Q^2}{2x_B^2} n^\mu \right\} \left(\frac{x_B}{Q^2} \right) = -\frac{1}{Q} . \quad (142)$$

As $s = m^2 + Q^2(1-x_B)/x_B$, this leads to a $1/Q^6$ behavior of $d\sigma_L/dt$ at large Q^2 .

5.6 Models for the off-forward parton distributions

Ultimately one wants to extract the OFPD's from data but in order to evaluate electroproduction observables, we need a first guess for the OFPD's. We shall restrict our considerations to the near forward direction because this kinematical domain is the closest to inclusive DIS, which we want to use as a guide. In this domain, the contribution of E and \tilde{E} , which goes like Δ , is suppressed. So in the following we shall keep only H and \tilde{H} . Furthermore, we assume that, at small $-t$, H^q is proportional to the unpolarized quark distribution for which we take the MRS (S_0) parametrization of Ref.[MRS93]

$$\begin{aligned} x d_V(x) &= A_d x^{0.78} (1-x)^{4.57} (1-0.87\sqrt{x}+0.82x) , \\ x (u_V(x) + d_V(x)) &= A_{ud} x^{0.26} (1-x)^{3.82} (1+14.4\sqrt{x}+16.99x) , \\ x S(x) &= 1.87(1-x)^{10} (1-2.21\sqrt{x}+6.22x) . \end{aligned} \quad (143)$$

The valence parts of the quark distributions are normalized as

$$\frac{1}{2} \int_0^1 dx u_V(x) = \int_0^1 dx d_V(x) = 1 , \quad (144)$$

and the sea quark distributions are parametrized as $u_S = \bar{u} = d_S = \bar{d} = 2s_s = 2\bar{s} = 5/9 S$. Our ansatz for the OFPD's H^q thus yields

$$H^{u/p}(x, \xi, t) = \frac{1}{2}u(x)F_1^{u/p}(t), \quad H^{d/p}(x, \xi, t) = d(x)F_1^{d/p}(t), \quad H^{s/p}(x, \xi, t) = 0, \quad (145)$$

and obviously the ansatz satisfies both Eq.(118) and the sum rule Eq.(122).

Similarly, we assume that $\tilde{H}^q(x, \xi, t)$ is proportional to the polarized quark distribution. For the latter we neglect the not well known sea part and we adopt the valence parametrizations of Ref.[Gos97]

$$\begin{aligned} \Delta u_V(x) &= \cos \Theta_D(x) \left[u_V(x) - \frac{2}{3}d_V(x) \right], & \Delta d_V(x) &= \cos \Theta_D(x) \left[-\frac{1}{3}d_V(x) \right], \\ \cos \Theta_D(x) &= \frac{1}{1 + H_0(1-x)^2/\sqrt{x}}, \end{aligned} \quad (146)$$

with $H_0 = 0.06$ such that the Bjorken sum rule is satisfied. This yields the normalization

$$\int_0^{+1} dx \Delta u_V(x) = 0.98, \quad \int_0^{+1} dx \Delta d_V(x) = -0.27, \quad (147)$$

which leads to the correct proton to neutron magnetic moment ratio $\mu_p/\mu_n \approx -1.47$. Our ansatz for \tilde{H}^q is thus

$$\tilde{H}^{u/p}(x, \xi, t) = \Delta u_V(x)g_A^{u/p}(t)/g_A^{u/p}(0), \quad \tilde{H}^{d/p}(x, \xi, t) = \Delta d_V(x)g_A^{d/p}(t)/g_A^{d/p}(0), \quad (148)$$

and one can check that both Eq.(119) and the sum rule of Eq.(123) are satisfied. Note that as suggested by the bag model estimate of Ref.[Ji97c], we have omitted any dependence of the OFPD's on ξ which should be justified for moderate Q^2 . At high values of Q^2 , this approximation is expected to break down and the Q^2 evolution has to be considered. The evolution of the OFPD's has recently been studied by several authors [Rad97][Bal97][Bel98][Fra98].

5.7 Results for DVCS and hard meson leptonproduction observables

We first show results for the ρ^0 electroproduction cross sections. In Fig.(17), the total longitudinal ρ_L^0 electroproduction cross section is shown as function of the C.M. energy W for different values of Q^2 . At high C.M. energies, it is well known that the Perturbative Two

$$\gamma^* + p \rightarrow \rho_L^0 + p : Q^2 = 6, 9, 17 \text{ GeV}^2$$

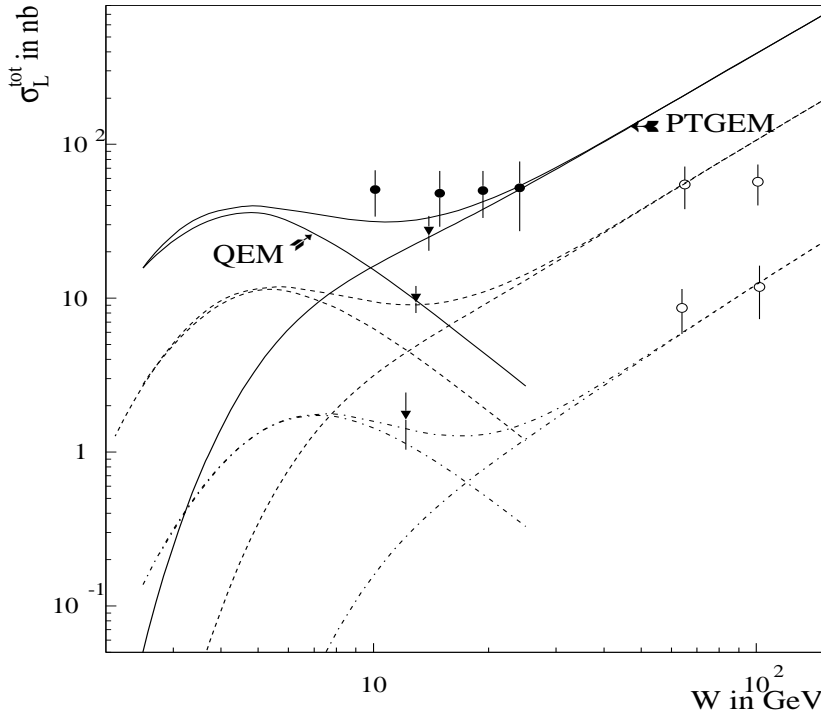


Figure 17: Total longitudinal cross section for ρ_L^0 electroproduction. Data from NMC [Arn94] (triangles) at $Q^2 = 5.5$ (highest point), 8.8 and 16.9 (lowest point) GeV^2 , E665 [Ada97] (black circles) at $Q^2 = 5.6 \text{ GeV}^2$ and ZEUS [Der95] (open circles) at $Q^2 = 8.8$ (upper points) and 16.9 GeV^2 (lower points). Calculations are shown at $Q^2 = 6 \text{ GeV}^2$ (full lines), $Q^2 = 9 \text{ GeV}^2$ (dashed lines) and $Q^2 = 17 \text{ GeV}^2$ (dashed-dotted lines). The curves which grow at high W correspond with gluon exchange whereas the curves which are peaked below $W \approx 10 \text{ GeV}$ correspond with quark exchange. The incoherent sum of both mechanisms is also shown.

Gluon Exchange Mechanism (PTGEM) dominates as soon as $Q^2 \geq 6 \text{ GeV}^2$ and this mechanism implies a $1/Q^6$ behavior of σ_L [Bro94][Fra96]. The PTGEM cross section calculated with Eq.(5) of Ref.[Fra96] is shown in Fig.(17). We used the CTEQ3L parametrization [Lai95] for the gluon distribution. The PTGEM explains well the fast increase at high energy of the cross section. Note that the data point shown on Fig.(17) are consistent with

the more recent ZEUS data [Cri97].

However, the PTGEM substantially underestimates the data at lower energies (around $W \approx 10 \text{ GeV}$), where the quark exchange mechanism (QEM) of Fig.(16b) is expected to contribute since x_B is then in the valence region. In Fig.(17) we show our predictions using the OFPD's proposed in the previous section. The incoherent sum of both mechanisms is also indicated. Fig.(17) provides a rather strong indication that the deviation from the PTGEM of the data at lower energies can be attributed to the onset of the QEM. The good agreement between the data in this region and our prediction gives us some confidence in our factorized ansatz for the OFPD's.

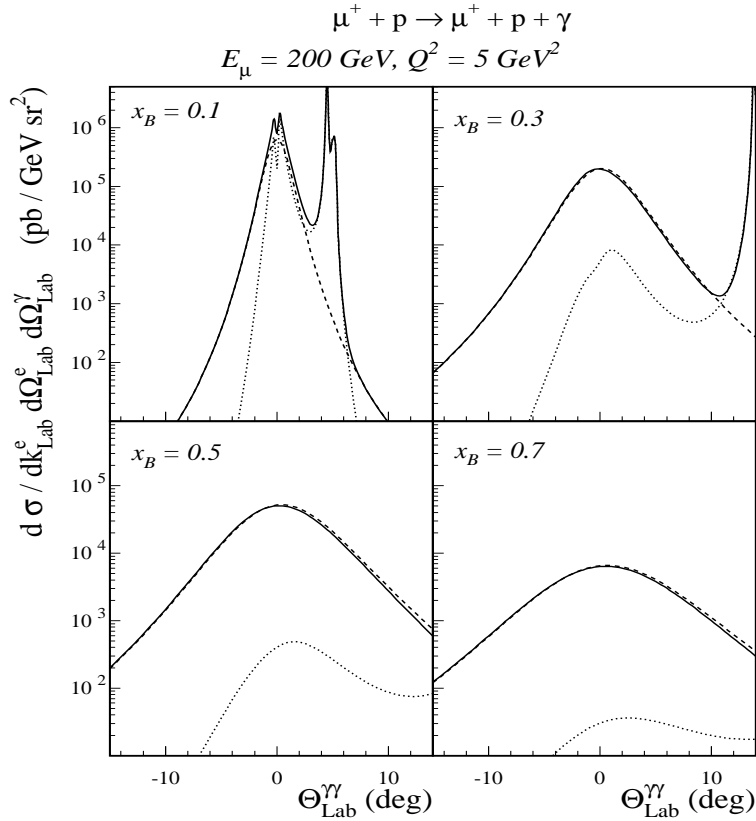


Figure 18: Comparison between BH (dotted lines), DVCS (dashed lines) and total γ (full lines) in-plane cross sections for COMPASS kinematics.

The QEM is studied further in Figs.(18),(19) where the angular dependence of the five-fold differential DVCS 8 , π^0 and ρ_L^0 muoproduction cross sections are shown for kinematics accessible at COMPASS. In our calculations we add coherently the BH and DVCS amplitudes. From a phenomenological point of view, it is clear that the best situation occurs when the BH process is negligible. For fixed Q^2 and s , the only way to favor the DVCS

⁸The small differences between the results shown here and those of Ref.[Gui97] are due to the use of different parton distributions.

over the BH is to increase the virtual photon flux and this amounts to increase the beam energy. According to our estimate, the unpolarized ($l, l' \gamma$) cross section in the forward region is dominated by the BH process in the few GeV region. To get a clear dominance of the DVCS process one needs a beam energy in the 100 GeV range. This is illustrated

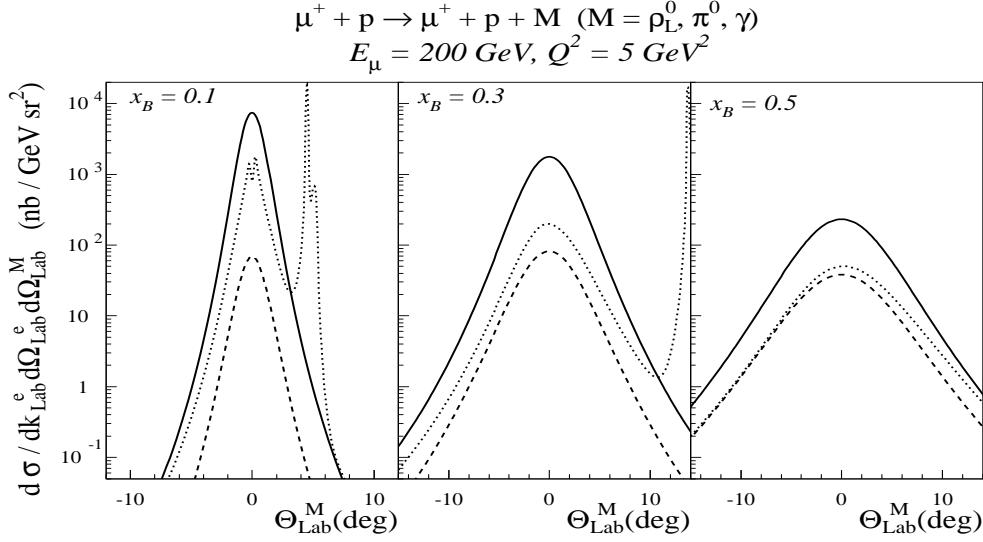


Figure 19: Comparison between ρ_L^0 (full lines), π^0 (dashed lines) and total γ (dotted lines) muoproduction in-plane cross sections for COMPASS kinematics.

in Fig.(18) where we show separately the BH, the DVCS and the coherent cross section at $E_\mu = 200 \text{ GeV}$ and $Q^2 = 5 \text{ GeV}^2$. In the valence region ($x_B \approx 0.3$), the DVCS cross section is more than one order of magnitude larger than the BH in the forward direction. The BH cross section increases if one goes to smaller x_B and becomes comparable to the DVCS cross section around $x_B \approx 0.1$. This is due to the fact that in the BH process the exchanged photon has 4-momentum ($q - q'$) which gives a $1/t$ behaviour to the amplitude. The value of t in the forward direction (t_{min}) is very small for small x_B values and it increases with x_B . At $x_B = 0.7$, the value of $-t_{min}$ in Fig.(18) is around 1 GeV^2 , which explains the sharp drop of the BH amplitude compared to the DVCS one. The sharp rise of the BH process in the forward direction at small x_B puts a limit on the region where the DVCS can be studied experimentally. At COMPASS kinematics, $x_B \simeq 0.1$ seems to be the lower limit. Although the BH is not a limiting factor at high x_B , one cannot go too close to $x_B = 1$ in order to stay well above the resonance region.

In Fig.(19), the x_B dependence of the ρ_L^0 , π^0 and γ fivefold differential muoproduction cross sections are compared in the same kinematics as in Fig.(18). The x_B dependence of the ρ_L^0 , π^0 and DVCS cross sections is a direct reflection of the x_B dependence of the OFPD's. In the valence region ($x_B \approx 0.3$), the ρ_L^0 cross section, which is sensitive to the unpolarized OFPD's, is about one order of magnitude larger than the π^0 cross section which is sensitive to the polarized OFPD's. The DVCS cross section is sensitive to both unpolarized and polarized OFPD's but, due to the additional electromagnetic coupling, it

is also about one order of magnitude below the ρ_L^0 cross section. Although the ρ_L^0 cross section is the easiest to measure, the π^0 and DVCS cross sections seem large enough to encourage a study of the feasibility of the experiments. The three reactions are highly complementary due to their different dependence on the OFPD's.

Before considering the extraction of the OFPD's from the data, it is compulsory to demonstrate that the scaling regime has been reached. In Fig.(20) we show the forward $\gamma^* + p \rightarrow M + p$ cross sections as a function of Q^2 . This illustrates the lever arm one has to test the scaling behavior, as the maximum value of Q^2 will be given by the count rate limit of an experiment. For the DVCS, the leading order amplitude is constant in Q and is predominantly transverse. Therefore, the leading order DVCS transverse cross section $d\sigma_T/dt$ shows a $1/Q^4$ behavior. To test this scaling behavior, one needs of course a kinematical situation where the DVCS dominates over the BH.

The leading order meson electroproduction amplitude was seen to behave as $1/Q$ and is predominantly longitudinal. Therefore, the leading order longitudinal cross section $d\sigma_L/dt$ for meson electroproduction shows a $1/Q^6$ behavior. Note that eventhough the ρ_L^0 electroproduction is not as clean as the DVCS due to its dependence on the ρ^0 wavefunction, a test of the $1/Q^6$ scaling behavior would nevertheless be meaningful. The reason is that an uncertainty in the meson wavefunction would influence mostly the normalization of the cross section, but not its behavior in Q .

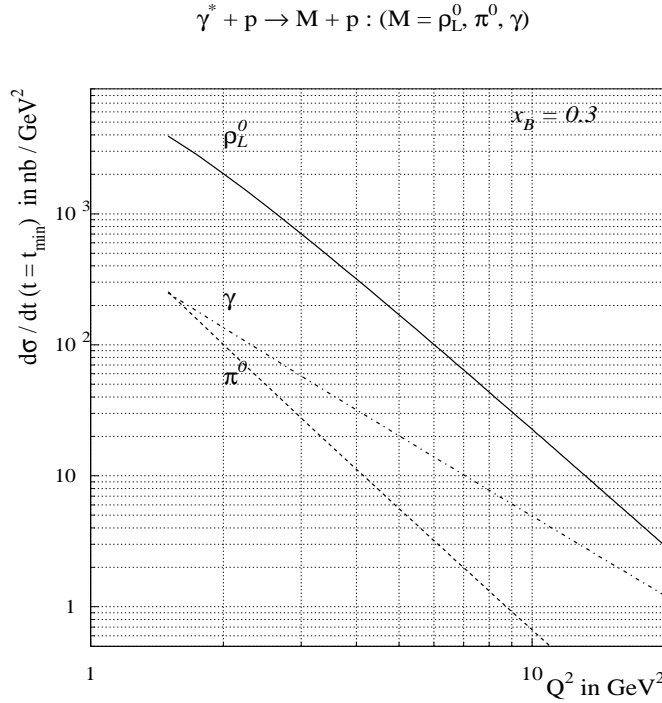


Figure 20: Scaling behavior of the forward ($t = t_{min}$) differential cross section $d\sigma_L/dt$ for ρ_L^0 and π^0 electroproduction and of $d\sigma_T/dt$ for the DVCS cross section.

Although a high energy such as planned at COMPASS is preferable, one can try to undertake a preliminary study of the hard electroproduction reactions using the existing facilities such as HERMES or CEBAF, despite their low energy. To this end, we compare in Fig.(21), the ρ_L^0 , π^0 and γ cross sections as function of the beam energy at a fixed $Q^2 = 2 \text{ GeV}^2$ and $x_B = 0.3$. Going up in energy, the increasing virtual photon flux factor boosts the ρ_L^0 , π^0 lepto-production cross sections and the DVCS part of the γ lepto-production cross section. For the γ electroproduction cross section the BH process is hardly influenced by the beam energy and therefore overwhelms the DVCS cross section at low beam energies.

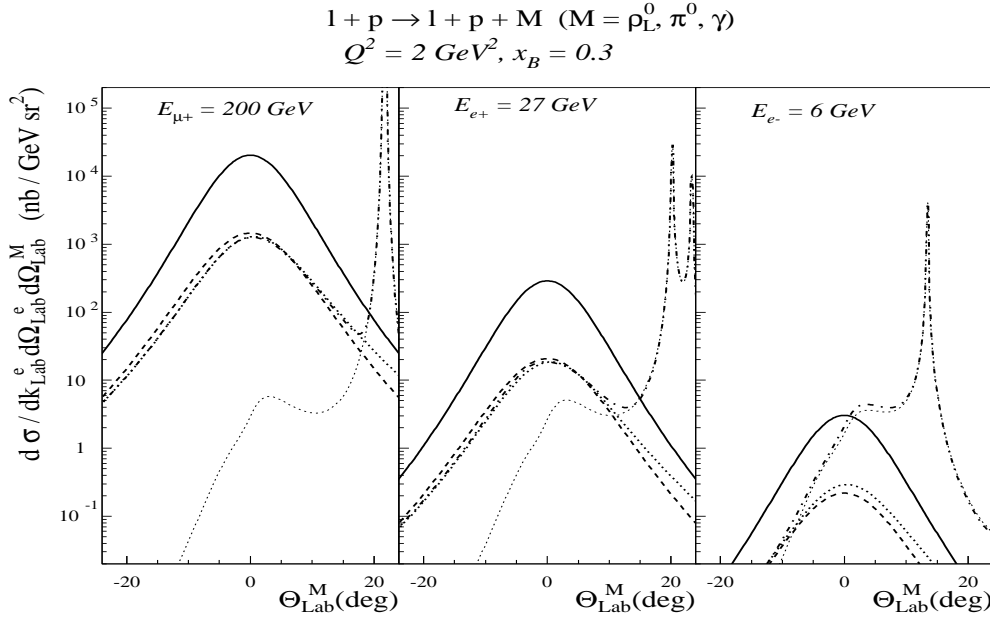


Figure 21: Comparison between ρ_L^0 (full lines), π^0 (dashed lines), DVCS (dotted lines), BH (thin dotted lines) and total γ (dashed-dotted lines) lepto-production in-plane cross sections at $Q^2 = 2 \text{ GeV}^2$, $x_B = 0.3$ and for different beam energies : $E_{\mu^+} = 200 \text{ GeV}$ (COMPASS), $E_{e^+} = 27 \text{ GeV}$ (HERMES), $E_{e^-} = 6 \text{ GeV}$ (CEBAF).

To make a preliminary exploration of the OFPD's in the few GeV range and to test the scaling, the measurement of the ρ_L^0 lepto-production through its decay into charged pions seems the easiest from the experimental point of view as the count rates are the highest. In particular, in the $Q^2 = 1 - 5 \text{ GeV}^2$ range, the ρ_L^0 cross section can be used to delineate the scaling region.

For the γ lepto-production at low energies, we suggest that an exploration of the DVCS part might be possible if the beam is polarized. The electron single spin asymmetry (SSA) does not vanish out of plane and is only due to the interference between the BH process and the imaginary part of the DVCS amplitude. Therefore, even if the cross section is dominated by the BH process, the SSA is *linear* in the OFPD's. To illustrate the point, we show on Fig.(22) the unpolarized cross section for a 6 GeV beam and the SSA at an

azimuthal angle $\phi = 120^\circ$. In the $0^\circ - 5^\circ$ region, a rather large asymmetry is predicted, even though the cross section is dominated by the BH process. Of course this does not exclude the risk that at this small Q^2 , higher twist effects might be important.

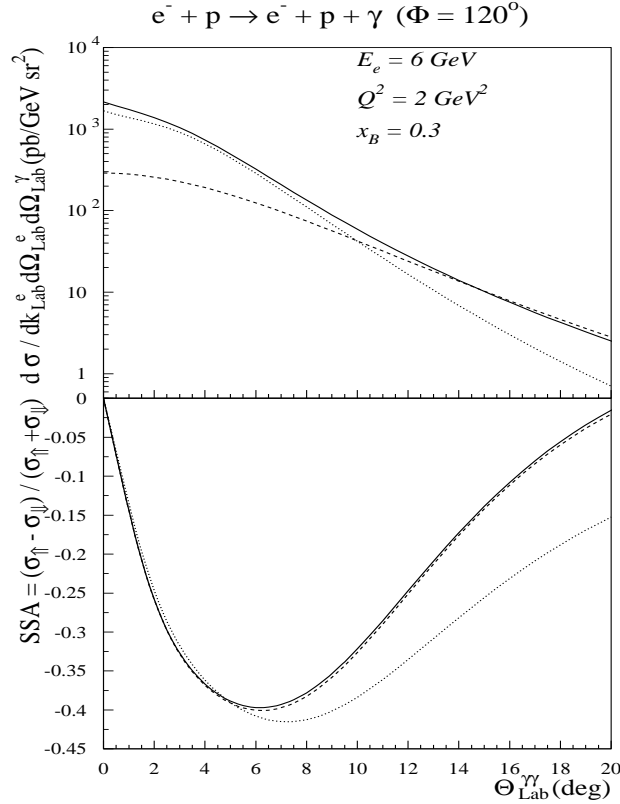


Figure 22: DVCS at CEBAF for out-of-plane kinematics ($\phi = 120^\circ$). Upper part shows the differential cross section : DVCS (dashed line), BH (dotted line) and total γ (full line). In the lower part, the electron single spin asymmetry is shown for the gaugeinvariant amplitude (full line) and for the leading order non-gaugeinvariant amplitude calculated in radiative gauge (dashed line) and in Feynman gauge (dotted line).

To illustrate the effect of the gauge restoring term in Eq.(135), we have plotted in Fig.(22) the SSA both for the gauge invariant and non gauge invariant amplitudes. For the non gauge invariant amplitude of Eq.(131), the SSA is shown both in the radiative gauge and in the Feynman gauge. As expected, all predictions are identical at small angle. At larger angles the gauge dependence clearly shows up, especially in the Feynman gauge.

Finally, we recall that the real part of the BH-VCS interference can be accessed by reversing the charge of the lepton beam since this changes the relative sign the BH and

FVCS amplitudes. This leads to the following charge asymmetry

$$\sigma_{e^+} - \sigma_{e^-} \sim 4\Re \left[T^{BH} T^{FVCS*} \right] . \quad (149)$$

Our estimate for the e^+e^- asymmetry is shown in Fig.(23) at 27 GeV. The comfortable asymmetry that one can see in the small angle region may offer an interesting opportunity for HERMES.

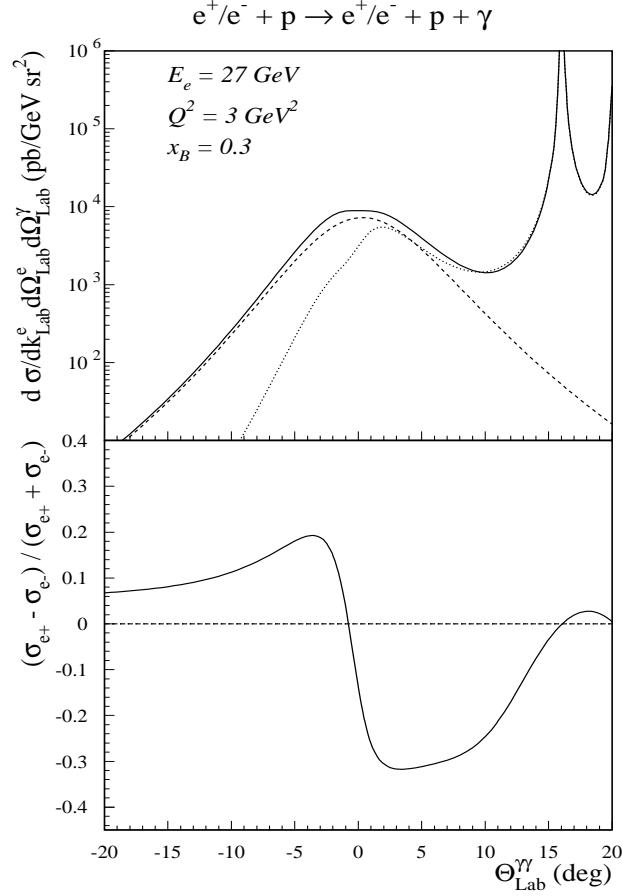


Figure 23: e^+e^- asymmetry at HERMES. Upper part shows the in-plane e^+ differential cross section : BH + DVCS (full line), DVCS (dashed line), BH (dotted line). Lower part : e^+e^- charge asymmetry with same curve conventions as in upper part of figure.

6 OUTLOOK AND PERSPECTIVES

As we have seen in the previous sections, virtual Compton scattering is a very versatile tool.

At threshold it gives us access to a new kind of electron scattering experiments where the target is submitted to an external electric or magnetic field. The outcome of the experiments are the form factors of the currents induced by the applied field. This generalizes the notion of polarizability in the sense that the spatial distribution of the induced current can be measured while in real Compton scattering only the dipole moment is accessible. For the proton there are six GP's which are functions of Q^2 . Their experimental determination is now under way but this is a delicate task. As explained in Section 3, the response at threshold is dominated by the global motion of the proton in the external field. Scattering on this moving object teaches us nothing more than what we already know such as its mass, its charge and its elastic form factors. To extract the true information one has to subtract this trivial but dominating part and this supposes very accurate experiments. To obtain the GP's, with an accuracy of 15% one needs cross sections with an accuracy of 3%.

The first experiment has been performed at MAMI [d'Ho95][Lhu97a] and at the time of writing, the analysis has not yet reached a stage where the polarizabilities can be extracted from the data. On the other hand the low energy theorem is well satisfied by the very low energy data [d'Ho97]. To our knowledge it is the first time that this theorem is tested. The next experiments will take place at CEBAF [Ber93] in 1998 where the higher beam energy is expected to help by allowing a better choice of the virtual photon polarization ϵ . Finally an experiment at small Q^2 has been accepted at Bates [Sha97] with the aim of testing Chiral perturbation theory predictions.

At present no experiments with polarization have been proposed. Though polarized beams exist now at the high duty cycle electron accelerators, we have seen that one needs to measure the polarization of the recoiling proton. Due to the low efficiency of the polarimeters, below 10%, one can foresee that this interesting physics will not start before the unpolarized program has achieved its task. We have demonstrated however that these recoil polarization observables provide three independent observables and complement the three unpolarized observables. Therefore, the measurement of these recoil polarization observables holds promise to disentangle the six independent GP's.

The hard scattering regime of VCS discussed in Section 4 gives access to the most elementary part of the nucleon structure, its 3 quark valence wave function. Thanks to the large energy-momentum transferred to the nucleon, the complex configurations which build the full confinement are eliminated from the amplitude. The price to pay is that the cross sections are extremely small and without a dedicated accelerator like ELFE [Arv93] the experiments look impossible. However a preliminary attempt will be performed at CEBAF [Ber93]. The beam energy is definitively too low to access the hard scattering regime but the use of the polarized beam to select the BH-VCS interference will provide the first test of the diquark model prediction for the phase of the VCS amplitude. Finally we recall that the physics case of real Compton scattering is similar to the one of VCS. Since the experiments are much easier it may be a good strategy to try to develop first the real Compton scattering in the hard scattering regime. Such experiments might become possible with a high intensity, high energy ($E_\gamma \sim 15$ GeV) photon beam at the existing HERA ring [d'Ho96][D'An97].

VCS in the Bjorken regime or DVCS is the most recent development in the VCS field.

Because of its strong connection with the time honoured inclusive DIS, it has become rapidly popular. In this regime one can access the so called off-forward parton distributions which may shed a new light on the nucleon spin problem. We have used a crude factorized model of the OFPD's to perform the first evaluation of the cross sections including the BH amplitude. Gauge invariance with respect to the outgoing real photon has been enforced in a minimal way in the sense that the corrective term is explicitly a higher twist effect. Its effect with respect to a calculation in the radiative gauge is about 1%.

To devise a convincing test of scaling of the DVCS amplitude and to access the OFPD's from this reaction one needs a very high energy in order that the BH process be negligible. The 100-200 GeV muon beam of COMPASS seems adequate, at least for not too small values of x_B .

However it is tempting to make use of the existing machines to open the way. The trick is to climb on the back of the BH amplitude using its interference with the DVCS amplitude. Even though the cross section may be completely dominated by the BH, the interference remains linear in the OFPD's that we are looking for. The first possibility is the single spin asymmetry which we have found to be large and which selects the imaginary part of the DVCS amplitude. A proposal of experiment is now in preparation [Ber98]. The energy might be too low to reach the scaling regime but since the experiment does not imply a huge effort it is worth an attempt. The second possibility is the beam charge asymmetry which is also large and selects the real part of the DVCS amplitude. In this case one does not need an out of plane experiment. This could be a good case for HERMES or SLAC and their higher energy as compared to CEBAF would be a serious advantage.

The high energy forward meson leptonproduction is closely related to DVCS because the same OFPD's enter the amplitudes. Moreover one can select the OFPD's by selecting the meson. In this way, the ρ_L^0 electroproduction gives access to the unpolarized OFPD's and the π^0 to the polarized OFPD's. One needs another input, the meson wave function, and therefore the information one gets from this process is less pure than in the DVCS case. However it is a useful complement and we have evaluated the cross sections using the (conservative) asymptotic wave function, which for the pion is able to describe the recent data for the $\pi^0\gamma^*\gamma$ transition form factor [Gro98]. We found comfortable cross sections especially for ρ_L^0 leptonproduction. In the meson case the BH problem is absent and therefore the measurement of the ρ_L^0 electroproduction may provide a nice test to see if one can access the scaling region already at CEBAF.

An important point which has not much been discussed in the text is the problem of radiative corrections, which is important in the case of experiments with electrons. All the Feynman diagrams contributing to the cross section of order α_{QED}^4 have been calculated [Vdh98b] using the dimensional regularisation both in the infrared and in the ultraviolet regions. The only approximation is that the radiative effects have been neglected for the proton. This approximation is justified by its large mass and has been tested to be numerically negligible using a model [Lhu97b]. The difficulty of the calculation is that it cannot be done analytically. After renormalization and cancellation of the infrared divergences, there remain multidimensional integrals over the Feynman parameters that one must evaluate numerically. The hard point is that the functions to integrate have sometimes wild variations, of the order E_{beam}/m_e in a range of the order m_e/E_{beam} . It has been necessary to develop very accurate integration methods to take care of this [Lhu97b]. Another problem, which is particular to VCS, is that the integrals may also have poles corresponding to the on shell propagation of the intermediate photon. To cope with that it has been necessary

to extend the integration in the complex plane of the Feynman parameters.

As pointed out in the introduction of this review, three interesting kinematical domains of VCS have been identified and discussed in some detail in this review. The threshold regime, the hard scattering regime and the DVCS have a well established physics case and are worth the experimental effort. This does not mean that VCS experiments cannot be done in other kinematical regimes. This is the case for the resonance region ($\sqrt{s} < 2$ GeV which will also be explored at CEBAF in 1998 [Ber93]. In this region the advantage of VCS over other probes is not so clear even if one forgets about the BH problem. The point is that in the resonance region the photon channel is, by unitarity, strongly coupled to the meson production channels. So the information is dominated by meson production and rescattering. This may be interesting by itself but it is much easier to study it directly using meson electroproduction rather than with the very difficult $(e, e'\gamma)$ experiments.

It seems now that, despite its experimental challenge, VCS has reached the status of a powerful and promising probe of nucleon structure. Nevertheless some work remains to be done to comfort this position. In particular, the higher twist effects need to be estimated and the model estimates of the OFPD's should be developed. Finally, since the OFPD's enter the amplitude through a convolution, one has to devise an efficient way to extract them from the data. We hope that this review will stimulate such work and that the experiments in the coming years will confirm our optimistic view of virtual Compton scattering.

Acknowledgements

This work was supported by the French Commissariat à l'Energie Atomique and in part by the EU/TMR contract ERB FMRX-CT96-0008. The authors thank P.Y. Bertin, V. Breton, N. d'Hose, H. Fonvieille, C. Hyde-Wright, L. Van Hoorebeke and P. Vernin for their experimental efforts as well as their stimulating interest for this work. The calculation of the radiative corrections would have been impossible without the enormous work of D. Lhuillier, D. Marchand and J. Van de Wiele. This work has been possible thanks to the collaboration with M. Guidal, P. Kroll, G.Q. Liu, M. Schürmann and A.W. Thomas. We thank D. Drechsel, A. Metz, and V. Brindejone for many stimulating discussions.

A Polarization vectors and spinors

The unit vectors $\vec{e}(1), \vec{e}(2), \vec{e}(3)$ of the C.M. frame have been defined in the text. The polarization vectors of a photon with momentum \vec{k} are

$$\vec{\varepsilon}(\vec{k}, 1) = \vec{\varepsilon}(\vec{k}, 2) \times \hat{k}, \quad \vec{\varepsilon}(\vec{k}, 2) = \frac{\hat{k} \times \vec{e}(1)}{|\hat{k} \times \vec{e}(1)|}, \quad \vec{\varepsilon}(\vec{k}, 3) = \hat{k}. \quad (150)$$

and the helicity states are

$$\vec{\varepsilon}(\vec{k}, \pm 1) = \mp \frac{1}{\sqrt{2}} \left[\vec{\varepsilon}(\vec{k}, 1) \pm i \vec{\varepsilon}(\vec{k}, 2) \right], \quad \vec{\varepsilon}(\vec{k}, 0) = \vec{\varepsilon}(\vec{k}, 3). \quad (151)$$

The 4-vector polarization states in the Lorentz gauge are then defined as

$$\varepsilon^\mu(\pm 1) = \begin{pmatrix} 0 \\ \vec{\varepsilon}(\pm 1) \end{pmatrix}, \quad \varepsilon^\mu(0) = \begin{pmatrix} k/k_0 \\ \vec{\varepsilon}(0) \end{pmatrix}. \quad (152)$$

The helicity spinors are

$$u(\vec{k}, h) = \begin{pmatrix} \sqrt{k_0 + m} \chi_h(\hat{k}) \\ 2h\sqrt{k_0 - m} \chi_h(\hat{k}) \end{pmatrix}, \quad (153)$$

with

$$\chi_{1/2}(\hat{k}) = \begin{pmatrix} \cos(\alpha/2) \\ e^{i\phi} \sin(\alpha/2) \end{pmatrix}, \quad \chi_{-1/2}(\hat{k}) = \begin{pmatrix} -e^{-i\phi} \sin(\alpha/2) \\ \cos(\alpha/2) \end{pmatrix}, \quad (154)$$

where (α, ϕ) are the polar and azimuthal angles of the direction \hat{k} . The rest frame spin projection spinors are

$$u(\vec{k}, \sigma) = \begin{pmatrix} \sqrt{k_0 + m} \chi_\sigma \\ \sqrt{k_0 - m} \vec{\sigma} \cdot \hat{k} \chi_\sigma \end{pmatrix}, \quad \chi_{1/2} = \begin{pmatrix} 1 \\ 0 \end{pmatrix}, \quad \chi_{-1/2} = \begin{pmatrix} 0 \\ 1 \end{pmatrix}. \quad (155)$$

These spinors are the positive energy solutions of the Dirac equation $(\gamma \cdot k - m)u(k) = 0$ and the Dirac matrices are those of Ref.[Bjo64].

B Vector basis

The vector spherical harmonics are defined according to

$$\vec{\mathcal{Y}}_{LM}^l(\hat{k}) = \sum_{\lambda, \mu} \langle l\lambda, 1\mu | LM \rangle Y_{l\lambda}(\hat{k}) \vec{e}(\mu), \quad \text{with } \mu = 0, \pm 1. \quad (156)$$

The magnetic, (transverse) electric and (electric) longitudinal vectors of the multipole expansion are, respectively

$$\begin{aligned} \vec{\mathcal{M}}_{LM}(\hat{k}) &= \vec{\mathcal{Y}}_{LM}^L(\hat{k}), \\ \vec{\mathcal{E}}_{LM}(\hat{k}) &= \sqrt{\frac{L+1}{2L+1}} \vec{\mathcal{Y}}_{LM}^{L-1}(\hat{k}) + \sqrt{\frac{L}{2L+1}} \vec{\mathcal{Y}}_{LM}^{L+1}(\hat{k}), \\ \vec{\mathcal{L}}_{LM}(\hat{k}) &= \sqrt{\frac{L}{2L+1}} \vec{\mathcal{Y}}_{LM}^{L-1}(\hat{k}) - \sqrt{\frac{L+1}{2L+1}} \vec{\mathcal{Y}}_{LM}^{L+1}(\hat{k}). \end{aligned} \quad (157)$$

They have the following useful properties

$$\vec{\mathcal{M}}_{LM}(\hat{k}) = \frac{\vec{L}_k Y_{LM}(\hat{k})}{\sqrt{L(L+1)}}, \quad \vec{\mathcal{E}}_{LM}(\hat{k}) = -i\hat{k} \times \vec{\mathcal{M}}_{LM}(\hat{k}), \quad \vec{\mathcal{L}}_{LM}(\hat{k}) = \hat{k} Y_{LM}(\hat{k}), \quad (158)$$

where \vec{L}_k is the angular momentum with respect to \vec{k} . The 4-dimensional basis $V^\mu(\rho LM, \hat{k})$ is defined as

$$\begin{aligned} V^\mu(0LM, \hat{k}) &= (Y_{LM}(\hat{k}), \vec{0}), \\ V^\mu(1LM, \hat{k}) &= (0, \vec{\mathcal{M}}_{LM}(\hat{k})), \\ V^\mu(2LM, \hat{k}) &= (0, \vec{\mathcal{E}}_{LM}(\hat{k})), \\ V^\mu(3LM, \hat{k}) &= (0, \vec{\mathcal{L}}_{LM}(\hat{k})). \end{aligned} \quad (159)$$

and one has the closure relation

$$\sum_{L, M} \sum_{\rho=0}^3 g_{\rho\rho} V^\mu(\rho LM, \hat{k}) V^{\nu*}(\rho LM, \hat{k}') = g^{\mu\nu} \delta(\hat{k} - \hat{k}'), \quad (160)$$

and the orthogonality relation

$$\int d\hat{k} V^{\mu*}(\rho LM, \hat{k}) V_\mu(\rho' L' M', \hat{k}) = g_{\rho\rho'} \delta_{LL'} \delta_{MM'}. \quad (161)$$

References

- [Ada97] Adams M.R. et al., Z.Phys.C **74** (1997) 237.
- [Ans87] Anselmino M., P. Kroll and B. Pire, Z Phys.C **36** (1987) 89.
- [Arn94] Arneodo M. et al., Nucl.Phys. **B429** (1994) 503.
- [Arv93] Arvieux J. and E. de Sanctis, The ELFE project, Italian Physical Society Conference Proceedings 44 (1993).
- [Arv95] Arvieux J. and B. Pire, Prog.Part.Nucl.Phys., Vol.35 (1995) 299.
- [Bal88] Balitsky I.I. and V.M. Braun, Nucl.Phys. **B311** (1988/89) 541.
- [Bal97] Balitsky I.I. and A.V. Radyushkin, Phys.Lett.B **413** (1997) 114.
- [Bal96] Ball P. and V.M. Braun, Phys.Rev.D **54** (1996) 2182.
- [Bel98] Belitsky A.V. and D. Müller, Phys.Lett.B **417** (1998) 129.
- [Ber67] Berends F.A., A. Donnachie and D.L. Weaver, Nucl.Phys. **B4** (1967) 1.
- [Ber58] Berg R.A. and C.N. Lindner, Phys.Rev. **112** (1958) 2072.
- [Ber61] Berg R.A. and C.N. Lindner, Nucl.Phys. **26** (1961) 259.
- [Ber93] Bertin P.Y., P.A.M. Guichon and C. Hyde-Wright, spokespersons TJNAF proposal, E-93-050.
- [Ber98] Bertin P.Y., private communication.
- [Bjo58] Bjorken J.D., S.D. Drell and S.C. Frautschi, Phys.Rev. **112** (1958) 1409.
- [Bjo64] Bjorken J.D. and S.D. Drell, *Relativistic quantum mechanics*, McGraw-Hill, New York (1964).
- [Bro73] Brodsky S.J. and G.R. Farrar, Phys.Rev.Lett. **31** (1973).
- [Bro80] Brodsky S.J. and G.P. Lepage, Phys.Rev.D **22** (1980) 2157.
- [Bro81] Brodsky S.J. and G.P. Lepage, Phys.Rev.D **24** (1981) 2848.
- [Bro94] Brodsky S.J. et al., Phys.Rev.D **50** (1994) 3134.
- [Che84] Cernyak V.L. and A.R. Zhitnitsky, Phys.Rep.**112** (1984) 173.
- [Che89] Chernyak V.L., A.A. Ogloblin and I.R. Zhitnitskii, Z.Phys. **C42** (1989) 569.
- [Col97] Collins J.C., L. Frankfurt and M. Strikman, Phys.Rev.D **56** (1997) 2982.
- [Col98] Collins J.C. and A. Freund, hep-ph/9801262.
- [Cri97] Crittenden J.A. (for ZEUS Collaboration), presented at Photon'97, May 1997.
- [D'An97] D'Angelo A. et al., Nucl. Phys. **A622** (1997) 226c.
- [Der95] Derrick M. et al., Phys.Lett.B **356** (1995) 601.
- [Deu73] Deutsch M. et al., Phys.Rev.D **8** (1973) 3828.
- [d'Ho95] d'Hose N. and Th. Walcher, spokespersons MAMI proposal (1995).
- [d'Ho96] d'Hose N. and G. Tamas, in Proceedings of the Workshop VCS'96, Ed. V. Breton, Clermont-Ferrand (1996).
- [d'Ho97] d'Hose N. et al., in Proceedings of the Conference on Perspectives in Hadronic Physics (Trieste 1997), Eds. S.Boffi, C. Ciofi degli Atti and M.M. Giannini, World Scientific, Singapore (1998).

- [Die97] Diehl M., T. Gousset, B. Pire and J.P. Ralston, Phys.Lett.B **411** (1997) 193.
- [Dit88] Dittes F.-M. et al., Phys.Lett.B **209** (1988) 325.
- [Dre97] Drechsel D., G. Knöchlein, A. Metz and S. Scherer, Phys.Rev.C **55** (1997) 424.
- [Dre98] Drechsel D., G. Knöchlein, A.Yu. Korchin, A. Metz and S. Scherer, Phys.Rev.C **57** (1998) 941.
- [Dud83] Duda J. et al., Z.Phys.C **17** (1983) 319.
- [Edm57] Edmonds A., *Angular Momentum in Quantum Mechanics*, Princeton University Press, Princeton N.J. (1957).
- [Ell77] Ellis J., in *Weak and Electromagnetic Interactions at High Energy*, Eds. R. Balian and C.H. Llewellyn Smith, North-Holland, Amsterdam (1977).
- [Far90a] Farrar G.R. and H. Zhang, Phys.Rev.D **41** (1990) 3348; Phys.Rev.D **42** (1990) 2413(E).
- [Far90b] Farrar G.R., K. Huleihel and H. Zhang, Nucl.Phys. **B349** (1991) 655.
- [Fra96] Frankfurt L., W. Koepf and M. Strikman, Phys.Rev.D **54** (1996) 3194.
- [Fra98] Frankfurt L.L., A. Freund, V. Guzey and M. Strikman, Phys.Lett.B. **418** (1998) 345.
- [Gel54] Gell-Mann M. and M.L. Goldberger, Phys.Rev. **96** (1954) 1433.
- [Geo71] Georgelin Y. and J. Stern, Nucl.Phys. **B27** (1971) 493.
- [Gos97] Goshtasbpour M. and G.P. Ramsey, Phys.Rev.D **55** (1997) 1244.
- [Gro98] Gronberg J. et al. (CLEO Collaboration), Phys.Rev.D **57** (1998) 33.
- [Gui95] Guichon P.A.M., G.Q. Liu and A.W. Thomas, Nucl.Phys. **A591** (1995) 606.
- [Gui97] Guichon P.A.M., in Proceedings of the 5th International Workshop on Deep Inelastic Scattering and QCD (DIS97), to be published.
- [Hem97a] Hemmert Th.R. and B.R. Holstein, G. Knöchlein and S. Scherer, Phys.Rev.D **55** (1997) 2630.
- [Hem97b] Hemmert Th.R. and B.R. Holstein, G. Knöchlein and S. Scherer, Phys.Rev.Lett. **79** (1997) 22.
- [Jac75] Jackson J.D., *Classical Electrodynamics*, John Wiley and sons, New York (1975).
- [Jaf96] R.L. Jaffe, "Spin, Twist and Hadron Structure in Deep Inelastic Processes, Lectures presented at the 1995 Erice Summer School on the Spin Structure of the Nucleon", in *Lectures on QCD*, 178-249, Ed. F.Lenz.
- [Jai93] Jain P. and J.P. Ralston, in Future Directions in Particle and Nuclear Physics at Multi-GeV Hadron Beam Facilities, BNL (March 1993).
- [Jak93] Jakob R., P. Kroll, M. Schürmann and W. Schweiger, Z.Phys.A **347** (1993) 109.
- [Ji97a] Ji X., Phys.Rev.Lett. **78** (1997) 610.
- [Ji97b] Ji X., Phys.Rev.D **55** (1997) 7114.
- [Ji97c] Ji X., W. Melnitchouk and X. Song, Phys.Rev.D **56** (1997) 5511.
- [Ji98] Ji X. and J. Osborne, hep-ph/9801260.
- [Kin87] King I.D. and C.T. Sachrajda, Nucl.Phys.**B279** (1987) 785.

- [Kro96] Kroll P., M. Schürmann and P.A.M. Guichon, Nucl.Phys. **A598** (1996) 435.
- [Kro91] Kronfeld A.S. and B. Nizic, Phys.Rev.D **44** (1991) 3445; Phys.Rev.D **46** (1992) 2272(E).
- [Lai95] Lai H.L. et al., Phys.Rev.D **51** (1995) 4763.
- [Lhu97a] Lhuillier D. et al., Virtual Compton Scattering at MAMI $\gamma^*p \rightarrow \gamma' p'$, in Proceedings of the 14th International Conference on Particles and Nuclei (PANIC96), 22-28 May 1996, Williamsburg, VA. Eds. C.E. Carlson and J.J. Domingo; World Scientific, Singapore (1997).
- [Lhu97b] Lhuillier D., PhD thesis, DAPNIA/SPhN-97-01T, 1997.
- [Low54] Low F.E., Phys.Rev. **96** (1954) 1428.
- [Low58] Low F.E., Phys.Rev. **110** (1958) 974.
- [MGi95] MacGibbon B.E. et al., Phys.Rev.C **52** (1995) 2097.
- [Met97a] Metz A. and D. Drechsel, Z.Phys. **A356** (1996) 351.
- [Met97b] Metz A. and D. Drechsel, Z.Phys. **A359** (1997) 165.
- [MRS93] Martin A.D., W.J. Stirling and R.G. Roberts, Phys.Rev.D **47** (1993) 867.
- [Rad96a] Radyushkin A.V., Phys.Lett.B **380** (1996) 417.
- [Rad96b] Radyushkin A.V., Phys.Lett.B **385** (1996) 333.
- [Rad97] Radyushkin A.V., Phys.Rev.D **56** (1997) 5524.
- [Rys93] Ryskin M.G., Z.Phys.C **57** (1993) 89.
- [Sha97] Shaw J., spokesperson MIT-Bates proposal.
- [Shu79] Shupe M.A. et al., Phys.Rev.D **19** (1979) 1921.
- [Sie37] Siegert A.J.F., Phys.Rev. **52** (1937) 787.
- [Siv89] Sivers D., Phys.Rev.D **41** (1990) 83.
- [Ste95] Sterman G. et al., Rev.Mod.Phys. **67** (1995) 157.
- [Ste97] Sterman G. and P. Stoler, Ann.Rev.Nucl.Part.Sci. **47** (1997) 193.
- [Sti96] Stiegler U., Phys.Rep. **277** (1996) 1.
- [vBi89] van Bibber K. and C. Hyde-Wright, in Pegasys project, Proceedings of Electronuclear Physics with internal targets, Stanford, 1989.
- [vdB95] van den Brand J.F.J. et al., Phys.Rev.D **52** (1995) 4868.
- [Vdh95] Vanderhaeghen M., K. Heyde, J. Ryckebusch and M. Waroquier, Nucl.Phys. **A595** (1995) 219.
- [Vdh96] Vanderhaeghen Marc, Phys.Lett.B **368** (1996) 13.
- [Vdh97a] Vanderhaeghen Marc, Phys.Lett.B **402** (1997) 243.
- [Vdh97b] Vanderhaeghen M., P.A.M. Guichon and J. Van de Wiele, Nucl. Phys. **A622** (1997) 144c.
- [Vdh98a] Vanderhaeghen M., P.A.M. Guichon and M. Guidal, Phys.Rev.Lett. **80** (1998) 5064.
- [Vdh98b] Vanderhaeghen M., D. Lhuillier, D. Marchand and J. Van de Wiele, article in preparation.
- [Wat82] Watanabe K., Prog.Theor.Phys. **67** (1982) 1834.